2005-09

Climatic variations of the California current system application of smart climatology to the coastal ocean

Feldmeier, Joel W.

Monterey, California. Naval Postgraduate School

NAVAL POSTGRADUATE SCHOOL

MONTEREY, CALIFORNIA

THESIS

CLIMATIC VARIATIONS OF THE CALIFORNIA CURRENT SYSTEM: APPLICATION OF SMART CLIMATOLOGY TO THE COASTAL OCEAN

by

Joel W. Feldmeier

September 2005

Co-Advisors: Tom Murphree
Robin T. Tokmakian

THIS PAGE INTENTIONALLY LEFT BLANK

REPORT DOCUMENTATION PAGE			Form Approved OMB No. 0704-0188
Public reporting burden for this collection of information is estimated to average 1 hour per response, including the time for reviewing instruction, searching existing data sources, gathering and maintaining the data needed, and completing and reviewing the collection of information. Send comments regarding this burden estimate or any other aspect of this collection of information, including suggestions for reducing this burden, to Washington headquarters Services, Directorate for Information Operations and Reports, 1215 Jefferson Davis Highway, Suite 1204, Arlington, VA 22202-4302, and to the Office of Management and Budget, Paperwork Reduction Project (0704-0188) Washington DC 20503.			
1. AGENCY USE ONLY *(Leave blank)*	**2. REPORT DATE** September 2005	**3. REPORT TYPE AND DATES COVERED** Master's Thesis	
4. TITLE AND SUBTITLE: Climatic Variations of the California Current System: Application of Smart Climatology to the Coastal Ocean		**5. FUNDING NUMBERS**	
6. AUTHOR(S) Joel W. Feldmeier			
7. PERFORMING ORGANIZATION NAME(S) AND ADDRESS(ES) Naval Postgraduate School Monterey, CA 93943-5000		**8. PERFORMING ORGANIZATION REPORT NUMBER**	
9. SPONSORING /MONITORING AGENCY NAME(S) AND ADDRESS(ES) N/A		**10. SPONSORING/MONITORING AGENCY REPORT NUMBER**	
11. SUPPLEMENTARY NOTES The views expressed in this thesis are those of the author and do not reflect the official policy or position of the Department of Defense or the U.S. Government.			
12a. DISTRIBUTION / AVAILABILITY STATEMENT Approved for public release; distribution is unlimited		**12b. DISTRIBUTION CODE**	

13. ABSTRACT (maximum 200 words)

The Northern Oscillation Index (NOI), an atmospheric climate index relating climate variations in the tropical Pacific and Northeast Pacific was used to selectively average output from the Parallel Ocean Climate Model (POCM 4C) for 1979-1998. Composites, or smart climatologies, were made representing El Nino (EN) and La Nina (LN) conditions, as well as a long term mean (LTM) average or traditional climatology, for November to March. Conditions in the California Current System (CCS) in the smart climatologies were consistent with large scale features noted in previously published studies of EN and LN. Overall, the patterns of anomalies (POCM 4C Smart Climatology minus POCM 4C Traditional Climatology) in salinity, temperature, and currents were opposite in sign and magnitude between the EN and LN composites. This was expected for opposite phases of the same climate variation, and many of the model's EN/LN differences were found to be statistically significant. Therefore, POCM 4C smart climatologies provide better estimates of ocean state and circulation patterns than traditional climatology. Such smart climatologies offer improved environmental information to Naval operational and strategic planners. They are also useful for studying climate variations, and in improving boundary and initial conditions for ocean and atmosphere models.

14. SUBJECT TERMS Smart Climatology, POCM 4C, El Nino, La Nina, Ocean Climatology, Northern Oscillation Index, NOI, Traditional Climatology			**15. NUMBER OF PAGES** 168
			16. PRICE CODE
17. SECURITY CLASSIFICATION OF REPORT Unclassified	**18. SECURITY CLASSIFICATION OF THIS PAGE** Unclassified	**19. SECURITY CLASSIFICATION OF ABSTRACT** Unclassified	**20. LIMITATION OF ABSTRACT** UL

NSN 7540-01-280-5500 Standard Form 298 (Rev. 2-89)
Prescribed by ANSI Std. 239-18

THIS PAGE INTENTIONALLY LEFT BLANK

Approved for public release; distribution is unlimited

CLIMATIC VARIATIONS OF THE CALIFORNIA CURRENT SYSTEM: APPLICATION OF SMART CLIMATOLOGY TO THE COASTAL OCEAN

Joel W. Feldmeier
Lieutenant Commander, United States Navy
B.S., Carnegie Mellon University, 1996
M.S., University of Idaho, 2003

Submitted in partial fulfillment of the
requirements for the degree of

MASTER OF SCIENCE IN METEOROLOGY AND PHYSICAL OCEANOGRAPHY

from the

NAVAL POSTGRADUATE SCHOOL
September 2005

Author: Joel W. Feldmeier

Approved by: Tom Murphree
Co-Advisor

Robin T. Tokmakian
Co-Advisor

Philip A. Durkee
Chairman, Department of Meteorology

Mary L. Batteen
Chairperson, Department of Oceanography

THIS PAGE INTENTIONALLY LEFT BLANK

ABSTRACT

The Northern Oscillation Index (NOI), an atmospheric climate index relating climate variations in the tropical Pacific and Northeast Pacific was used to selectively average output from the Parallel Ocean Climate Model (POCM 4C) for 1979-1998. Composites, or smart climatologies, were made representing El Nino (EN) and La Nina (LN) conditions, as well as a long term mean (LTM) average or traditional climatology, for November to March. Conditions in the California Current System (CCS) in the smart climatologies were consistent with large scale features noted in previously published studies of EN and LN. Overall, the patterns of anomalies (POCM 4C Smart Climatology minus POCM 4C Traditional Climatology) in salinity, temperature, and currents were opposite in sign and magnitude between the EN and LN composites. This was expected for opposite phases of the same climate variation, and many of the model's EN/LN differences were found to be statistically significant. Therefore, POCM 4C smart climatologies provide better estimates of ocean state and circulation patterns than traditional climatology. Such smart climatologies offer improved environmental information to Naval operational and strategic planners. They are also useful for studying climate variations, and in improving boundary and initial conditions for ocean and atmosphere models.

THIS PAGE INTENTIONALLY LEFT BLANK

TABLE OF CONTENTS

LIST OF ACRONYMS

AC	-	Alaska Current
AL	-	Aleutian Low
ASW	-	Antisubmarine Warfare
AUV	-	Autonomous Underwater Vehicle
AXBT	-	Air Dropped Expendable Bathythermograph
CALCOFI	-	California Cooperative Oceanic Fisheries Investigation
CC	-	California Current
CCS	-	California Current System
CDC	-	NOAA Climate Diagnostics Center
CFS	-	Climate Forecast System
CTD	-	Conductivity Temperature and Depth Profiling Instrument
CTZ	-	Coastal Transition Zone
CUC	-	California Undercurrent
DC	-	Davidson Current
EBC	-	Eastern Boundary Current
ECMWF	-	European Center for Medium Range Weather Forecasting
EN	-	El Nino
ENSO	-	El Nino/Southern Oscillation
GCM	-	General Circulation Model/Global Climate Model
GDEM	-	Generalized Digital Environmental Model
GFS	-	Global Forecast System
LAS	-	Live Access Server
LN	-	La Nina
LTM	-	Long Term Mean
MEI	-	Multivariate El Nino Index
METOC	-	Meteorology and Oceanography
MJO	-	Madden Julian Oscillation
MODAS	-	Modular Ocean Data Assimilation System
MOM3	-	Modular Ocean Model Version 3
MOODS	-	Master Oceanographic Observation Data Set
NAVO	-	Naval Oceanographic Office
NOAA	-	National Oceanic and Atmospheric Association
NOI	-	Northern Oscillation Index
NPC	-	North Pacific Current
NPH	-	North Pacific High
NRL	-	Naval Research Lab
OCL	-	NOAA Ocean Climate Laboratory

OFCM	-	Office of the Federal Coordinator for Meteorology
PDO	-	Pacific Decadal Oscillation
PFEL	-	NOAA Pacific Fisheries and Environmental Lab
POCM	-	Parallel Ocean Climate Model
POCM 4C	-	Parallel Ocean Climate Model Version 4C
POP	-	Parallel Ocean Program
SCC	-	Southern California Countercurrent
SCE	-	Southern California Eddy
SLA	-	Sea Level Anomaly
SLP	-	Sea Level Pressure
SLPA	-	Sea Level Pressure Anomaly
SODA	-	Simple Ocean Data Assimilation Ocean Reanalysis
SOI	-	Southern Oscillation Index
SSH	-	Sea Surface Height
SSHA	-	Sea Surface Height Anomaly
SST	-	Sea Surface Temperature
SSTA	-	Sea Surface Temperature Anomaly
USW	-	Undersea Warfare
UUV	-	Unmanned Underwater Vehicle
UW	-	University of Washington
WBC	-	Western Boundary Current
WOA	-	World Ocean Atlas
WOCE	-	World Ocean Circulation Experiment
WOD	-	World Ocean Database
WS	-	Wind Stress
WSC	-	Wind stress curl
WSCA	-	Wind stress curl anomaly
XBT	-	Expendable Bathythermograph

LIST OF FIGURES

THIS PAGE INTENTIONALLY LEFT BLANK

LIST OF TABLES

THIS PAGE INTENTIONALLY LEFT BLANK

ACKNOWLEDGMENTS

I would especially like to thank both Tom Murphree and Robin Tokmakian for their patience, help, and guidance. Steven Ramp and Peter Guest provided some valuable insight via their Operational Meteorology and Oceanography course. Additionally, Leslie Rosenfeld provided some valuable guidance as to the literature of the California Current System.

I would also like to thank my parents and brother for inspiring me and sharing their love of science. Special thanks are due to my brother and mother for some key statistical advice. My father also offered special inspiration as a past United States Air Force weather officer. Finally, to Hiromi and Reese my wonderful wife and daughter, thanks for the love, support, and most of all for just putting up with me.

THIS PAGE INTENTIONALLY LEFT BLANK

I. INTRODUCTION

A. MOTIVATION

The Navy Meteorology and Oceanography (METOC) Community is increasingly interested in both ocean forecasting and coupled air-ocean modeling (Estis et al. 2004; Oceanographer of the Navy 2000). Experience has shown that atmospheric forecasting improves when atmospheric climatological variability is taken into account (Reeves et al. 2004). Therefore as part of improving air-ocean modeling and forecasting it is reasonable to examine the state of ocean climatology, to ask how that climatology might be improved, and to ask how atmospheric climate variability affects the ocean and vice versa.

1. Naval Ocean Climatologies

a. History and Current State

The U.S. Navy has been recording, in one form or another, atmospheric and ocean data for over two hundred years. The landmark work of Matthew F. Maury at the Naval Observatory in the 19th century culled observations from ships' logs to create worldwide average seasonal and monthly representations of winds and currents. This data mining effort led to important realizations about the atmosphere and oceans. Perhaps the most important of these realizations was that although there is a lot of day to day variability in the atmosphere and oceans, distinct, recognizable, and repeatable patterns can be observed (Hearn 2002).

Maury's work was practically oriented. His target audience was captains of sailing vessels who could, given an accurate picture of winds and ocean currents

significantly shorten their voyage times. That had profound implications for both trade and Naval warfare (Hearn 2002). In the modern Navy, with fast propeller driven vessels not dependent on the wind, the benefits of Naval climatology have somewhat shifted. Submariners and those involved in antisubmarine warfare/undersea warfare (ASW/USW) are very interested in underwater acoustics. To find an adversary via sonar, and to avoid detection themselves, they need a detailed understanding of the temperature and salinity structure of the ocean, which effects sound velocity (Grembowicz and Howell 2002).

Additionally, the positions of temperature and salinity fronts, and the strength and position of currents are of wider Naval interest. It should be said that modern ships' navigators cannot completely neglect the effect of winds and seas on their voyage planning. Also, amphibious landings can be dramatically affected by ocean conditions, while search and rescue operations are very concerned with ocean temperatures (for survivability), and currents (for locating personnel). Increased use is being made of unmanned and autonomous underwater vehicles (AUVs and UUVs) for both sensing the environment and tactical jobs like minehunting. UUVs and AUVs have limited range and power, so knowledge of currents, temperature, and salinity features can help optimize where they are launched and where they transit to (Estis et al. 2004). To support these needs from an ocean climate perspective, the U.S. Navy METOC Community has several complimentary products in place. Among these are:

(1) MOODS. The Master Oceanographic Observation Dataset (MOODS) is maintained by the Naval Oceanographic Office (NAVO). It consists of approximately 10 million oceanic temperature and salinity versus depth profiles (T and S profiles) from expendable bathythermographs (XBTs), air dropped XBTs (AXBTs), conductivity temperature and depth instruments (CTDs), and other instruments dating from 1870 to the present. NAVO has made recent efforts to improve quality control of this data. All of these in situ station profiles are stored in a common MOODS format, and flagged if they are outliers a specified number of standard deviations from a prior climatological mean. Additional steps are underway to visually compare profiles with others in the same area as they are entered into the database (Grembowicz and Howell 2002).

(2) GDEM. The Generalized Digital Environmental Model (GDEM), also maintained by NAVO, provides global seasonal and monthly profiles of ocean temperature, salinity, and sound velocity on a regular 3-D grid. The current publicly available version (GDEM-V 3.0) has 78 vertical levels and a standard resolution of 0.25° in both latitude and longitude. The GDEM database was created by sampling the profiles available from MOODS. Various interpolation techniques have been used in different versions of GDEM to give realistic horizontal depictions of water masses. Vertical resolution is also a challenge for the creators of GDEM. The MOODS contains profiles from different types of instruments, with differing levels of reliability and depth range. In particular, profiles from XBTs and AXBTs cover mostly shallow depths, while CTDs and

other devices provide the data from deeper waters (NAVO 2005).

(3) MODAS. The Modular Ocean Data Assimilation System (MODAS) has been developed by the Naval Research Lab (NRL). Like GDEM, it incorporates data from MOODS to create a static climatology (i.e., a traditional long term mean climatology). This provides a 3-dimensional representation of the ocean at monthly intervals created from an optimum interpolation of selected MOODS profiles. It has 37 vertical levels, and variable horizontal resolution (from 0.125° to 0.5° latitude and longitude). In the bottom 11 vertical layers, and in open oceans areas where MOODS has few profiles, the static climatology is the World Ocean Atlas 1994 (WOA 94) produced by the National Oceanographic and Atmospheric Association (NOAA). These monthly MODAS fields can be further interpolated to give a representation at a specific location on a specific day of the year. There is another mode of MODAS that is referred to as a "dynamic" climatology, or Dynamic MODAS. Dynamic MODAS tries to improve on static climatology by using satellite sea surface temperature and sea surface height (SST and SSH) data. Basically, correlations are determined between historical T and S profiles and co-located SST and SSH data. Those correlations are then used to make corrections (or estimates) of the static climatology given observed SST or SSH data at a particular time and location (Fox et al. 2002a).

b. Problems and Limitations

As noted above, the U.S. Navy has a large amount of oceanographic data in the MOODS database. However, there are non-trivial problems with using that data to create a realistic picture of the world ocean. Most of the data is

from ships and submarines operating along well established shipping lanes and in training areas. Therefore some parts of the ocean are very well sampled, while other large areas of the open ocean (as well as the territorial waters of potential adversaries) have few or no observations. As was also noted above, MOODS contains well over 100 years of observations. However, using those observations all together can be challenging because the measurement instruments used and their associated reliability have changed through the years.

With the exception of Dynamic MODAS, GDEM and MODAS can be described as traditional climatology products. In meteorology and oceanography, traditional climatology involves getting as long a time series as possible for a certain variable, such as the daily maximum temperature at a specific location on a specific day. Then a simple average (long term mean, or LTM) of that time series (often a specific 30 year period is used as a standard) is taken. Traditional climatology is most useful in geographic areas where variability is low. However, over the last few decades it has been recognized that in some locales, large-scale atmosphere-ocean events like Madden Julian Oscillations (MJOs), El Nino (EN), La Nina (LN), and the Pacific Decadal Oscillation (PDO) can cause intraseasonal, interannual, interdecadal, and longer period variability (Reeves et al. 2004). For those locales the LTM can be a very poor representation of the actual atmosphere or ocean state.

An alternative to traditional climatology is based on recognizing variability in the ocean and atmosphere. Basic meteorology courses teach students that

weather can be studied over different spatial and temporal scales. A weather forecaster cannot ignore the synoptic scale (spanning 1000s of kilometers and affecting an area for several days) when making a local forecast. Mesoscale events, such as an afternoon thunderstorm, can be heavily influenced by synoptic forcing. Instead of viewing climate as static, its variability can, in part, be viewed as a forcing function on synoptic and global scale weather over large temporal and spatial scales.

One way to understand variability is to selectively average data from long time series. For example, some locations are much warmer or have more precipitation during an EN year than during a LN year or average (non-EN or non-LN) year. In such cases, it might make sense to separately average all of the EN years in the time series, all the LN Years, and all of the other years. Each of the three cases (or composites) then is a representative of the ocean or atmosphere relating to the climate signal of interest. How to select which years go into each such composite is debatable, and is discussed further in Chapter II. This selective averaging technique is sometimes referred to as smart climatology. The standard interfaces to GDEM and MODAS do not allow a user to do such selective averaging. Instead only a LTM for the day, month, or season of interest is provided.

2. Non-Naval Ocean Climatologies

a. Types of Climate Studies

Many oceanographic and atmospheric research studies can be classified as observational studies or modeling studies. Each has type of study has its benefits and drawbacks.

(1) Observational Studies. The civilian oceanographic community has been compiling hydrographic data from observational studies (cruises, coastal surveys, fixed instruments) for over a century (Gould 2003). Some of that data was collected as part of studies designed to define the mean state of the ocean. Other data sets conveniently have long enough time series, or can be combined with similar data sets, to be used in climate research. Of course, the same sorts of problems exist with these data as with the MOODS database. MOODS actually contains civilian profile data, but only for as far back as 1870 (Grembowicz and Howell 2002). Other observations are available from as far back as the 18th century (Conkright et al. 2002). In either case, these historical observations are not regularly spaced temporally or spatially, but represent conditions along major shipping routes, random opportunistic sampling, and specific research projects.

Additionally, as was noted above, instruments have changed and improved over the years. Data has been recorded in all sorts of hardcopy and digital formats. Data collected from remote sensing, such as satellite derived SST and SSH, have tremendous potential for use since they have global coverage and standardized formats. However, SST data has only been operationally reliable since the early 1980s, and SSH since approximately the early 1990s so their use in climate studies is limited (Gould 2003; Martin 2004). So, although there is a mass of real world data available for climate studies, it can be challenging to sort through and process into useful forms. Given these limitations, many observationally based studies focus on specific small geographic areas and limited time ranges, for which sufficient data is available.

(2) Modeling Studies. Numerical modeling studies can have many benefits. Chief among these for climate studies is consistency of the output. General circulation models (GCMs), typically calculate a standard set of variables (such as velocity, temperature, and salinity), at regular vertical, horizontal (e.g., isopycnal surface), and temporal resolutions (Semtner 1995). Therefore when a GCM simulates several years or decades, the time series are complete (spatially and temporally) and consistent.

Ocean modeling has improved drastically over the last several decades. Many GCMs now realistically simulate basin and global circulations, major currents, temperatures, and salinity fluxes (Semtner 1995; Stammer et al. 1996; Tokmakian 1996; Tokmakian 1998). However, there is an important distinction between realistic and accurate. A model may realistically portray a trend, such as warming or strengthened currents, but not accurately portray the amplitude (or geographic position and extent) of that trend. Also, models rely on past observational datasets to provide initialization and boundary conditions. Thus modeling studies are further limited in areas where few observations exist.

b. Climatology Atlases and Datasets

Efforts are ongoing to standardize oceanographic data and make it more accessible (Gould 2003). Different research initiatives such as WOCE (World Ocean Circulation Experiment) and CALCOFI (California Cooperative Oceanic Fisheries Investigation) make their historical data available online both through their own websites, and by requesting the data from online live access servers (LAS) run by organizations such as NOAA (see for example the

National Virtual Ocean Data System maintained at http://ferret.pmel.noaa.gov/NVODS/servlets/dataset, accessed July 2005).

NOAA's Ocean Climate Laboratory (OCL) has been a leader in taking on the challenges of non-standard data formats and coverage, and has produced several WOAs, and accompanying databases, often colloquially referred to by the leading OCL investigator's surname, Levitus. This work has provided a standard for modelers to use in verifying their work, and also for providing initial and boundary conditions for models (Stephens et al. 2002). As noted above, the Naval oceanographic community makes use of this data. Levitus data is available for global fields of temperature, salinity, and ocean chemistry at standardized depth levels for monthly, seasonal, and annual averages. The data is typically presented with 1° of latitude and longitude horizontal resolution, as that is the best available for the chemistry data (Stephens et al. 2002). However very recent analysis of T and S data has been done to 0.25° resolution from WOA 2001 (Boyer et al. 2005).

The data listed above has limited direct usefulness to the Navy. The WOA data is quite useful filling in gaps in the MOODS database. However, 1° horizontal resolution, on the order of 100 km, is not adequate for a Naval planner who may need to understand mesoscale ocean features which are on the order of much less than 100 km in size. Also, the Levitus data set represents traditional ocean climatologies by providing LTMs of individual months or seasons, but can not be easily and selectively averaged for a particular year. By contrast, for example, at the NOAA Climate Diagnostics

Center (CDC) website, data from an atmospheric reanalysis data derived from an atmospheric model can be averaged for individual atmospheric variables over specific days, months, seasons, or years to create smart climatology-type atmospheric composites (see http://www.cdc.noaa.gov/cgi-bin/Composites/printpage.pl, accessed July 2005). Such reanalysis data sets for the ocean have become available in recent years, but they also rely heavily on modeling due to the lack of observations, and users must typically conduct extensive data processing to develop smart ocean climatologies from these data sets (e.g., the Simple Ocean Data Assimilation ocean reanalysis (SODA); Carton et al. (2000)).

3. Aims of this Research

The research described in this thesis tests the idea of applying smart climatology concepts, especially selective compositing of historical or model data, to oceanographic data. It investigates whether smart ocean climatology is a reasonable and useful way to reflect the ocean's state in real time in the context of the data and models that are presently available. Additionally, this study addresses the question of whether using smart climatology versus traditional climatology has significant potential to improve Naval planning and operations perspective.

More details on the model and analysis techniques used are provided in Chapter II. Some essential questions, though, are: what resolution ocean model is necessary, what features are resolved by the model, how is the model forced, and how should one construct the composites? In this case a 0.25° horizontal resolution model, capable of

resolving large eddies, with realistic wind, heat, and freshwater forcing was examined. The use of atmospheric climate indices (to look for large scale air-sea interaction) in selecting the composites was also explored.

The ultimate motivations for this research are twofold. First, on the basic science side, meaningful analyses based on large scale changes of the ocean and atmosphere-ocean interaction can lead to a better understanding of the mechanisms for climate variability. Second, the Naval METOC community would benefit from improved information about the ocean's mean state and variability both for forecasting and for presenting useful environmental information to strategic and operational planners. It should be noted that the research presented in this thesis is an initial effort towards these goals. The research attempts to establish the feasibility of creating such products and to lay the groundwork for further research.

B. REGION OF FOCUS

Some geographic regions are more advantageous than others for testing the smart climatology concepts outlined above. One needs a region where large climate variability in both the atmosphere and ocean has been noted. Preferably the area has been well studied, with large amounts of real world observations available to compare with model output. Additionally, one would like to study an area routinely operated in by the Navy. That could lead to analysis of past Naval operations to see if smart climatology could have had a positive impact. The North Pacific along the west coast of North America is such an area.

1. California Current System

a. Choice of Geographic Region

This thesis will focus on the California Current System (CCS) off the west coast of North America. The CCS was chosen because of its position relative to large scale air-sea interactions (further discussed below; Schwing et al. 2002a), the large number of past studies done on the CCS (e.g., Miller et al. 1999), and because the Navy already uses the CCS as a test area for oceanographic and atmospheric models and products (e.g., Miller et al. 1999; NRL 2005).

b. LTM State of the CCS

The CCS has been highly measured, but is 'yet to be convincingly understood' (Miller et al. 1999). In part it is the large volume of published, sometimes contradictory, work on different portions of the CCS that makes it difficult to form a coherent picture. However, if we wish to understand atmospheric and oceanic long term variability, and how they affect and are expressed in the CCS, we first describe its LTM. The synopsis that follows draws heavily on the excellent works of Hickey (1998) and Gangopadhyay et al. (web page cited in 2005, from a document written in planning for 2003 Monterey Bay Circulation Portion of the AOSN-II experiment).

(1) Large-scale Structure. The California Current (CC) (as distinct from the CCS) is part of a large gyre in the North Pacific basin that also includes the North Equatorial Current (NEC), the Kuroshio, and the North Pacific Current (NPC). Broadly speaking, the NPC, also known as the West Wind Drift, connects the Northwest Pacific to the Northeast Pacific (NEP). The NPC starts around the termination of the Kuroshio and crosses the

Pacific until it splits into the Alaska Current (AC) and CC off the coast of British Columbia (Strub and James 2000). Flow in the CC is equatorward and can extend south of the 20° N parallel (Strub and James 2002). A basic depiction is given below. See Figure 1.

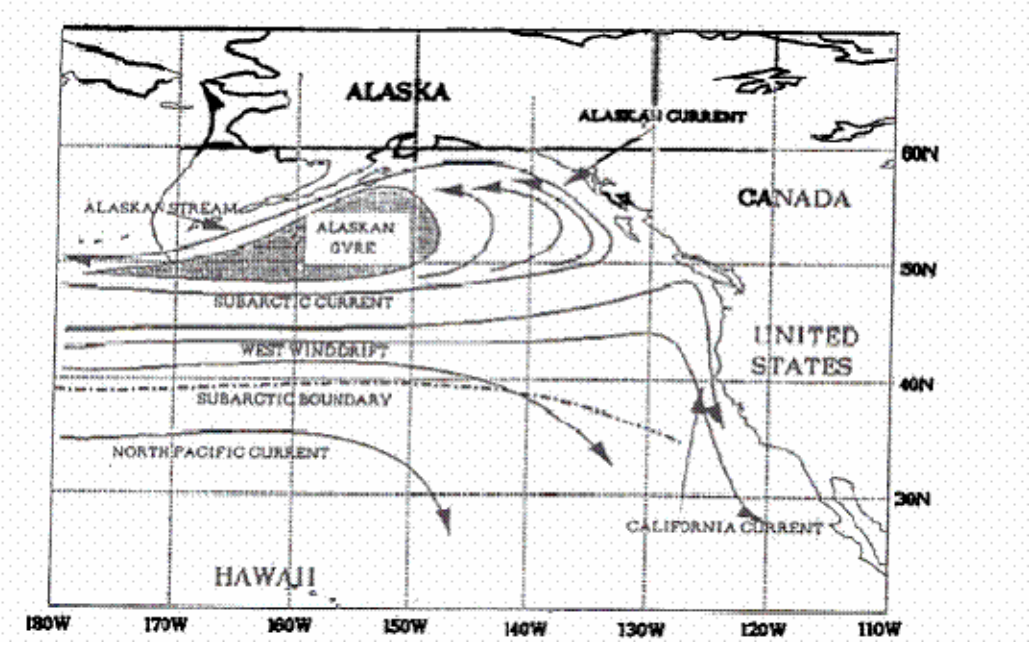

Figure 1. Large-scale current Structure of the NEP (From Matthews et al. 1992)

Over the last several decades, as more has been learned about ocean circulation, the picture of the CCS has become more complex. Older texts had focused on the CC as an example of a broad and slow eastern boundary current (EBC; Pickard and Emery 1990). This is opposed to distinct and strong western boundary currents (WBCs), such as the Gulf Stream and Kuroshio. Within its broad scope though, the CCS has a complex structure.

The CCS occurs approximately from Oregon to Baja California, extending from the shoreline 1000 km seaward (Miller et al. 1999). In addition to general

equatorward flow, there is a meandering equatorward jet at the core of the CC (Brink et al. 1991). A less well sampled poleward California Undercurrent (CUC) has been detected, inshore of the CC in observational studies (Gangopadhyay et al. 2005). The strength, extent, and continuity of the CUC are not always clear (Ramp et al. 1997b). There is also a surface inshore poleward current, or Davidson Current (DC) (Collins et al. 2003). The DC is strongest in fall, and the suggestion has been made that the DC is actually a surfacing of the CUC (Hickey 1998). A seasonal equatorward jet, well inshore of the CC and associated with upwelling is also sometimes observed (Collins et al. 2003). Between the inshore CUC/DC and the main CC is an area with current meanders and mesoscale eddies defined as the Coastal Transition Zone (CTZ) (Collins et al. 2003).

(2) Current Strength and Position (Mean and Variances). The CC mean flow is southward, and spans from 100-1350 km offshore (Gangopadhyay et al. 2005). It ranges in depth from 0-500 m, with strongest flow at the surface and weakens with depth (Collins et al. 2003). Typical current speeds are 10 cm/s (Hickey 1998). A meandering jet superimposed on this mean flow has been shown from drifter studies to have core velocities (during summer and fall) on the order of 50 cm/s, with meanders of approximately 300 km alongshore wavelength and 100-200 km cross-shore wavelength (Brink et al. 1991). However, an analysis of over ten years of hydrographic data off Monterey, California suggests that there is a mean CC jet 100-200 km offshore, with speeds only on order of 10 cm/s, with broader weaker mean flow to the west of that (Collins et al. 2003). This may indicate that the higher current

magnitudes determined by Brink were the result of frontal features, while the mean main CC flow is on the order of 10 cm/s (Collins et al. 2003). Such frontal features, associated with seasonal upwelling (see below), have been investigated in connection with an equatorward coastal jet along Oregon, which at times separates from the coast and becomes part of the CC (Barth et al. 2000). Cape Blanco (43° N), serves as a dividing point for upwelling and jets. North of Cape Blanco, upwelling is typically within 30 km of the shoreline (Barth et al. 2000). South of Cape Blanco, a strong upwelling front and an associated jet move further offshore, on order of 100 km (Barth et al. 2000). Barth et al. (2000) also suggest that a portion of the CUC turns equatorward near Cape Blanco and joins with the separating jet to strengthen southward transport.

A recent survey of much of the CCS (from 33° N to 51° N) yielded a mean structure for the CUC. Flow in the CUC is generally confined from 100-300 m depth (Hickey 1998). The CUC was found to have a core speed of about 10 cm/s, spanned from 200-275 m in depth, and was located 20-25 km off the continental shelf break (Pierce et al. 2000). That survey also suggested that some of the CUC is a continuous poleward flow, while some of the current turns offshore and also forms eddies (Pierce et al. 2000). The CUC has been observed to flow very close to the coast north of 37° N, while shifting offshore at 36.8° and 36.47° N (Gangopadhyay et al. 2005). In this same area, close to the Monterey Bay, 3-4 month increases (or bursts) in the speed of the CUC to speeds over 40 cm/s have been recorded although these increases were not found to be correlated with seasonal variability (Ramp et al. 1997b).

The DC has significant seasonal variability (see below). Observations suggest that sometimes two distinct cores of the DC may be observed: one along the coast, and another 50 km offshore (Collins et al. 2003). At times, poleward speed in both current cores of over 10 cm/s has been detected (Collins et al. 2003).

(3) Water mass characteristics. Hickey (1998) lists three main types of water in the CCS: Pacific Subarctic, North Pacific Central, and Southern (or Equatorial). The Pacific Subarctic water is carried equatorward by the CC, and is distinguished from other CCS waters by relatively low salinity and temperature. Entering the CCS from the west, North Pacific Central waters have relatively high salinity and temperature. Equatorial waters, carried poleward mainly by the CUC, also have relatively high temperatures and salinity, but are distinguished from North Pacific Central waters by a higher level of nutrients (Hickey 1998).

In coastal waters, wind induced upwelling also has a major effect on temperature and salinity. Colder saltier water (with high nutrient content) is brought to the surface from depths on the order of 10-100 m. This can create a 'cool band' of upwelled water, several 10s of km wide, along the coast (Pennington and Chavez 2000). Pennington and Chavez (2000) also cite several sources who note a separation of the upwelled waters from warmer waters by fronts, plumes, and eddies sometimes extending over 100 km offshore (this roughly corresponds to the CTZ).

Additionally outflow from the Columbia River (around 46.2° N) in northern Oregon can have a measurable impact. Hickey (1998) notes several studies in which the fresher water associated with the Columbia River was

identifiable in plumes extending several 100 kilometers. These plumes shifted position with the seasonally shifting currents (as will be described below). In general, the overall pattern of the CCS is cooler fresher waters to the north, warmer saltier waters to the south, with seasonally varying cool salty waters along the coast (Hickey 1998).

(4) Seasonal Variability. A major driving force in the CCS, and the source of much variability, is the wind (Hickey 1998; Pennington and Chavez 2000; Murphree et al. 2003a, 2003b). On the large scale, this variability is caused by shifting positions of the North Pacific High (NPH) (with clockwise winds) off the coast of California, and the Aleutian Low (AL) (with counterclockwise winds) in the Gulf of Alaska or north central Pacific. There are two major transition patterns in the wind field. The first occurs in spring when the AL moves northwest and the NPH moves north, strengthening northerly (note northerly is equivalent to southward) winds (Pennington and Chavez 2000). This is often termed the 'spring transition,' which occurs from south to north along the coast as the winds shift. In winter, the NPH and AL shift back and southerly winds from storms increase (Pennington and Chavez 2000).

A major feature of the spring transition is an increase in upwelling along the coast (Hickey 1998). Upwelling can be caused by alongshore coastal wind stress and/or wind stress curl (Murphree et al. 2003; Pickett and Paduan 2003). Alongshore coastal wind stress leads to Ekman transport of near surface waters away from the coast and upwelling of colder saltier waters and a drop in coastal sea level (Pickard and Emery 1990). Wind stress curl (WSC) leads to Ekman pumping or suction, with positive

WSC causing upwelling and lowered SSH, and negative WSC causing downwelling and increased SSH (Pickard and Emery 1990).

Additionally, the large scale winds caused by the AL and NPH can be differentiated from local winds. Chelton and Davis (1982) found that with respect to climate variations of coastal sea level, basin scale winds were more important than local winds. Of course, local wind variations can impact WSC and thus Ekman pumping. However, high correlation has been found between the large scale WSC anomalies and temperature (indicating upwelling or downwelling) anomalies in the NEP (Murphree et al. 2003a). An increase in upwelling also leads to elevated surface salinity (as discussed above).

Maximum anti-cyclonic northerly (southward) surface winds flow around the NPH, roughly parallel to the California coast, during spring and summer. Following in large part the wind forcing, the CC has its maximum equatorward flow in summer to early fall. During this same period, near Point Conception (approximately 34.5° N), a portion of the CC turns shoreward and then poleward and is termed the South California Countercurrent (SCC), or South California Eddy (SCE) if it does not continue poleward up the coast but returns to the main CC flow (Hickey 1998).

The DC generally develops in the fall and lasts through winter, flowing northwards from Point Conception to the vicinity of Vancouver Island (Hickey 1998). The development of the DC pushes a plume of fresh water from the Columbia River north. As the DC weakens, the Columbia River plume will extend more directly offshore (about 100 km), and with the spring transition has been observed to move far south (approximately 3-5 degrees of

latitude) along the coast with the CC or coastal jet (Hickey 1998).

As noted above, the CUC is not sampled as well as the other currents in the CCS. However the strength of the CUC is at a maximum in the summer and early fall. In winter there is a secondary maximum of the CUC (possibly associated with the DC), followed by a minimum poleward flow (with some equatorward flow observed in the California Bight) in spring (Hickey 1998).

Several altimeter based studies of seasonal variability in the circulation of the NEP have been carried out, notably by Strub and James (2000, 2002a). By examining sea surface height (SSH) and SSH anomalies (SSHA) they were able to infer approximate geostrophic currents. In Strub and James (2002a) several key points were enumerated. Among these are that during winter the cyclonic circulation in the AC is strengthened while the equatorward flow in the CC weakens. The equatorward flow in the CC is strongest in summer. Also, the variability of the NPC was found to be much smaller than the seasonal changes in the AC and CC. Additionally, seasonal highs and lows of SSH are seen to appear close to the coast and migrate offshore, causing meanders in the CCS. Strub and James (2000) describe the CC as a seasonally meandering equatorward jet that is created close to the coast in early spring and which then moves offshore, with poleward currents developing inshore in the late summer and early fall. Based on these studies, Strub and James (2000) provided the following conceptual schematic (Figure 2):

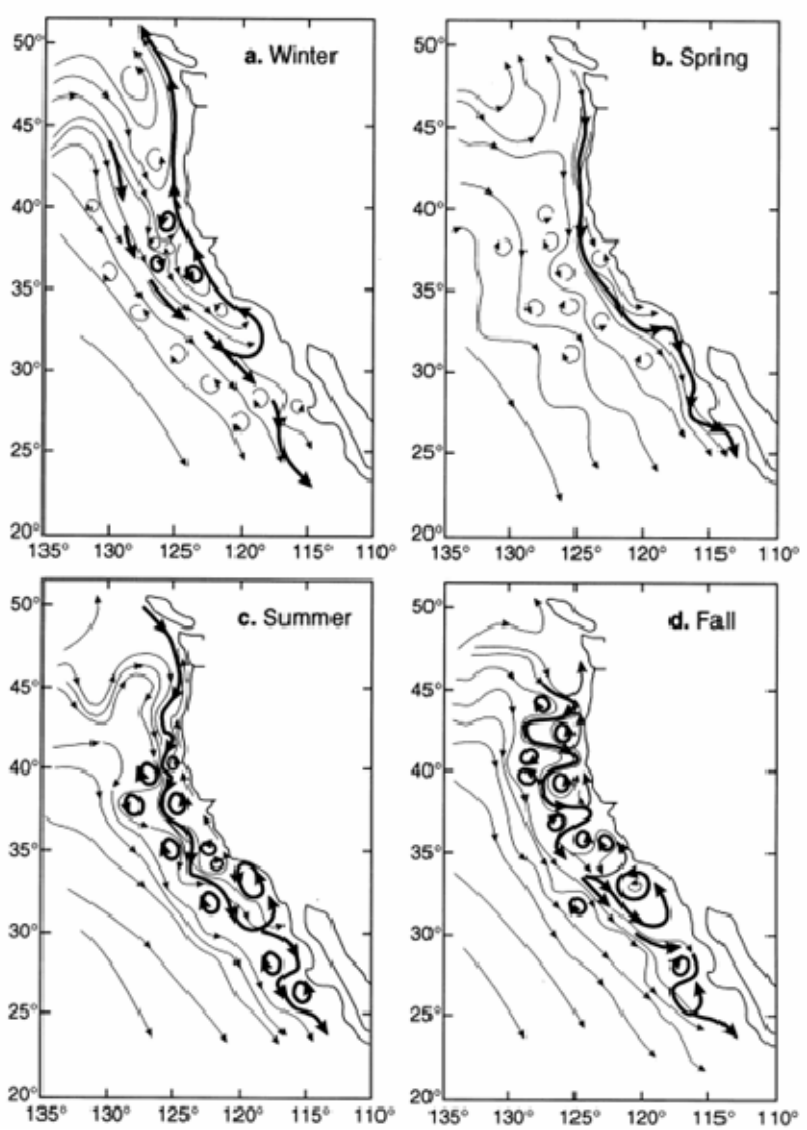

Figure 2. Conceptual schematic of surface current variability in the CCS. Note the dramatic shift from winter to spring, followed by the slower migration of the CC offshore with increasing eddies and the eventual re-formation of the DC (From Strub and James (2000)).

(5) LTM Hadley-Walker Circulation. The tropical and equatorial atmosphere is connected to and directly influences the extratropical atmosphere over the CCS (Schwing et al. 2002a). A primary mechanism for this is the Hadley-Walker Circulation. The warmest waters in the Pacific are generally in the vicinity of Indonesia or

northern Australia. That leads to the most active atmospheric convection in the western tropical Pacific. The air lifted into the atmosphere in that region is carried in the upper atmosphere towards the northeast by the thermally driven Hadley-Walker circulation. In the vicinity of the NPH that air returns to sea level causing a high pressure area. That air then continues as surface trade winds until it is carried back to the vicinity of the warmest Pacific waters and lifted again (Schwing et al. 2002a; see Figure 3)

.

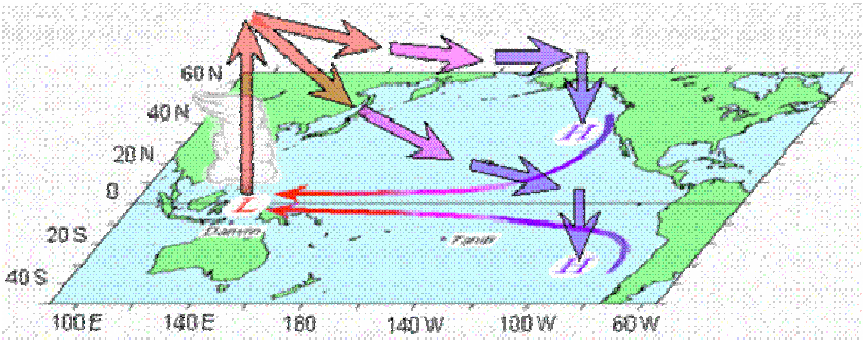

Figure 3. The Hadley-Walker circulation in the Pacific (from Schwing et al. 2002a)

2. Northeast Pacific Atmosphere and Ocean Regimes

a. Shift of Hadley-Walker Circulation

The existence of the Hadley-Walker circulation provides motivation for examining air-sea climate interaction in the CCS. During EN/LN events, the position of the warmest waters in the Pacific shifts (Cane 1983; numerous others). That leads to changes in the position of associated winds in the CCS, which lead to changes in the relative strength and position of the NPH and AL, which lead to changes in currents and water properties (Schwing et al. 2002a).

During EN, the warm water in the equatorial Pacific moves to the east (Mysak 1986). This shifts the Hadley-Walker pattern eastward. Normally high pressure regions in the NEP atmosphere are thus shifted east. An examination of wind anomaly fields indeed shows a large area of negative sea level pressure anomalies (SLPA) with associated counterclockwise winds in the region of the CCS (Schwing et al. 2002b). Note a SLPA is defined as the average sea level pressure (SLP) for a particular period minus the LTM SLP. A roughly opposite effect occurs during LN. More details of these patterns are presented below.

b. Oceanic Connections to EN/LN

In addition to atmospheric connections between the NEP and the equatorial Pacific during EN/LN, research has been done on oceanic connections (see for example Mysak 1986; Collins et al. 2002; Strub and James 2002b, 2002c; Huyer et al. 2002; Ramp et al 1997a). The general concept is that equatorial ocean Kelvin waves, associated with the shifting warm water in the tropical Pacific, travel to the eastern boundary of the Pacific. Some of that wave energy is channeled into coastally trapped ocean Kelvin waves traveling toward both poles (Mysak 1986).

c. Relative Effects of Atmospheric and Oceanic Teleconnections

There is a great deal of interest in whether the teleconnection between the tropics and the NEP is driven more by the atmosphere or by the ocean and which forcing leads. Huyer et al. (2002) found that sea level anomalies corresponding to EN were observed along the Oregon coast prior to downwelling winds both in 1982-83 and 1997-98. That suggests the oceanic pathway was dominant. However, Schwing et al. (2002b) suggest that at least in the 1997-98

case, non-EN related events prior to the 1997-98 EN were already effecting SSH along Oregon. Collins et al. (2002) conclude from hydrographic data from off central California that the oceanic pathway dominated the 1997-98 EN signal into the CCS. However, other investigators (Strub and James 2002b, 2002c) have suggested that oceanic teleconnections are most important from the Gulf of California south, while atmospheric teleconnections dominate further north. Ramp et al. (1997) also found evidence, from a combined modeling and observational study, of anomalous winds causing SSH changes to the north (with the signal propagating north to south) and Kelvin waves in the ocean causing SSH anomalies farther south (strongest south of the Gulf of California), with the two signals meeting somewhere off the southern California coast. This thesis will not attempt to determine the relative importance of atmospheric and oceanic teleconnections, but prior studies clearly indicate that the CCS can be strongly affected by atmospheric teleconnections during EN/LN. Thus, this supports the notion of considering periods of atmospheric climate variability to select model output for smart ocean climatology analyses.

d. Observed Conditions in the CCS During EN/LN

Distinct patterns of anomalies in wind, currents, sea surface height, temperature, and salinity have been reported in the atmosphere and ocean around the CCS during EN and LN (e.g., Schwing et al. 2002b). The following discussion of those anomalies focuses on the EN anomalies. Unless otherwise noted, the LN anomalies are approximately opposite in sign to those described for EN.

(1) Wind. Schwing et al. (2002b) sampled historical and atmospheric model reanalysis data

from 10 EN events, and 10 LN events to create composite EN and LN anomalies. Specifically, they looked at the effects in the NEP averaged over the November to February period, when EN/LN events are usually in a fully developed stage (Schwing et al. 2002b). Their composite anomalous wind field at 850 mb is shown in Figure 4. Anomalous winds at the surface will be similar, but friction will cause a turning in towards low pressure anomalies, and a turning away from high pressure anomalies (Danielson et al. 2003).

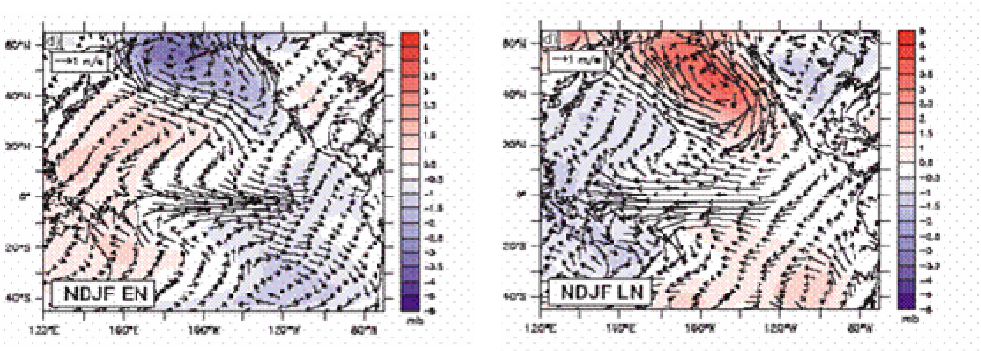

Figure 4. Typical 850 mb wind anomaly patterns during EN/LN. Color represents SLPA (in mb). The left figure depicts typical November to January (NDJF) conditions for EN. The right figure shows typical LN NDJF.(From Schwing et al. 2002b)

If we compare Figure 4 with Figure 3 we see, as expected, that a shifted Hadley-Walker circulation during EN leads to low SLPA off the California coast, with anomalous poleward winds along much of the coast. This is in contrast to LN which has enhanced equatorward/northerly winds over the CCS.

(2) Currents. On the large scale, given the anomalous wind forcing, the expected CCS anomalies during EN are an enhanced DC along the northern California-Oregon Coast, a weakened CC, and a strengthened AC (anomalous wind forcing will channel more of NPC into the CC than the AC). During LN we expect roughly the opposite pattern: enhanced

CC, diminished or absent DC, and weakened AC (Chelton and Davis 1982; Strub and James 2002b). These expected relationships are summarized for EN in Strub and James (2002b)'s Figure 1, and reproduced here as Figure 5.

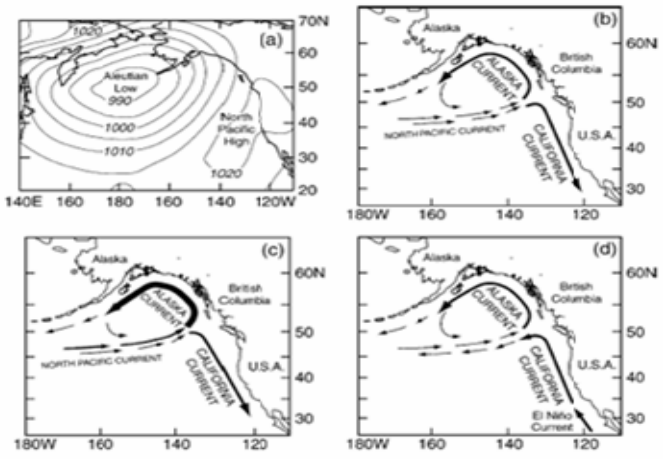

Fig. 1. Schematic of the NE Pacific atmospheric forcing and surface circulation. (a) The two major atmospheric pressure systems: the Aleutian Low and the North Pacific High (shown with a strengthened Aleutian Low and weakened North Pacific High); (b) the surface circulation in the North Pacific Current, the Alaska Gyre and the California Current; (c) the change in circulation hypothesized to occur during El Niño periods; (d) the hypothesized anomaly in circulation during an El Niño (the fields in (c) minus those in (b)).

Figure 5. Expected Large-scale Current Anomalies During EN (From Strub and James 2002b)

Many hydrographic surveys have been made during EN and LN events. The major limitation of these is that they can only cover limited spans of latitude and longitude. However, they do help identify repeatable trends during EN/LN. Collins et al. (2002) reported observations from the 1997-98 El Nino, along the CalCOFI line 67, which extends about 300 km at direction 240 degrees true from the central California coast at Moss Landing. They found upper ocean currents in the region 50-100 km from shore to be strongly poleward (approximately 0.5 m/s) in November 1997, equatorward in January 1998, and onshore in March 1998. Also in January 1998, they did a limited drift bottle experiment and found a net poleward drift rate of about 0.2 m/s along the coast of Northern California and Oregon.

During the same 1997-98 EN event, further north (along the 44.6° N parallel of latitude), strong poleward flow extending from the surface to 200 m inshore of 100 km off the coast were observed (Huyer et al. 2002). This was a dramatic departure from a ten year mean recorded along the same hydrographic line. This is illustrated in their Figure 5.b. of geostrophic current velocity, reproduced here as Figure 6.

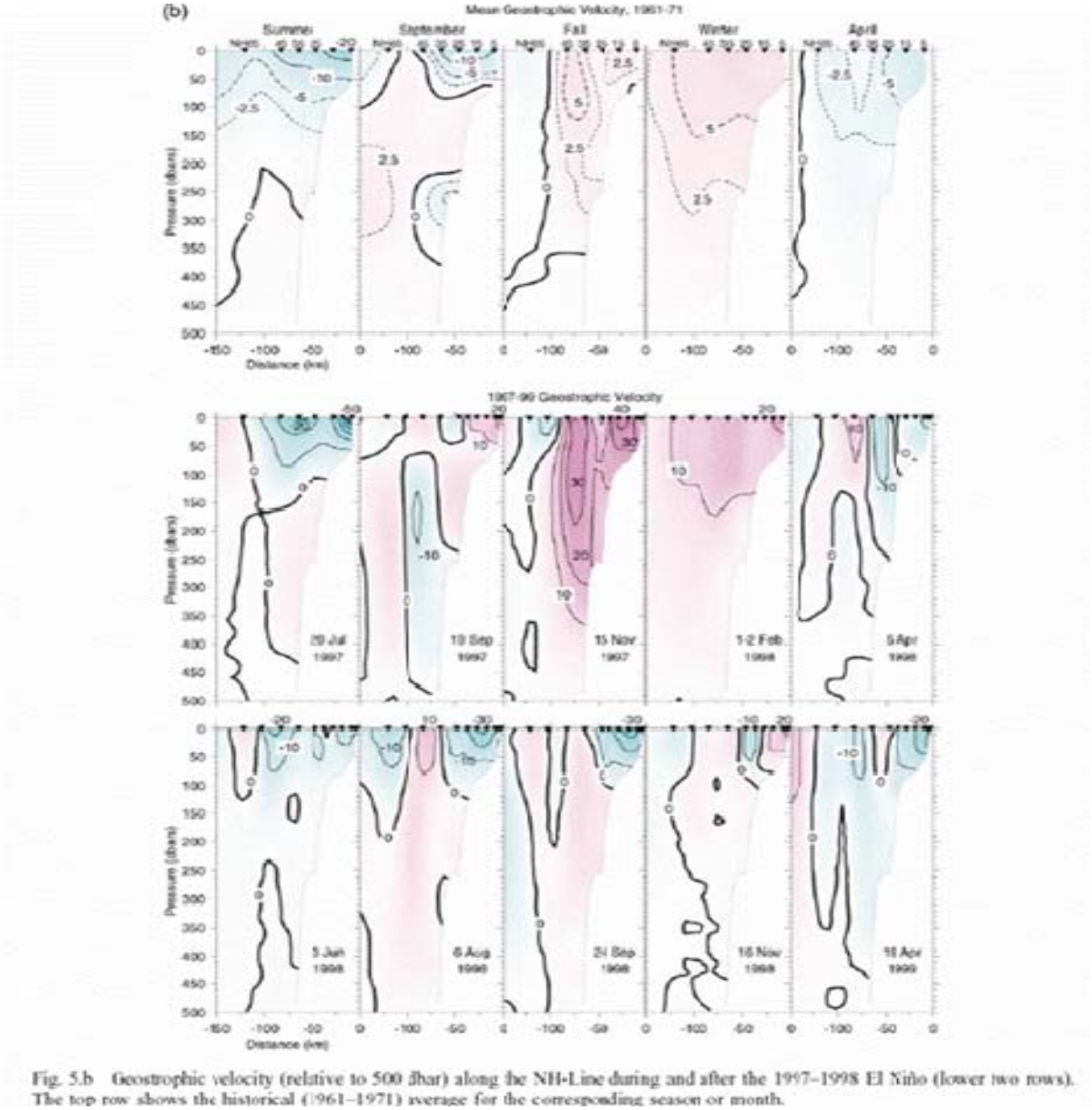

Fig. 5.b Geostrophic velocity (relative to 500 dbar) along the NH-Line during and after the 1997–1998 El Niño (lower two rows). The top row shows the historical (1961–1971) average for the corresponding season or month.

Figure 6. Geostrophic Velocities (in cm/s) along 44.6° N (From Huyer and Smith (2002)).

Note summer in these figures is 22 June – 31 August, fall is 1 November – 21 December, and winter is 1 January – 29 February.

Huyer et al. (2002) also reported observations along 4 hydrographic lines successively south of 44.6° N. Figure 7 below reproduces their Figure 9, which presents geostrophic velocity at these locations at various times during the 1997-98 EN. Of note is the variable strength of the southward coastal jet.

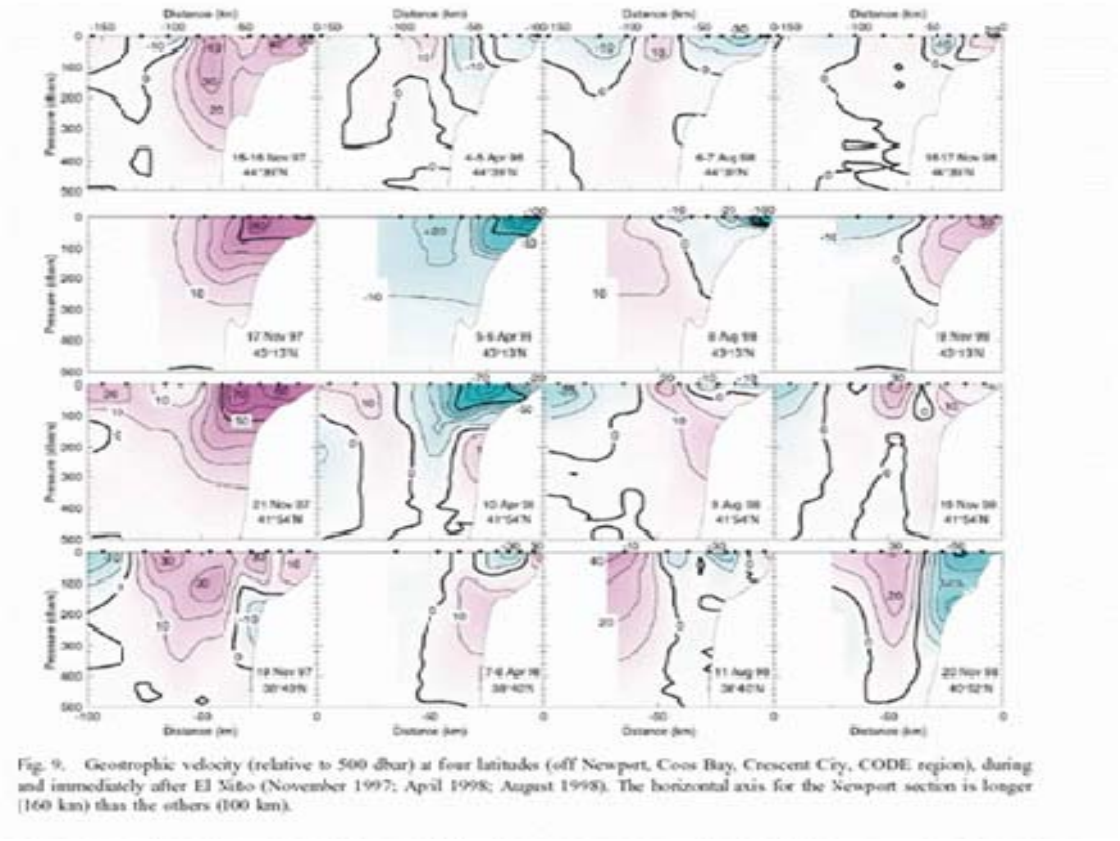

Fig. 9. Geostrophic velocity (relative to 500 dbar) at four latitudes (off Newport, Coos Bay, Crescent City, CODE region), during and immediately after El Niño (November 1997; April 1998; August 1998). The horizontal axis for the Newport section is longer (160 km) than the others (100 km).

Figure 7. Geostrophic Velocities off Northern California and Oregon (From Huyer et al. 2002).

(3) SSH. SSH differences can be used to infer horizontal pressure gradients in the ocean. Those pressure gradients can then be used to estimate geostrophic currents. Geostrophic current is a major component of the total current and can reflect the underlying temperature

and upwelling phase in the ocean. Strub and James have made extensive studies (2000, 2002a, 2002b, 2002c, among others) of satellite altimeter derived SSH anomalies. Others have relied on hydrographic surveys and tidal gauge data for analysis (see for example Chelton and Davis 1982; Mysak 1986).

Altimetry studies have confirmed that during EN, SSH is anomalously high along the west coast of North America (Strub and James 2002a, 2002b). As previously noted, it is unclear whether this is caused primarily by atmospheric teleconnections, oceanic teleconnections via coastally trapped Kelvin waves, or some combination thereof. However, it was noted that during the 1997-98 EN SSH anomalies were noted along southern California first, with the signal propagating northward and into the AC by the fall (Strub and James 2002a). This signal began weakening in January and February 1998. Processed and gridded altimetry data is readily available online, and analysis of that data is part of this thesis.

Much data reported in the literature is from the 1997-98 EN and 1998-99 LN. These were quite strong events relative to others in the record (Strub and James 2002c). In their analysis of multiple EN and LN events, Schwing et al. (2002b) present averaged November to February SSH anomalies from these events, presented as Figure 8 below.

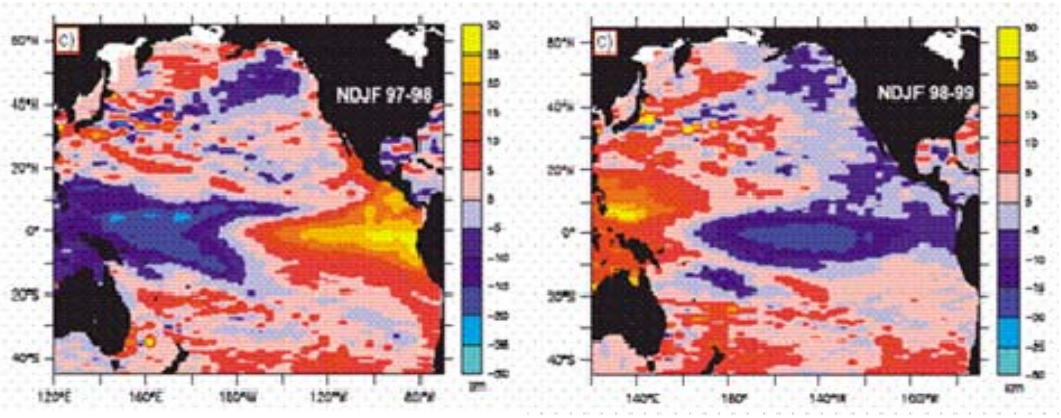

Figure 8. SSH anomalies (in cm) of recent strong EN (97-98) and LN (98-99) events (From Schwing et al. 2002b).

Similar patterns have been observed in other EN events. Researchers at NOAA noted that anomalously high sea level was noted along the coast in the Pacific Northwest (approximately 47°N) during the 1982-83, and 1957-58 EN (Wooster and Fluharty 1985). However, they noted that between 1958 and 1982 large SSH anomalies were not recorded in the Pacific Northwest during several EN events. This may be due to longer scale climate variations such as the PDO acting simultaneously, and biasing the sea level low. Miller and Schneider (2000) discuss a Pacific climate shift in the late 1970s which may explain why EN signals were apparent in SSH in the 1980s, but not in the 1970s or '60s.

(4) Temperature. As with current observations, temperature data is collected with two major methods: remote sensing via satellite and hydrographic surveys. SST is an important dataset particularly because of the relative ease of obtaining global coverage via satellite. However, it should be analyzed in combination with SSH for a more complete description of the ocean state because remotely sensed SST directly represents only a thin surface layer (Martin 2004).

Although open ocean data is sparse, Schwing et al. (2002b) describe temperature anomalies at the surface and at 100 m depth for their composite EN and LN events (Figure 9). These were derived by monthly averaging, interpolating, and gridding observations from the Global Temperature-Salinity Profile Program database and subtracting Levitus data. The anomalies were averaged into 5 degree by 5 degree spatial boxes (Schwing et al. 2002b). The results in Figure 9 suggest that during EN and LN winters, CCS temperature anomalies at the surface tend to be qualitatively very similar to those at 100 m.

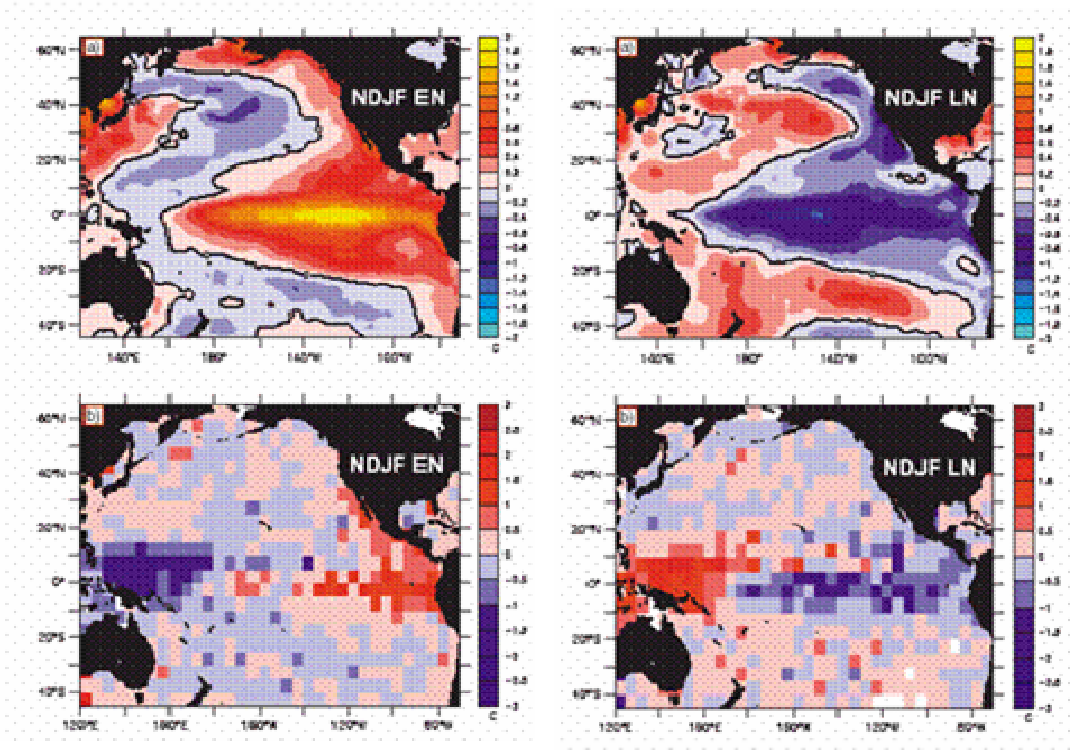

Figure 9. Temperature anomalies (in °C) during composite EN and LN events (From Schwing et al. 2002b). Note upper figures are for the surface, while lower figures are for 100 m depth.

Similar to current plots above, Huyer et al. (2002) provided analyses of cross-sections in the vicinity of the Oregon coast, showing temperature and salinity

structures in the LTM and for the 1997-98 EN. Temperature is shown in Figure 10 and Figure 11.

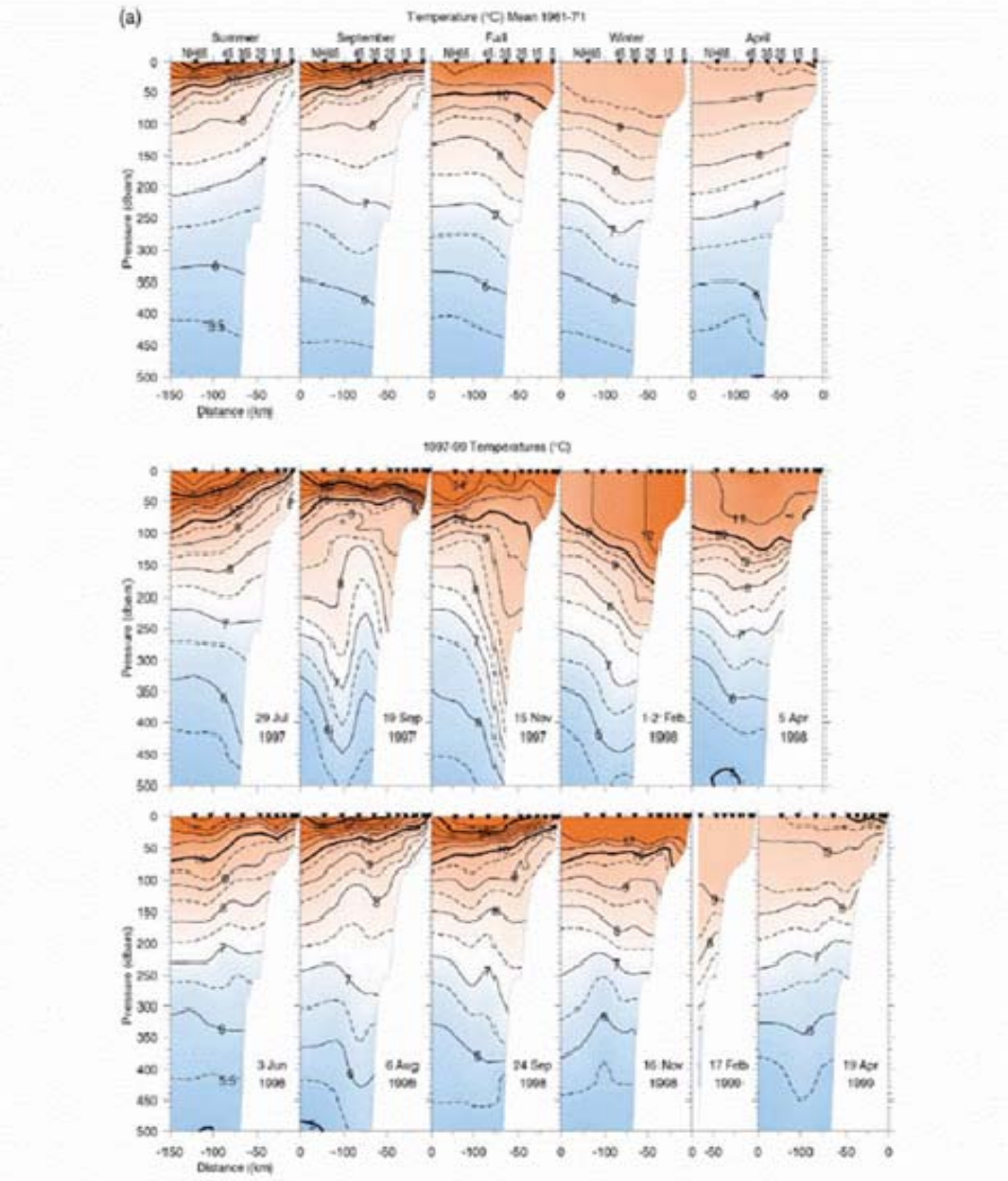

Fig. 3.a Temperature along the NH-Line during and after the 1997–1998 El Niño (lower two rows), with historical (1961–1971) averages (top row) for the corresponding season or month: summer (22 June – 31 August), September, late fall (1 November – 21 December), winter (1 January – 29 February), and April.

Figure 10. Temperature along 44.6°N during 1997-98 (From Huyer et al. 2002)

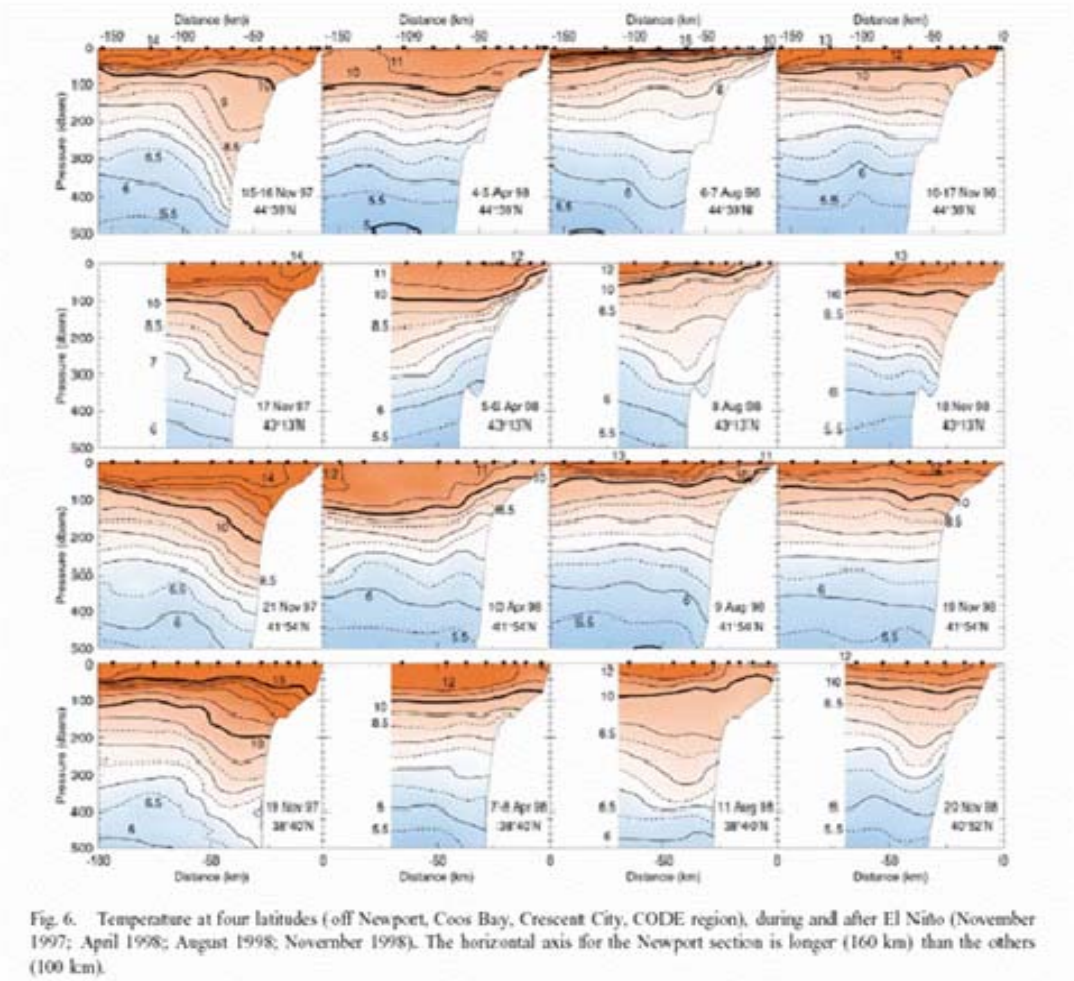

Fig. 6. Temperature at four latitudes (off Newport, Coos Bay, Crescent City, CODE region), during and after El Niño (November 1997; April 1998; August 1998; November 1998). The horizontal axis for the Newport section is longer (160 km) than the others (100 km).

Figure 11. Temperature cross-sections off the northern California and Oregon coast during 1997-98 (From Huyer et al. 2002)

Farther south during the same 1997-98 EN event, Collins et al. (2002) observed similar patterns off central California. Namely warming at the surface and at depths (mainly above 200m), corresponding with SSH increases. Some warming was also noted below 200 m (Collins et al. 2002). Slightly further north, observations reported by Ramp et al. (1997a) from the 1991-92 EN from near the Farallon Islands (offshore from San Francisco) saw familiar trends. Maximum warm anomalies were seen in the 100-150 m depth range and may be caused by anomalous advection of

Southern waters, decreased upwelling corresponding to anomalous southerly winds, or both (Ramp et al. 1997a). A representative figure from their analysis is reproduced below (Figure 12). Similar patterns for both temperature and salinity for earlier EN events are available in Wooster and Fluharty (1985)

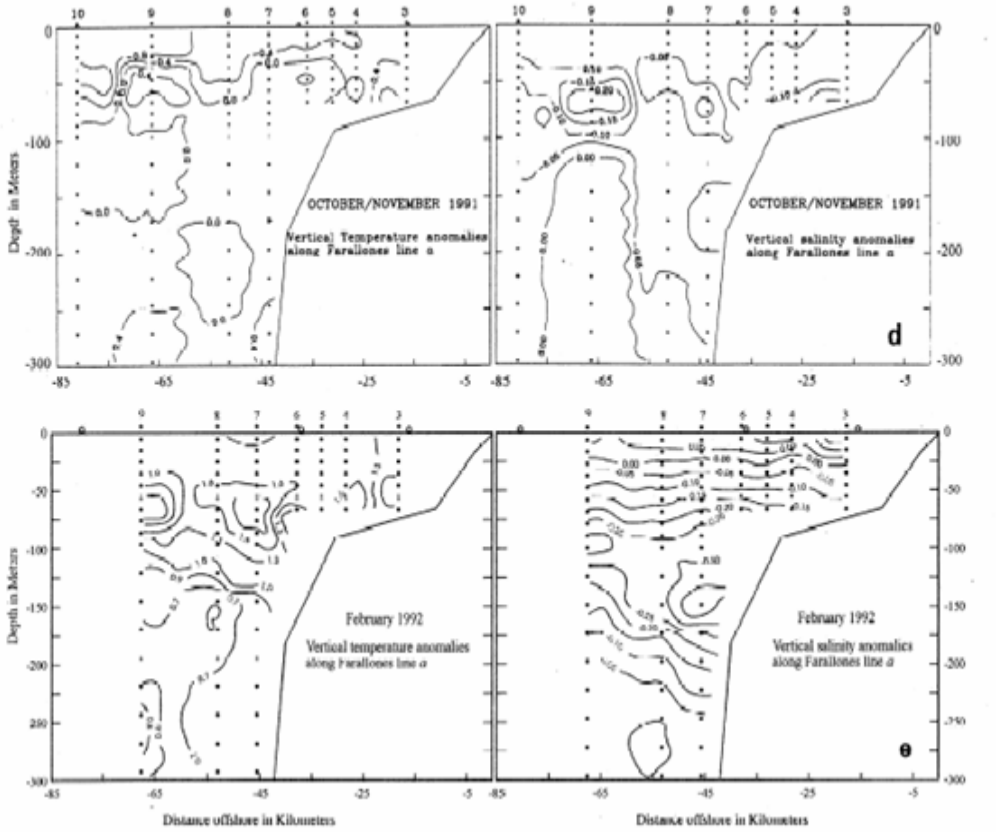

Figure 12. Temperature and Salinity anomalies (in ˚C/PSU) during the 1991-92 EN in the vicinity of the Farallones (From Ramp et al. 1997a). Note study area encompassed roughly from 37-38˚ N, from coast to about 90 km offshore.

(5) Salinity. Salinity variability has also been addressed and other researchers' figures are included in this section. Temperature and salinity, or density, anomalies should be considered in concert, to help determine if T-S anomalies are driven by anomalous advection of different waters, upwelling/downwelling

anomalies, or some combination thereof. Huyer et al. (2002) found that warm fresh anomalies were associated with EN along the central and northern California and Oregon coasts (Figure 13 and Figure 14).

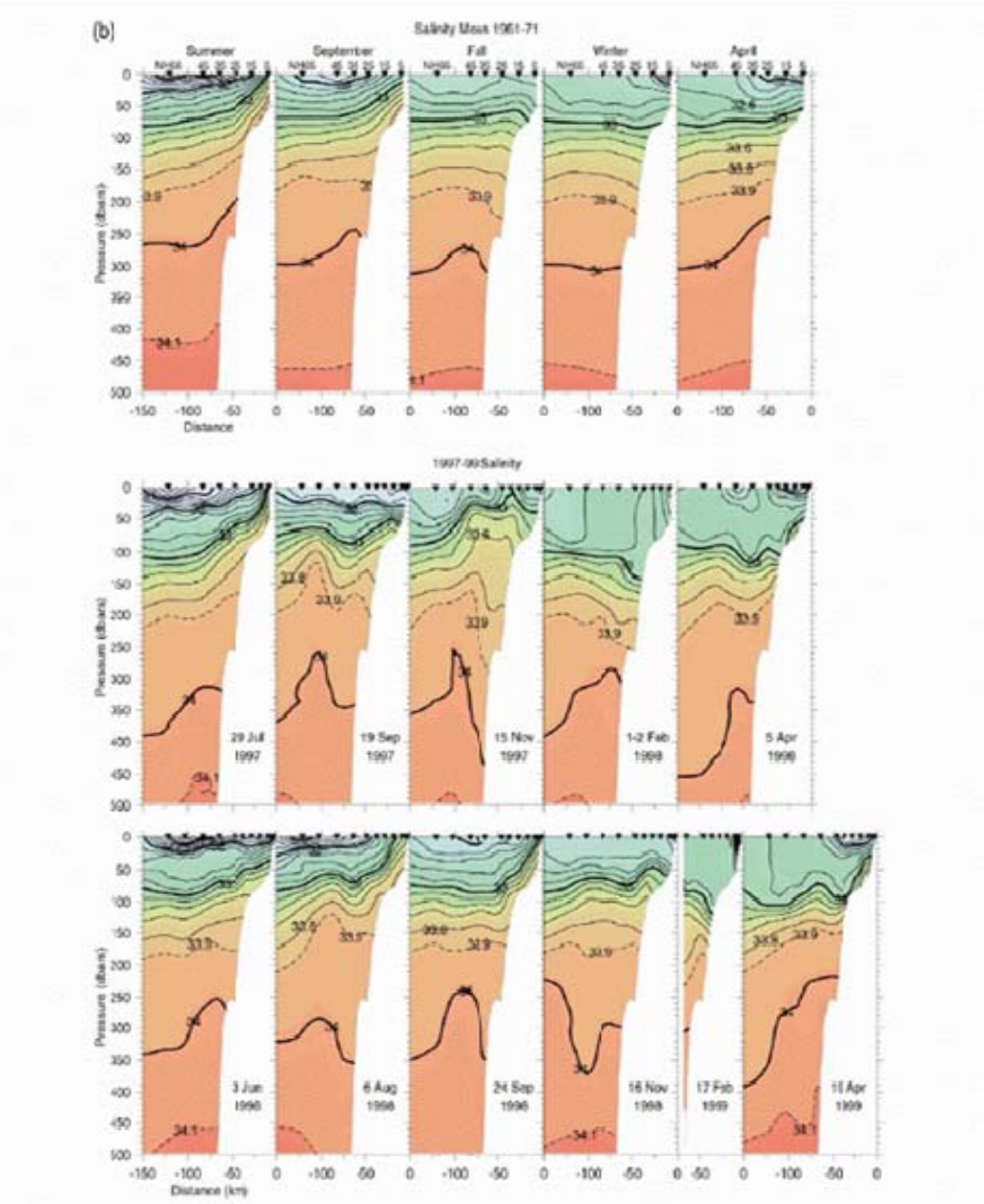

Fig. 3.b Salinity along the NH-Line during and after the 1997–1998 El Niño (lower two rows), with historical (1961–1971) averages (top row) for the corresponding season or month).

Figure 13. Salinity (in PSU) along 44.6° N during the 1997-98 EN (From Huyer et al. 2002)

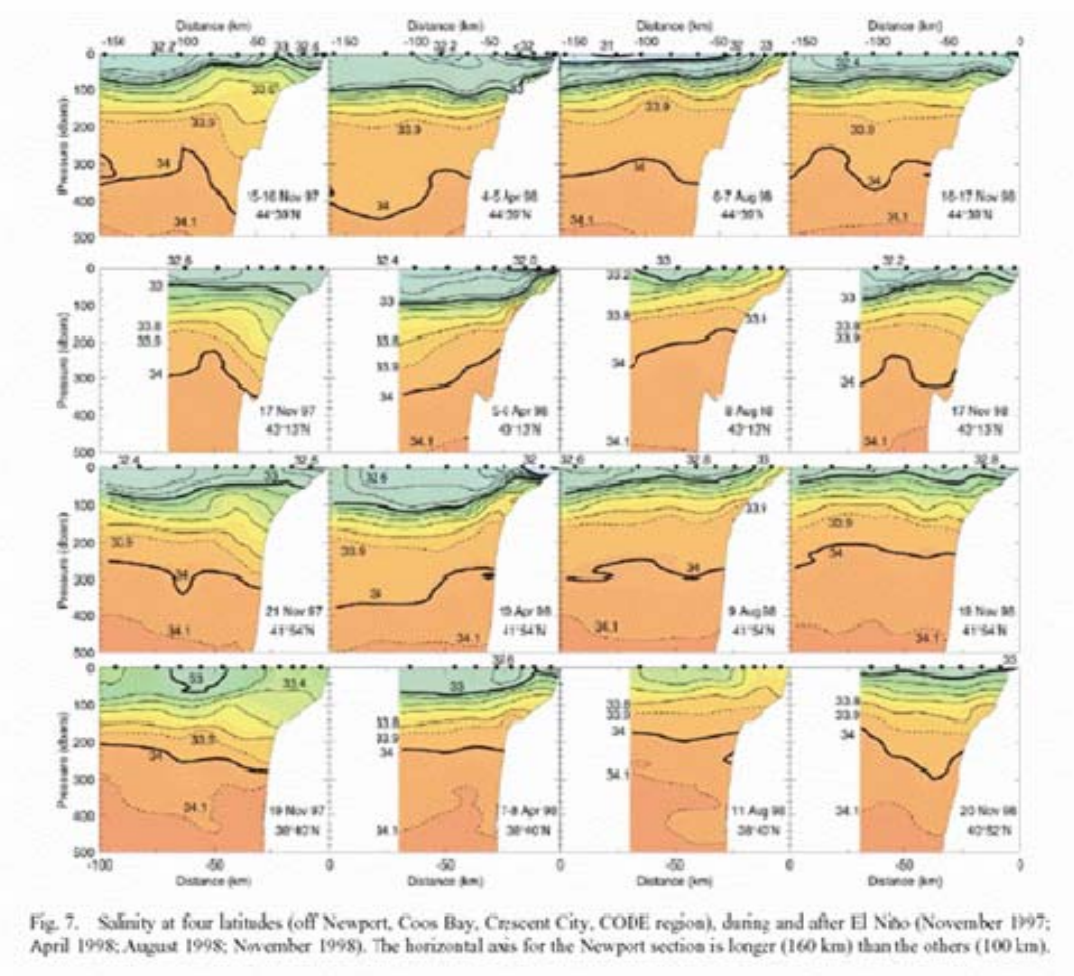

Fig. 7. Salinity at four latitudes (off Newport, Coos Bay, Crescent City, CODE region), during and after El Niño (November 1997; April 1998; August 1998; November 1998). The horizontal axis for the Newport section is longer (160 km) than the others (100 km).

Figure 14. Salinity (in PSU) along the Oregon and north California coast during the 1997-98 EN (From Huyer et al. 2002)

C. PROBLEMS AND HYPOTHESES

As mentioned above, this thesis will test the feasibility and usefulness of creating a smart climatology composite based on atmospheric climate indices related to EN and LN. Given the sparseness of in situ data in the ocean, a model will have to be used. The model provides both a LTM, and variations from that mean, for creating climate variation composites. This thesis focuses on the following analyses:

- Determine how well the selected ocean model reproduces the LTM state of the CCS as defined by

position and strength of CCS currents, temperature, salinity, and SSH.

- Identify trends in the difference between the selected model's LTM and in situ data to aid in proper analysis of model output.
- Determine if the POCM 4C is a reasonable test bed for this project, using the results from the preceding tasks.
- Use atmospheric climate indices to select years available within the ocean model run for creating EN and LN composites (EN and LN being chosen for study as they are large climate variations). This allows us to examine how atmospheric variability varies with the ocean's signal.
- Create November to March average EN and LN events from the years of data selected above. November to March has been chosen to cover the time period where the maximum extratropical impact of EN/LN is felt (Schwing et al. 2002a, b). This will allow us to look for systematic differences between EN, LN, and the LTM presumably caused by variability.
- Compare the November to March composite EN and LN events with available in situ data, such as summarized for the CCS in section B above. This will give a sense of the accuracy and usefulness of the smart climatology composite. If the model composites reasonably reproduce in situ observational trends, we will be more confident that the EN/LN/LTM differences observed in the model are realistic.

It should be noted that other modeling studies of the CCS during EN have been done (see for example Ramp et al. 1997a; Johnson and O'Brien 1990). However, the overall focus of these studies was on the processes by which EN events exhibit themselves in the CCS (e.g., by atmospheric or oceanic pathways) and not on characterizing the CCS during EN and LN periods. Specific EN events were the focus, rather than the similarities between events (Ramp et

al. 1997a). Those studies also typically used regional models instead of global. Using a global model with realistic surface forcing to study variability in the CCS allow for remote processes to influence the circulation in the coastal region.

We hypothesize that EN/LN composites of ocean parameters will show realistic and identifiable anomaly patterns in temperature, salinity, currents, and SSH. Further, we hypothesize that the differences between the EN/LN composites and the LTM state of the CCS will be significant and should be accounted for when Naval planners consider ASW operations, UUV and AUV operations, search and rescue, and transits.

THIS PAGE INTENTIONALLY LEFT BLANK

II. DATA AND METHODS

A. MODEL DESCRIPTION AND VERIFICATION

1. Model Development

The model used in this research is the Parallel Ocean Climate Model (POCM) version 4C, an ocean GCM based on the general formulation created and modified by Bryan, Cox, and Semtner among others over the last several decades. Although many other successful models exist and are in development, the Bryan-Cox-Semtner formulation is very widespread and serves as something of a standard among ocean modelers (Semtner and Chervin 1992; Killworth et al. 1991).

The general formulation was designed to handle the complex bathymetry and coastlines of the oceans (Bryan 1969). The original algorithm used modified primitive equations for horizontal motion as well as temperature and salinity transport, was hydrostatic, assumed incompressibility, and relied on an empirical equation for density (Semtner 1995). Multiple vertical levels, and variable horizontal grid spacing was included (Bryan 1969). Additionally, a 'rigid-lid' formulation, meaning a boundary condition of no vertical motion at the top level, was used. This was done to eliminate the calculation of high speed gravity waves in the model and provide savings in computational time (Bryan 1969; Semtner 1995). However, additional calculations at the surface level were required at each time step to fully resolve currents, and diagnose such variables as SSH (Killworth et al. 1991; Semtner 1995).

Cox made some of the first attempts to use the formulation globally in the 1970s (Semtner 1995). In 1974, Semtner undertook to modify the Bryan-Cox scheme for vector processing (Semtner and Chervin 1988). However, limitations on computer speed and memory led to a greater focus on regional models, since global models could only be run with a resolution of a degree of latitude. Additionally, it was realized that mesoscale features in the ocean, with horizontal extent on the order of 10s of kilometers were of interest, motivating models of higher resolution in smaller geographic areas (Semtner 1995). As technology continued to improve, models were better able to handle larger areas. By the late 1980s it was possible to run models based on the Bryan-Cox-Semtner formulation on a global scale (featuring resolution of less than a degree of latitude) with realistic eddy activity (Semtner and Chervin 1988; Semtner 1995).

By the early 1990s Semtner and colleagues had demonstrated the feasibility of GCMs including eddies (Semtner and Chervin 1992). Semtner and Chervin created a global model, at 0.5° resolution, with coastlines simplified and smoothed from available data. The model was forced with annual mean wind stress, and temperature and salinity were interpolated from Levitus data (Semtner and Chervin 1988). Initial improvements were made by using monthly mean wind stress (Semtner and Chervin 1992). Further improvements have been made by use of ever more realistic external forcing.

The POCM 4C is the Semtner-Chervin variation of the Bryan-Cox-Semtner formulation (Stammer et al. 1996). POCM 4C has an average horizontal resolution of 0.25°. Also, in

the early 1990s, the rigid lid formulation was replaced with a free-surface formulation (Killworth et al. 1991; Stammer et al. 1996). It had been noted that with the newer global models the computational effort required at the top model level in a rigid-lid scheme was becoming about the same as that which would be required for a free-surface model. Having a free surface model has the advantage of SSH being a prognostic variable. This allows for direct assimilation of satellite altimetry data, and for studying tides via the model (Killworth et al. 1991).

POCM 4A was run for the 1986-1989 period. It used monthly mean wind stress fields, and restored T and S fields towards monthly Levitus values on a 30 day time scale (Stammer et al. 1996). POCM 4B covered 1987-1994, and used European Center for Medium Range Weather Forecasting (ECMWF) derived daily wind stress fields, monthly climatological surface heat fluxes produced from ECMWF products, and T and S restored towards Levitus 1994 fields (Stammer et al. 1996; Tokmakian 1998). POCM 4B was initialized from POCM 4A. Important lessons were learned during this timeframe, including that it was better to use ECMWF 10 meter wind fields, rather than 1000 mb winds, and that you should temporally interpolate between daily averaged wind fields at shorter model time steps (Stammer et al. 1996; Jayne and Tokmakian 1997). Also, model SSH fields improved, reflecting altimetric variability spatially as improved wind stress and heat flux forcing was used.

2. POCM 4C Specifications

The POCM 4C run used for this thesis covers the period from 1979-1998. For 1979-1993, ECMWF reanalysis data was

used for the daily forcing fields, while for 1994-1998, the daily operational ECMWF fields were used (Tokmakian 1998). The reanalysis and operational fields are consistent with each other. The model has an average horizontal grid spacing of 0.25°. Global coverage is provided with a 902 x 507 longitude by latitude grid (Tokmakian 2005). Calculations are made at 20 vertical, irregularly spaced levels (Tokmakian 2005). Model bathymetry was derived from the 5′ gridded Earth topography dataset (Matano et al. 2002).

POCM 4C differs from its predecessors primarily in the tracer equations for temperature and salinity. These equations have been modified to provide more realistic time varying fluxes using daily heat and freshwater fluxes, in addition to daily wind forcing (Tokmakian 1998). At individual model time steps, ECMWF wind fields interpolated from between daily averages were used (Jayne and Tokmakian 1997).

3. Prior POCM 4C Verification Work

Before utilizing the POCM 4C run to study variations in the CCS, it is important to examine the model's general performance. Although the purpose of this thesis work is not to verify the model, a working knowledge of model accuracy and biases will aid in the interpretation of results obtained from POCM 4C output. POCM 4C is a global model, so most verification work done to date involves comparison of model data fields to in situ data fields on very large scales.

In general, POCM 4C shows good qualitative agreement with the general circulation of the ocean. The Antarctic Circumpolar Current (ACC), Kuroshio, Gulf Stream, and other

basin scale western boundary currents (WBCs) and their associated mesoscale eddies are resolved in the approximately correct locations (Stammer et al. 1996). Analysis of POCM 4B showed that the model simulated well the location, timing, and variance of the large scale mean circulation, but the modeled variance tended to be too weak by a factor of 2 to 4 (Stammer et al. 1996).

Comparisons between model and in situ data have primarily been done with sea surface height (SSH). The sources of observational SSH data are tide gauges and satellite altimetry. Tokmakian (1996) found that satellite altimetry SSH and POCM 4B SSH had approximately the same correlation (approximately 0.5) to tide gauge data. Comparisons of POCM 4B with tide gauge data have shown that the model captured the phase of SSH variations, but tended to show weaker magnitudes than the observed data (Tokmakian 1996). Similar but more limited comparisons of POCM 4C with tide gauge data has produced similar results (Tokmakian 1998).

The situation is somewhat different with regard to temperature and salinity fields. In one comparison, at Ocean Weather Station Papa (50° N 145° W), POCM 4C slightly overestimated sea surface temperature (SST), but captured the phase of variations well (Tokmakian 1998). Compared to the Station Papa salinity, the POCM 4C salinity variations were too large, and did not capture the phase of salinity changes as well as it did temperature (Tokmakian, 1998).

Comparisons of POCM 4C output with altimetry data found the model had larger absolute SSH errors than the altimetry (Tokmakian and Challenor 2000). Correlations of model SSH with tide gauge data showed a low correlation in

regions such as in the North Pacific around 20° North. As noted in Stammer et al. (1996), the model tends to underestimate the magnitude of variability. Thus, in eddy rich areas such as the Kuroshio and Gulf Stream, the model error is relatively large (Tokmakian and Challenor 2000).

Examinations have also been made of heat fluxes in POCM 4C. Tokmakian (1998) found that in the Pacific, at 24°N latitude, the mean overturning heat flux over the 20 year POCM 4C run was within the range of that reported by other researchers from observational data. It was also noted that overturning heat flux is highly correlated with the climatological North Pacific Index (Tokmakian 1998). That may indicate that in the northern Pacific POCM 4C variability is closely tied to Ekman processes, as overturning is closely tied to wind driven Ekman transport (Tokmakian 1998).

Freshwater flux was also examined. The model does not resolve the Arctic explicitly (latitudinal grid stops at 65.11°N), so an offset of flow into and out of the Arctic in the Pacific and Atlantic had to be made. The model reasonably resembles fluxes estimated from observations worldwide, but there is a noticeable difference in the South Atlantic (Tokmakian 1998).

POCM 4C has been used in a study of the southern Indian Ocean, as well as in a study of the Antarctic Circumpolar Current (Matano et al. 2002; Gille et al. 2001). A comparison of current strength via volume transport calculations in the southwest Indian Ocean showed that POCM 4C was “statistically indistinguishable” from observations (Matano et al. 2002). It was also noted however that POCM 4C’s upper circulation energy is lower

than that observed from altimetry (Matano et al. 2002; Stammer et al. 1996). Gille et al. (2001) studied the relation of wind stress and wind stress curl to model transport in the Antarctic. They found that POCM 4C matched observations in that transports are coherent with the wind. However, phase lags seen in observational data were not reproduced in the model. They suggest that the POCM 4C effective viscosity may be too large (Gille et al. 2001).

For this study, additional verification and comparison work was done on the scale and in the vicinity of the CCS. That work is described in Chapter III along with a summary of POCM 4C trends and biases.

B. SOURCES OF COMPARISON DATA

1. Levitus T and S Data

As mentioned in Chapter I, the work of NOAA's Ocean Climate Laboratory in compiling and analyzing historical ocean observations is often referred to by the name of the principle investigator, Levitus. Levitus and colleagues have compiled, with the cooperation of numerous scientists and institutions worldwide, a highly comprehensive set of data including ocean temperature, salinity, and (recently) chemistry (Stephens et al. 2002). This data goes as far back as the late 18^{th} century, and is perhaps the most comprehensive collection of such data in the world. They have also done analyses of these data to provide global ocean annual, seasonal, and monthly climatologies at 1° and 0.25° (T and S only) (Boyer et al. 2005). In so doing they have produced a series of World Ocean Databases (WOD) and World Ocean Atlases (WOA).

The most recent Levitus products are WOD 2001 and WOA 2001. WOA 2001 was initially assembled for 1° of

latitude/longitude resolution, at standardized depth levels (depth resolution varies with temporal resolution: monthly fields at 24 levels, seasonal fields at 33 levels) (Stephens et al. 2002). Subsequent analyses (using the same data) for T and S at 0.25° resolution have been accomplished and are available from NOAA and other data-servers online. All of the Levitus climatologies provide both simple means of raw data, which has been objectively analyzed. Essentially objective analysis is a process to average and weight data sampled inconsistently in instrumentation, time, and space to a regular 4-D (3 spatial dimensions and time) data set. The Levitus climatologies use a first-guess field for each variable, taking an average of all observations (that have been interpolated to a standard depth level, and are from the appropriate temporal frame) within a grid box, and compare that grid box mean to the first guess fields of neighboring grid boxes (to some specified distance; this procedure is done multiple times over decreasing distances), and then applying horizontal and vertical smoothing techniques (Boyer et al. 2005).

Any grid square in the Levitus (WOA 2001) climatologies that contains land is excluded from analysis. This led in general to an increased number of observations averaged for the 0.25° objective analyses (of WOA 2001 data), because a 1° **x** 1° grid box close to the coast can contain a large number of observations. Excluding a 1° **x** 1° grid box removes far more observations than removing several 0.25° **x** 0.25° boxes along the coastline (Boyer et al. 2005). The first guess field for the 1° fields is a zonal average of all values in the immediate vicinity of the grid-box. The 0.25° fields use the 1° fields as the first guess, so in data

sparse areas there is not much difference between the 1° and 0.25° fields. In comparison with 1° resolution data from WOA 2001, the 0.25° resolution analyses were able to better represent such features as the Gulf of Mexico Loop Current, and improved resolution in the Agulhas Retroflection and Gulf Stream (Boyer et al. 2005).

The Levitus climatologies are easily accessible and widely used traditional climatologies for the world ocean. However, it would be very difficult to create a smart climatology from the Levitus climatologies because of the limited number of observations for each grid-box, and because they are based long term means calculated from all data (regardless of year or century collected).

As part of the data analysis for this thesis, POCM 4C T and S fields are compared with objectively analyzed, 0.25° resolution, Levitus fields. Where possible, comparisons with MODAS and GDEM data are also done. However, because there is significant overlap between the MOODS and Levitus climatologies, and because one version of Levitus and POCM 4C share a common 0.25° resolution, Levitus climatology is the preferred source for observational LTM T and S in this thesis. Unless otherwise indicated, all future references to 'Levitus' are to the 0.25° resolution analysis from WOA 2001.

2. Reynolds SST

In order to compare POCM 4C simulation data from individual months or years with the observational data sets, the product commonly referred to as Reynolds SST will be used. This is currently available from the CDC website (www.cdc.noaa.gov, accessed September 2005) for weekly average fields, monthly average fields, as well as LTM

fields covering 1961-1990 and 1971-2000. The specific product name is Optimum Interpolation Sea Surface Temperature Version 2 (OI SST V2). This product merges satellite observations with in situ data, taking into account ice cover and satellite biases. Interpolation and bias correction methods are described in Reynolds et al. (2002). The spatial resolution of Reynolds SST is 1° x 1°, which is coarser than POCM 4C output, so only large scale comparisons will be made between POCM 4C and Reynolds SST. Despite its coarser resolution, Reynolds SST is a convenient and commonly used source of real world data against which model output can be compared.

3. Satellite Altimetry Data

As noted above, POCM 4C calculates SSH directly. Therefore, comparison with satellite altimeter derived SSH is very convenient. Satellite altimetry's main advantage over data from oceanographic cruises is global coverage. For our climatology study, the principal disadvantage is that data is only available since the early 1990s (Gould 2003), so any LTM will be from less than two decades of data. Although altimetry data from the GEOSAT mission in the mid 1980s is also available, this study will compare model fields with those readily available on the Aviso website (see below).

Altimetric radar instruments measure distance by the time it takes a signal to leave the satellite and return after reflecting off Earth's surface. Because the satellite is in a known orbit, an estimate can be made of SSH variation by computing the difference between the satellite's orbit and the change in distance. This difference accounts for Earth's geoid, long-term mean ocean

circulation, and shorter period oceanic anomalies (CNES 2005). The geoid is not globally well known on scales of tens of kilometers, so an average SSH is subtracted from altimeter SSH fields resulting in a sea level anomaly (SLA) field. See discussion of Aviso data below for more detail on such average SSH fields. A climatological mean height field, computed from historic or model T and S data, can be added back onto this anomaly field to include long term mean currents (see for example Strub and James 2000).

For POCM 4C SSH fields, a 20 year average of SSH can be calculated and subtracted from a field of interest to produce a POCM 4C SLA dataset. For this study, the twenty year average of a specific time period is used. For example, if one wanted the SLA field for March 1995 from POCM 4C, one would average the SSH data from all twenty Marches in the POCM 4C field. That average would be your LTM. Then the LTM would be subtracted from the March 1995 SSH data to yield the POCM 4C SLA. In equation form:

POCM 4C March 1995 SSHA =

$$\text{POCM 4C March 1995 SSH} - \langle \text{POCM 4C March}_{1979\text{-}98} \rangle$$

Aside from figures in the references, the main source of altimetry data for this research was the Aviso live access server website (http://las.aviso.oceanobs.com/las/, accessed June 2005) run by the French space agency, CNES. Aviso provides, among other products, a merged SLA field. That is a merged product (spatially and temporally) of data from the Topex/Poseidon, Jason, ERS-1/2, and Envisat altimeters. The delayed time merged product optimally interpolates the data spatially and temporally, providing

global coverage over the October 1992 to January 2005 timeframe (in 7-day or monthly increments) (CNES 2005).

The Aviso product gives SLA fields by subtracting a 3 year annual mean sea level from within its own data set. Therefore to compare with POCM 4C SSHA fields calculated as shown above, an additional step is required. For example, to compare the POCM 4C March 1995 SLA field with Aviso, we must first average all of the March fields available in Aviso (e.g. March 1993, March, 1994… March 2004), and subtract that from an Aviso March data field we wish to compare to POCM 4C. The Aviso data covers 1992-2005. So in equation form, an example of what would be compared to POCM SSHA is:

Aviso March 1995 SLA for comparison with POCM 4C =

Aviso March 1995 SLA - $\langle \text{Aviso SLA March}_{1992\text{-}2005} \rangle$

In this way, the average March signal as well as an annual mean is removed.

C. SMART CLIMATOLOGY ANALYSES

1. Northern Oscillation Index (NOI)

The NOI is a relatively new climate index that has been found to track well the effects of EN and LN on the northeast Pacific (Schwing et al. 2002a). The NOI is calculated by taking the difference between sea level pressure anomalies (SLPA) at the average position of the North Pacific High (NPH) off the west coast of North America and at Darwin, Australia. This is very similar to the Southern Oscillation Index (SOI) which tracks the difference in SLPA between Tahiti and Darwin. The SOI is one of many indices that have been used to track EN. During EN, as noted above, warm waters and associated convection move eastward from Darwin. Therefore, during EN, Darwin

tends to have a positive SLPA, while Tahiti has a negative SLPA. Thus during an EN, the SOI is a negative value (negative at Darwin minus positive at Tahiti) (Schwing et al 2002a).

Similarly, as also discussed above, during EN we expect a weakened NPH, causing a negative SLPA. Thus during EN the NOI should also be negative (positive during LN). The NOI has particular appeal for this study since the NPH is a major driver of the CCS. Schwing et al. (2002a) created the NOI, and in studying historical data they found that it is dominated by EN and LN events. They also found that the NOI and SOI were highly correlated, but that in 40% of "strong" NOI events (a large value of NOI in combination with EN/LN type variations in the northeast Pacific), the SOI was much smaller or even opposite in sign from the NOI. The NOI is calculated monthly, and is available for 1948-present from the NOAA Pacific Fisheries Environmental Lab website (www.pfel.noaa.gov/products/PFEL/modeled/indices/NOIx/noix.html cited August 2005).

2. Creation of EN and LN Composites

As mentioned in Chapter I, we primarily examine the November to March period. Table 1 below provides some basic statistics. We first averaged all NOI values in each complete November to March period available in the NOI time series. For example:

Nov 1948 - Mar 1949 Average NOI = (Nov 48 NOI + Dec 48 NOI + Jan 49 NOI + Feb 49 NOI + Mar 49 NOI)/5

Table 1. NOI November to March Long Term Character

Average November to March NOI (from November 1948 – March 1949 through November 2003 – March 2004)	-0.011 mb
Median November to March NOI	0.787 mb
Standard Deviation (over 56 year period)	2.6327 mb

Then we examined the 20 year POCM 4C time frame, 1979-1998. For different key variables (e.g., salinity, temperature, current), we averaged the values from the four November to March periods with the highest positive average NOI to form composites representative of LN winters, and with the lowest average NOI to form a composite representative of EN winters. The 4 most negative periods in 1979-1998 were all in the top 5 negative values for all November to March averages during 1948-2005. However, only one of the four most positive periods was among the top 10 positive November to March periods in the 1948-2004 timeframe. Therefore, our EN representation is a composite of several strong EN events; while our LN representation includes several relatively weak events (see tables 2-4).

Table 2. Ten most negative Nov-Mar Values During 1948-2004

November to March Period	NOI Value (mb)
1982	-8.291
1997	-6.6648
1977	-5.2068
1991	-4.5694
1994	-4.0388
1957	-3.6552
1979	-3.5722
1992	-3.2742
1968	-2.4828
1985	-2.4118
Note: years in bold are in NOI Based EN composite	

Table 3. Ten most positive NOI Nov-Mar Values During 1948-2004.

November to March Period	NOI Value (mb)
1952	2.1666
1949	2.238
1963	2.255
1971	2.6006
1970	2.8632
1954	3.0132
1948	3.1146
1988	3.3132
1998	3.4674
1975	4.2506
Note: years in bold are in NOI Based LN composite. 1998 refers to Nov 1998 – Mar 1999, and thus is not covered by POCM 4C	

Table 4. Nov-Mar Periods used for LN NOI Based Composite

November to March Period	NOI Value (mb)
1988	3.3132
1987	2.0036
1984	1.5774
1989	1.2282

D. OVERALL METHODOLOGY

In summary, the twenty year average of all variables from November to March for the years in POCM 4C serve as a LTM in this study. For example, the LTM salinity is taken as:

POCM 4C Nov-Mar LTM Salinity =

(<POCM 4C Salinity Nov 79 – Mar 80> +

<POCM 4C Salinity Nov 80 – Mar 81> + … + <POCM 4C Salinity Nov 97 – Mar 98> +

<POCM 4C Salinity Jan-Mar 79 and Nov 98-Dec 98>)/20

Note that the Jan-Mar 1979 and Nov-Dec 98 time periods are included to yield 20 distinct Nov-Mar periods for calculating LTMs. Unless otherwise specified, references below (in Chapter III and Chapter IV) to any POCM 4C LTM are the averages of all 19 continuous November to March periods from 1979-1998, with January-March of 1979 and November-December of 1998 combined to provide a 20^{th} November to March period. Each POCM 4C LTM is compared to a November to March LTM from both Levitus and Aviso data. EN and LN composites, based on the NOI, are constructed from POCM 4C as specified above. The POCM 4C LTM, EN, and LN composites are compared to identify distinct trends and mechanisms for the differences between EN, LN, and LTM states of the CCS. The EN and LN composites are also compared against the Levitus and Aviso LTMs to see if the same trends are observed. Finally, the EN and LN composites are compared against the results from prior studies (see Chapter I) to determine how representative the model is of observed conditions.

III. RESULTS

A. POCM 4C CCS LTM TRENDS

Initial work was done to find possible systematic biases in POCM 4C and assess how well the POCM 4C LTM fields match observations. Many comparisons of surface features such as SST, SSH, surface salinity, and surface currents, are shown in this chapter. Selected depth-longitude and depth-latitude cross-sections are also shown. Prior experience with POCM 4C has shown that the surface forcing in the model retains too much heat. Therefore the average of the model's upper two vertical levels, representing the upper 50 m of the ocean, is used surface conditions (Tokmakian, personal communication).

1. Large-scale Structure

Hickey (1998) estimated large-scale seasonal variations in the surface currents of the CCS based on a synthesis of past observations. These are compared to POCM 4C surface current streamlines in the figures below (compare also with Figure 2 in Chapter I).

a. Winter

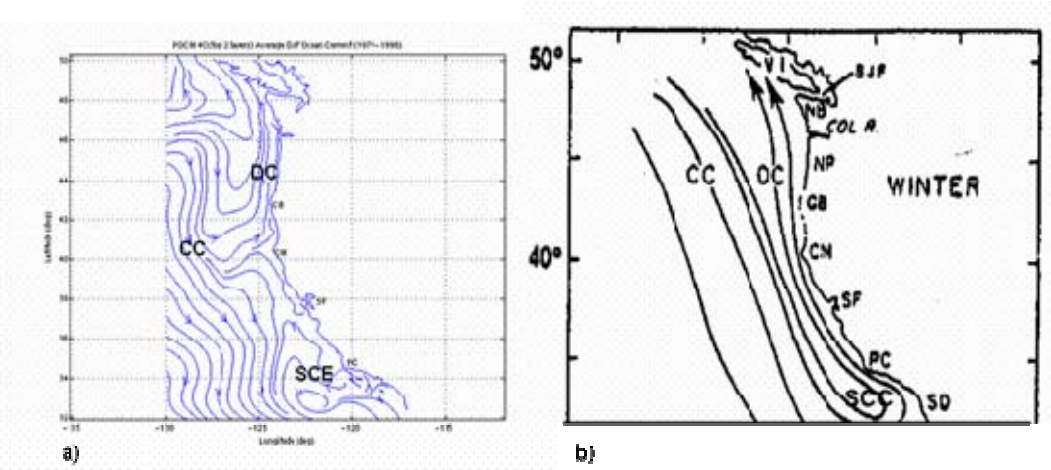

Figure 15. Winter Surface Current Streamlines: (a) POCM 4C LTM; (b) Schematic From Hickey (1998)

Figure 15a shows the POCM 4C 20 year average of December, January, and February (DJF) surface current streamlines. The 20 winters in this average are December 1979-February 1980 through December 1997–February 1998 (19 winters) plus a constructed winter, January-February 1979 combined with December 1998. Figure 15b is from Hickey (1998). We see that POCM 4C does simulate the DC. However, POCM 4C has a distinct SCE rather than a SCC (see Chapter I), and poleward flow is not distinct or continuous along the coast from Point Conception to Cape Mendocino in POCM 4C.

b. Spring

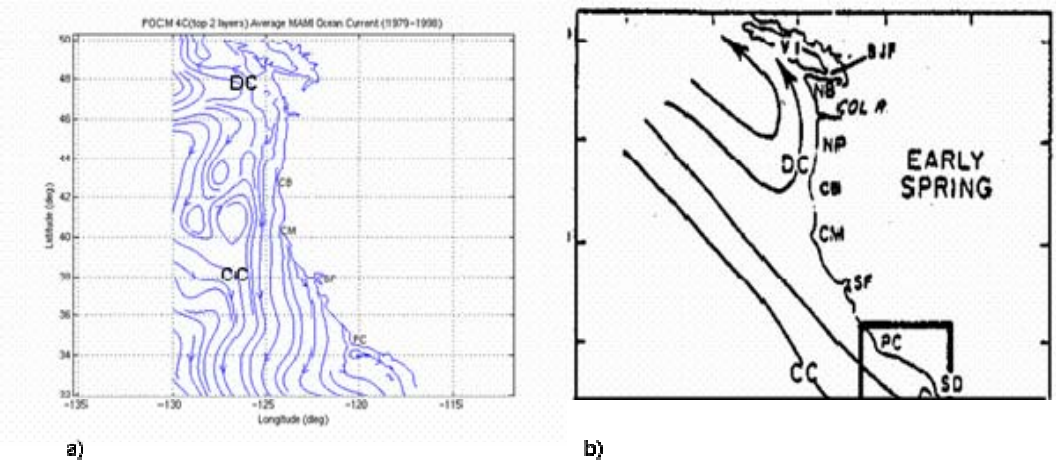

Figure 16. Spring Surface Current Streamlines: (a) POCM 4C LTM; (b) Schematic From Hickey (1998)

Figure 16a shows the POCM 4C 20 year average of March, April, and May (MAM). Figure 16b is from Hickey (1998). We see that the POCM 4C LTM Spring shows strong equatorward flow all along the coast from the Columbia River south. Note that 'Early Spring' in Figure 16b refers to March-April (Hickey, personal communication). POCM 4C places the surface DC further north in spring than in Hickey (1998).

c. Summer

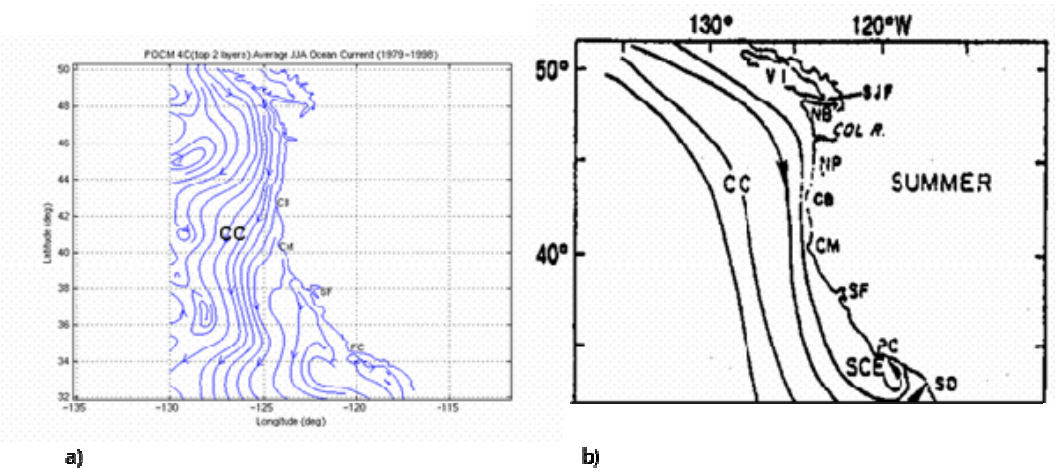

Figure 17. Summer Surface Current Streamlines: (a) POCM 4C LTM; (b) Schematic From Hickey (1998)

Figure 17a is the POCM 4C 20 year average of June, July, and August (JJA). Figure 17b is from Hickey (1998). We see that the POCM 4C summer is in broad agreement with Hickey (1998). Surface flow is equatorward all along the coast, although POCM 4C does not simulate a distinct SCE.

d. Fall

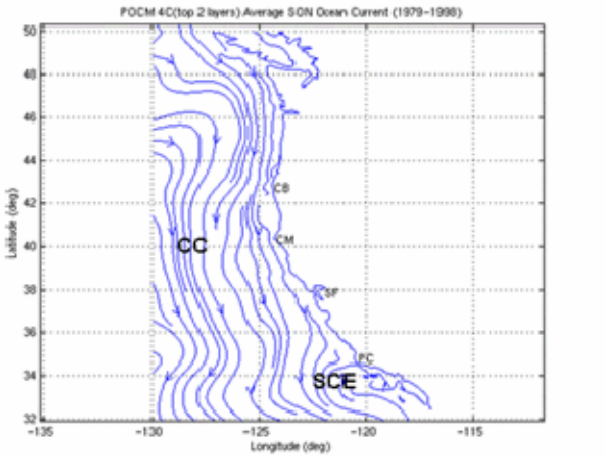

Figure 18. Fall Surface Current Streamlines: POCM 4C LTM

No schematic fall current diagram was available from Hickey (1998). However, note that the POCM 4C fall shown in Figure 18 defined by the 1979-1998 September-November average (SON), is more similar to the POCM 4C JJA pattern (Figure 17) than with the POCM 4C DJF pattern (Figure 15). Therefore the transition to the winter current pattern with poleward DC present along the coast does occurs very late in the year of the model simulation. POCM 4C does show a SCE but does not simulate distinct poleward flow anywhere along the coast, which observations show in the transition to winter.

1. Current Strength/Position and SSH

a. Winter

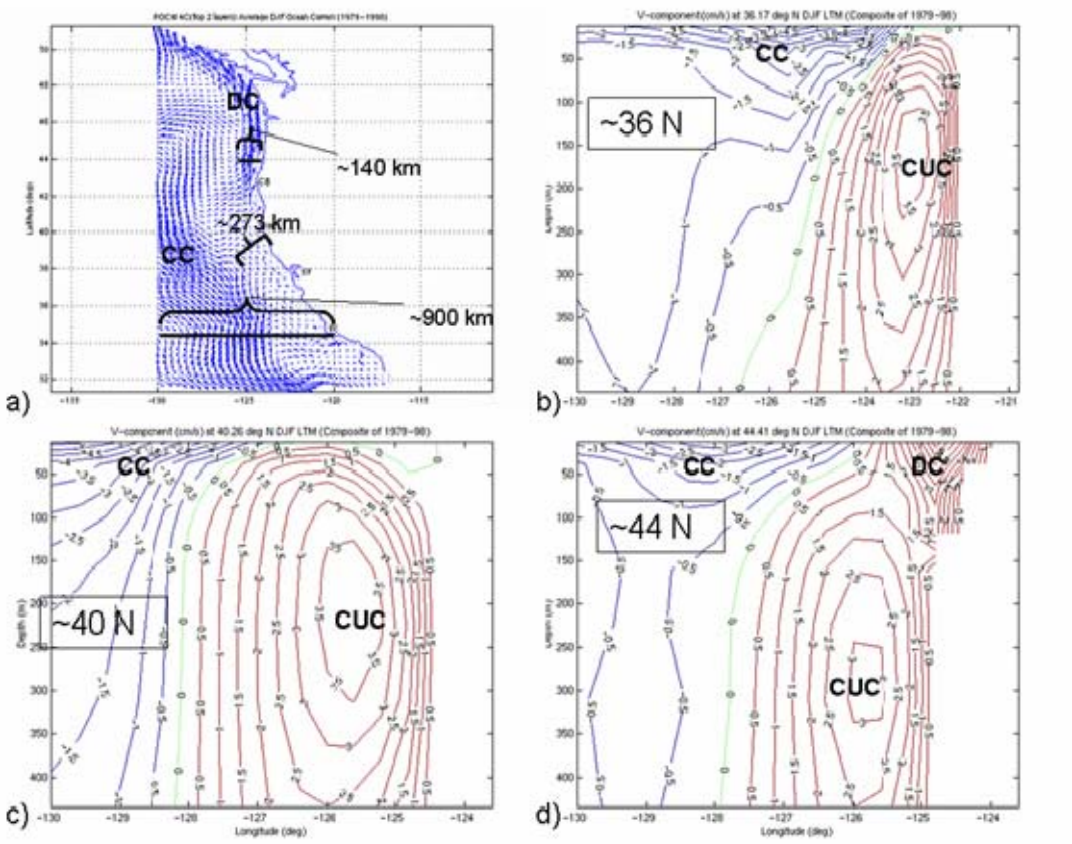

Figure 19. DJF LTM Winter Currents in POCM 4C: (a) Surface Current Vectors; (b) Depth-Longitude Cross-section along 36° N; (c) Depth-Longitude Cross-section along 40° N; (d) Depth-Longitude Cross-section along 44° N

Figure 19a shows a surface depiction of the DJF POCM 4C LTM CCS. Figure 19b-d show east-west cross-sections, to approximately 500 m depth, of the CCS at 36° N, 40° N, and 44° N respectively. The shoreline/bottom is indicated on the right hand side of these figures where no contours are drawn. Red contours correspond to a positive v-component of velocity (poleward) while blue contours are

negative (equatorward), with green contours showing zero v-component. These three lines of latitude were chosen to examine the coastal area from south of San Francisco to mid-Oregon and show three distinct and separate sections across the CCS, as this is an area of strong seasonal variability in the CCS. The geographic views seen here will be repeated for T and S comparisons, and also for November to March LTM, EN, and LN comparisons.

At 36° N, the weak equatorward flow dominates the surface within 200-300 km of the coast. This flow is contiguous with the main CC, the core of which is approximately 360 km offshore with maximum speed of about 5 cm/s equatorward. The CUC is distinct, lying very close to the surface, centered about 140 km offshore and at approximately 140 m depth with a maximum poleward speed of 3.5 cm/s. The DC is not present.

Moving north to 40° N, the core of the CC moves farther offshore to approximately 540 km, and increases slightly in equatorward speed. The poleward CUC again appears close to the surface, but there is no distinct DC. The CUC has broadened, and the core has deepened to about 250 m.

At 44° N, POCM 4C simulates a DC that extends about 160 km from the coast, and has relatively strong poleward flow of about 6 cm/s. A weaker CUC, with maximum speed of 3 cm/s and centered at approximately 300 m, is simulated within 200 km of the coast. The CC equatorward flow is centered about 200 km offshore and is weak, at 3 cm/s.

b. Spring

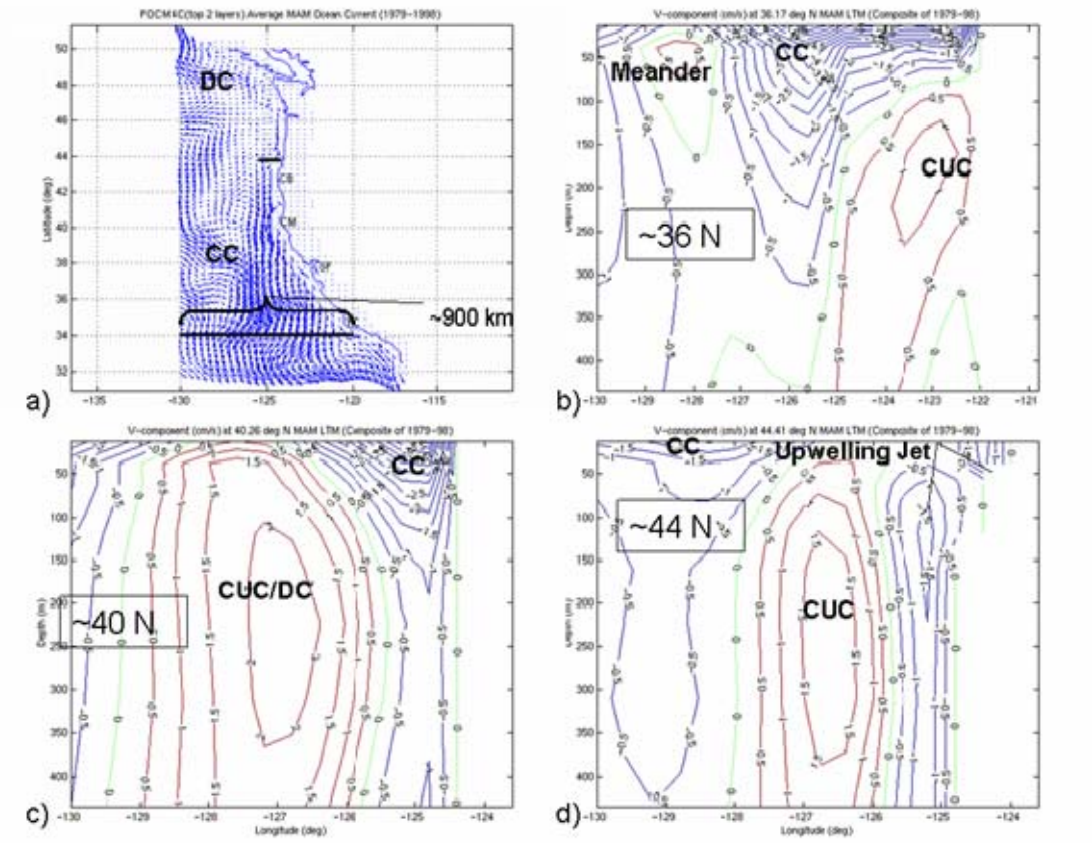

Figure 20. MAM LTM Spring Currents in POCM 4C: (a) Surface Current Vectors; (b) Depth-Longitude Cross-section along 36° N; (c) Depth-Longitude Cross-section along 40° N; (d) Depth-Longitude Cross-section along 44° N

The spring (March-May) transition is apparent in Figure 20. Figure 20a is a surface depiction of POCM 4C LTM MAM currents. Figure 20b-d are as in the previous figure, cross-sections of POCM 4C current at approximately 36° N, 40° N, and 44° N respectively. Figure 20a shows that the DC has disappeared from the California-Oregon-Washington coast. At 36° N, when compared to winter, the core of the equatorward flow of the CC has moved inshore approximately 50 km, and strengthened to about 7 cm/s. The CUC is still centered at about 140 m depth, but has weakened substantially and spans a much smaller depth range than it does in winter.

At 40° N, the strongest equatorward flow in the CC has moved inshore substantially from the winter season to about 270 km, although the speed is about the same as for winter. The CUC has weakened and moved further offshore.

At 44° N, an equatorward upwelling jet close to the coast is simulated, although the speed is very low at 2 cm/s. Further out to sea, at approximately 129° W, there is weak equatorward flow corresponding to the NPC feeding into the CC. The CUC has weakened and moved farther offshore than in winter.

c. Summer

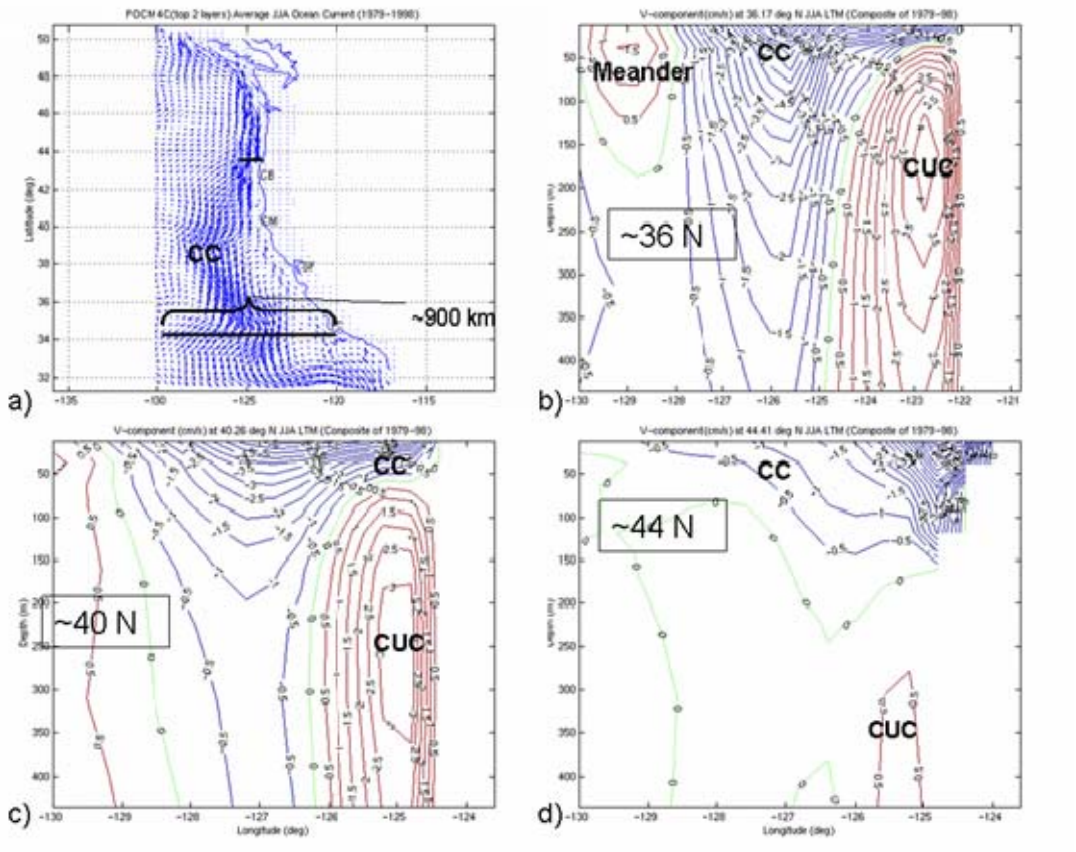

Figure 21. JJA LTM Summer Currents in POCM 4C: (a) Surface Current Vectors; (b) Depth-Longitude Cross-section along 36° N; (c) Depth-Longitude Cross-section along 40° N; (d) Depth-Longitude Cross-section along 44° N

Figure 21 follows the pattern of the previous two figures. Panel a shows LTM POCM 4C surface currents in JJA, while panels b-d show cross sections of POCM 4C JJA current at approximately 36° N, 40° N, and 44° N respectively. In summer, POCM 4C simulates a stronger CC than in the preceding seasons shown all along the California-Oregon-Washington coast. Notably, no DC is seen. At 36° N, an almost 10 cm/s equatorward CC core is seen approximately 360 km offshore. The vertical extent of the CC is larger as well. A stronger CUC immediately adjacent to the coast is

also apparent, with a core speed of about 4 cm/s centered at around 150 m depth.

This pattern continues at 40° N. All flow in the upper 100 m of this cross-section is equatorward, corresponding to the CC. The core speed of the CC is about 6 cm/s. The CUC at 40 N has moved adjacent to the shore and is slightly stronger than what is seen in spring.

At 44° N the CC/upwelling jet has also strengthened to close to 10 cm/s. The strongest flow is within 100 km of the coast. The CUC has mostly disappeared, although a weak poleward flow centered at 350 m depth is seen.

d. Fall

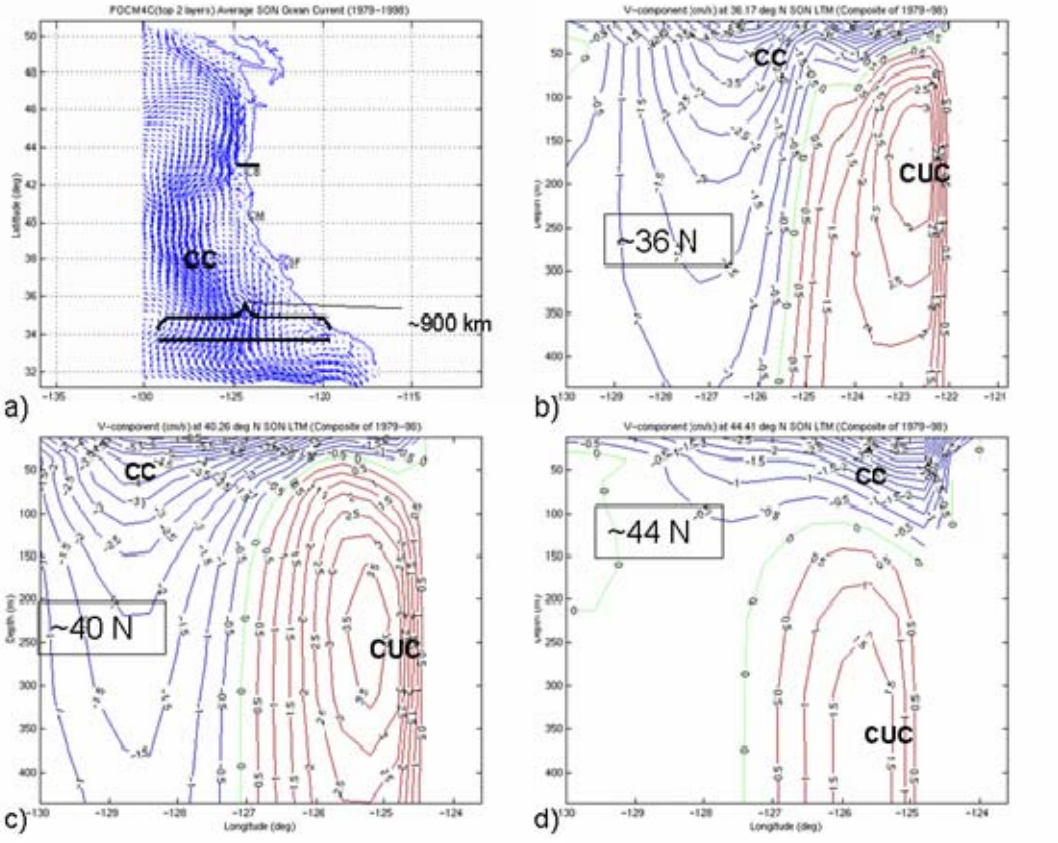

Figure 22. SON LTM Fall Currents in POCM 4C: (a) Surface Current Vectors; (b) Depth-Longitude Cross-section along 36° N; (c) Depth-Longitude Cross-section along 40° N; (d) Depth-Longitude Cross-section along 44° N

Following the format of the previous 3 figures, Figure 22a depicts POCM 4C LTM surface currents for SON. Panels b-d show cross-sections at approximately 36° N, 40° N, and 44° N respectively. The fall pattern largely follows that of summer. At 36° N the CC and CUC are in approximately the same positions as for summer, but both have weakened by about 30% from the summer values.

At 40° N, the CUC shoals toward the surface. It also has increased slightly in speed. The horizontal extent of the CC is the same as for summer, although the largest

equatorward speeds have moved several hundred kilometers offshore.

At 44° N, the CUC is more distinct than seen in summer. The CC/upwelling jet is immediately adjacent to the coast. However the CC core speed is slightly weaker than the summer LTM and is simulated slightly further offshore.

e. SSH

To make further large scale comparisons of current strength and position to observational data, SSH fields were examined. Strub and James (2000) produced bimonthly LTM SSH fields for the general region of the CCS. These fields were calculated from 6 years of satellite altimeter height anomalies and tide gauge heights. Additionally, a mean annual dynamic height field based on Levitus (WOA 2001, 0.25° horizontal resolution) data was added to include the mean circulation (Strub and James 2000). POCM 4C SSH is not referenced to the annual mean field that the Strub and James figures are and therefore, the gradient of SSH is compared, and the apparent location of currents.

Because POCM 4C and observations show similar currents in somewhat different locations, direct comparisons were of limited value. Instead, comparisons were made of dynamically similar portions of the CCS. For example, the SSH gradient at the location where the NPC feeds into the CC in POCM 4C is compared with the same feature in altimetry fields, even if the geographic coordinates are not exactly the same.

This procedure involves subjective selection of comparison locations in each field. Where possible, the strengths of the NPC, DC, and CC were examined, as

represented by the direct link between SSH gradient and geostrophic current. Table 5 below summarizes the results. Note that for ease of comparison, the SSH gradient is shown as:

SSH = 100 *(SSH change along sample line (cm))/range (km).

Figures 23-28 show the patterns for each bimonthly period. The analysis procedure involved looking at three separate figures for each period. The POCM 4C surface depiction of currents was examined to determine the apparent location of the CC. The approximate boundaries of the CC from that figure were then transferred onto contour plots of SSH from both POCM 4C and Strub and James (2000). A visual comparison of POCM 4C CC boundaries and regions of large SSH gradients in POCM 4C with regions of large SSH gradients in the Strub and James figures was made and allowed for a characterization of POCM 4C current placement. SSH gradients were calculated from SSH contour plots. For brevity, only the SSH contour plots, with lines indicating the CC, are shown with SSH gradient calculations also illustrated. Panel a in the figures is from the POCM 4C LTM, while panel b is from Strub and James (2000).

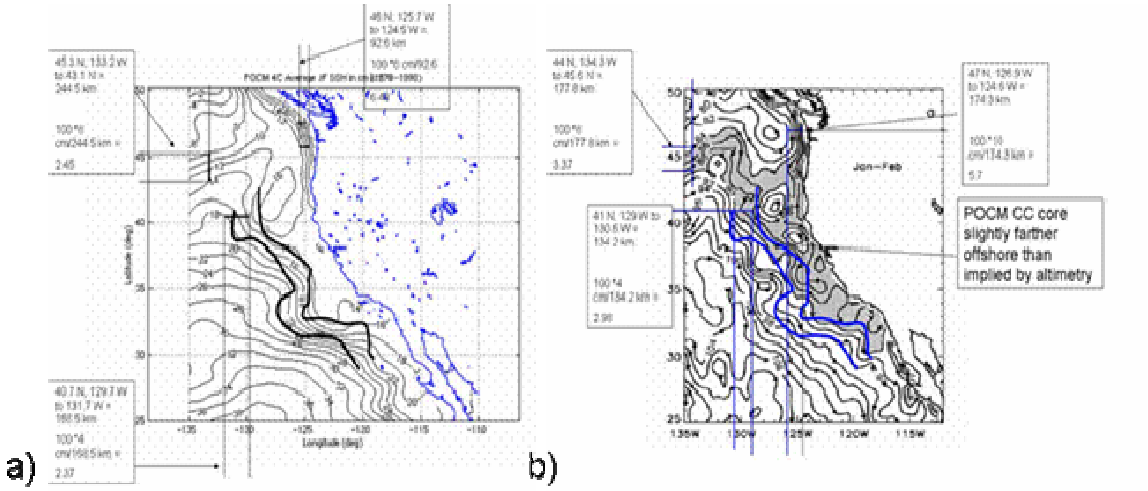

Figure 23. January-February SSH Fields: (a) POCM 4C; (b) From Strub and James (2000)

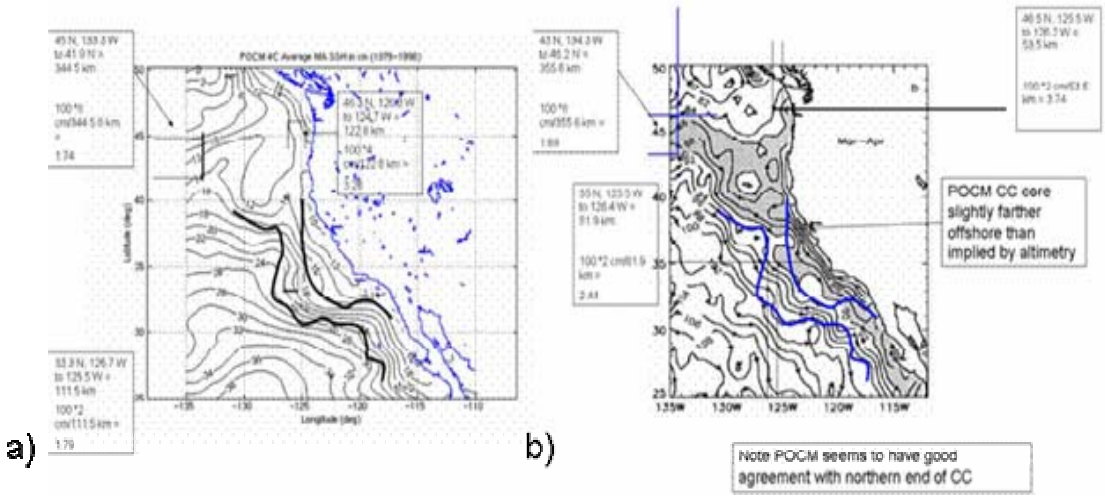

Figure 24. March-April SSH Fields: (a) POCM 4C; (b) From Strub and James (2000)

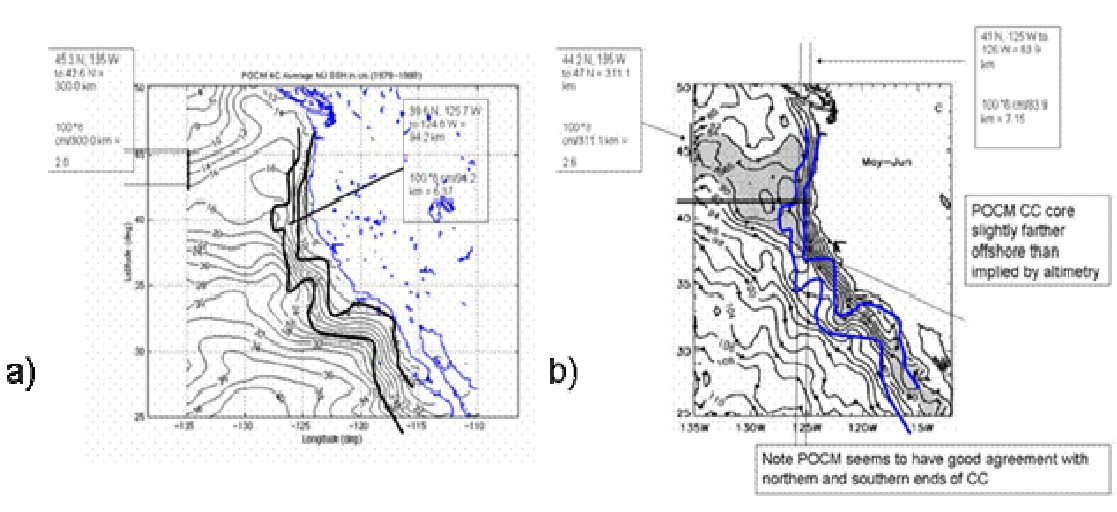

Figure 25. May-June SSH Fields:
(a) POCM 4C; (b) From Strub and James (2000)

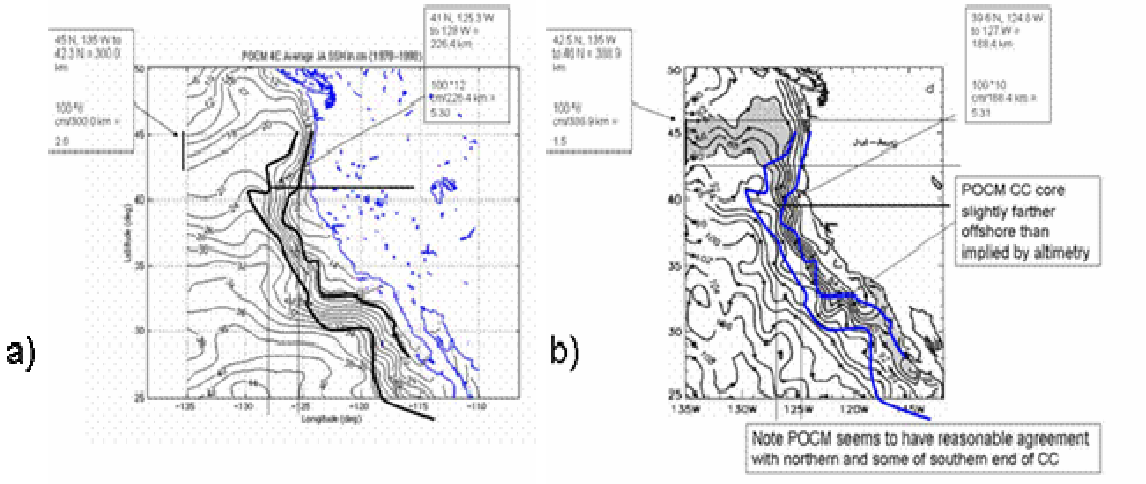

Figure 26. July-August SSH Fields:
(a) POCM 4C; (b) From Strub and James (2000)

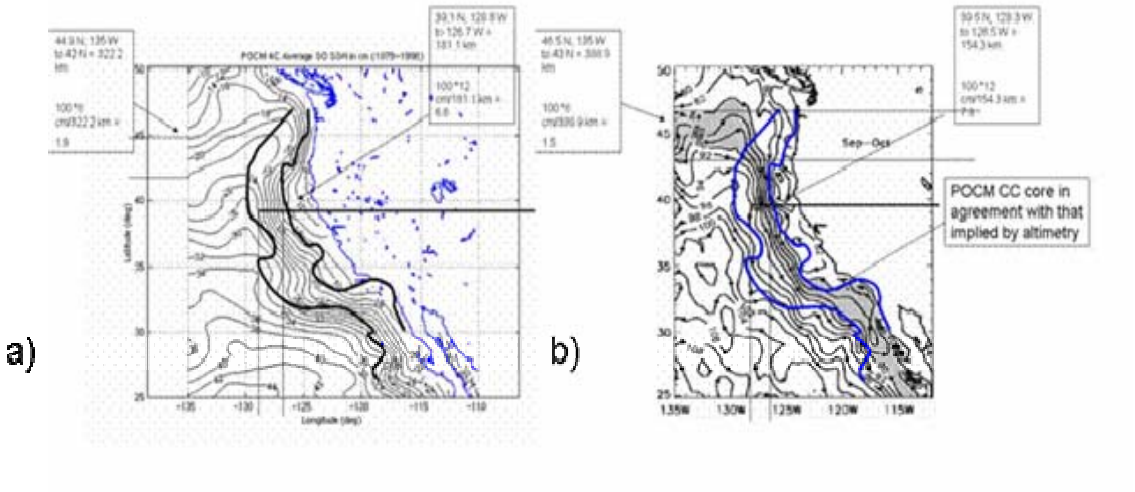

Figure 27. September-October SSH Fields: (a) POCM 4C; (b) From Strub and James (2000)

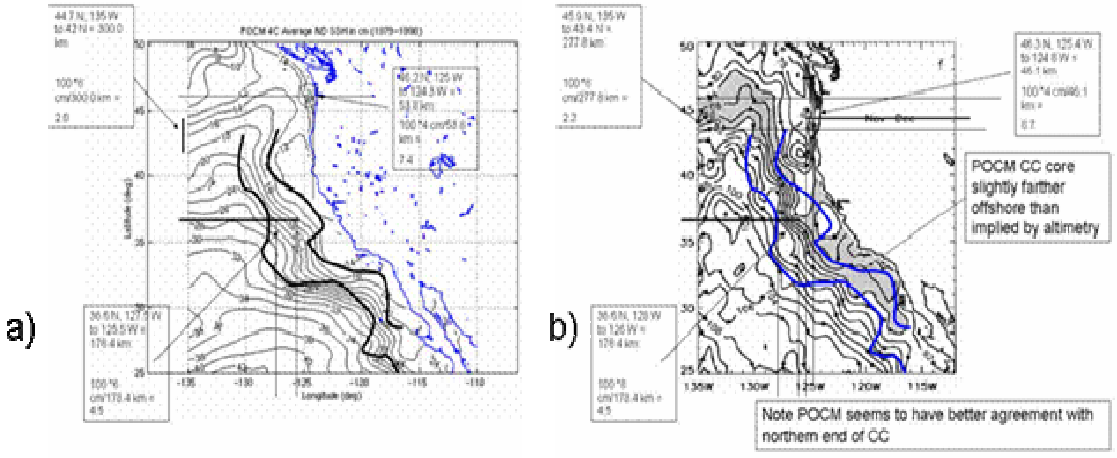

Figure 28. November-December SSH Fields: (a) POCM 4C; (b) From Strub and James (2000)

Table 5. Comparison of POCM 4C and Satellite Altimetry derived SSH

Height Gradient Comparisons						
	Jan-Feb	Mar-Apr	May-Jun	Jul-Aug	Sep-Oct	Nov-Dec
NPC from Altimetry (100*cm/km)	3.4	1.7	2.6	1.5	1.5	2.2
NPC from POCM (100*cm/km)	2.5	1.7	2.0	2.0	1.9	2.0
Anomaly (POCM NPC Gradient - Altimetry NPC Gradient) (100*cm/km)	-0.9	0.0	-0.6	0.5	0.4	-0.2
% Difference ((POCM-Altimetry)/Altimetry)	-26.5	0.0	-23.1	33.3	26.7	-9.1
DC from Altimetry (100*cm/km)	5.7	3.7	N/A	N/A	N/A	8.7
DC from POCM (100*cm/km)	6.5	3.3	N/A	N/A	N/A	7.4
Anomaly (POCM DC Gradient - Altimetry DC Gradient) (100*cm/km)	0.8	-0.4	N/A	N/A	N/A	-1.3
% Difference ((POCM-Altimetry)/Altimetry)	14.0	-10.8	N/A	N/A	N/A	-14.9
CC from Altimetry (100*cm/km)	3.0	2.4	7.2	5.3	7.8	4.5
CC from POCM (100*cm/km)	2.4	1.8	6.4	5.3	6.6	3.4
Anomaly (POCM CC Gradient - Altimetry CC Gradient) (100*cm/km)	-0.6	-0.6	-0.8	0.0	-1.2	-1.1
% Difference ((POCM-Altimetry)/Altimetry)	-20.0	-25.0	-11.1	0.0	-15.4	-24.4

Figures 23-28 and Table 5 indicate that POCM 4C generally simulates a weaker CC and a weaker DC than what is indicated by altimetry. Additionally, from January to June POCM 4C seems to simulate the CC further offshore than expected from altimetry. The POCM 4C CC strength best matches altimetry in periods when no DC is present (i.e. late spring-early fall). The NPC in POCM 4C is stronger than that represented in the Strub and James figures for late summer-early fall, and is weaker in winter-early summer. Overall, the simulation of the CCS by POCM 4C is

realistic and the seasonal variability seen within POCM 4C is similar to that seen in observations.

2. Water Mass Characteristics

Figures 29-43 show the POCM 4C seasonal LTM values of temperature and salinity along with seasonal averages from the 0.25° resolution WOA 2001. Temperature plots are in the top row of the figures, while salinity is in the bottom row. POCM 4C data is on the left hand side while WOA 2001 data is shown on the right. The seasons are DJF, MAM, JJA, and SON. The POCM 4C LTM shown is the 20 year average of each season (i.e., (MAM 1979 + MAM 1980 + … + MAM 1998)/20). Some limited comparisons with GDEM data were also done, but as no major differences were seen between GDEM and WOA 2001 plots, the GDEM plots are not included here.

a. Winter

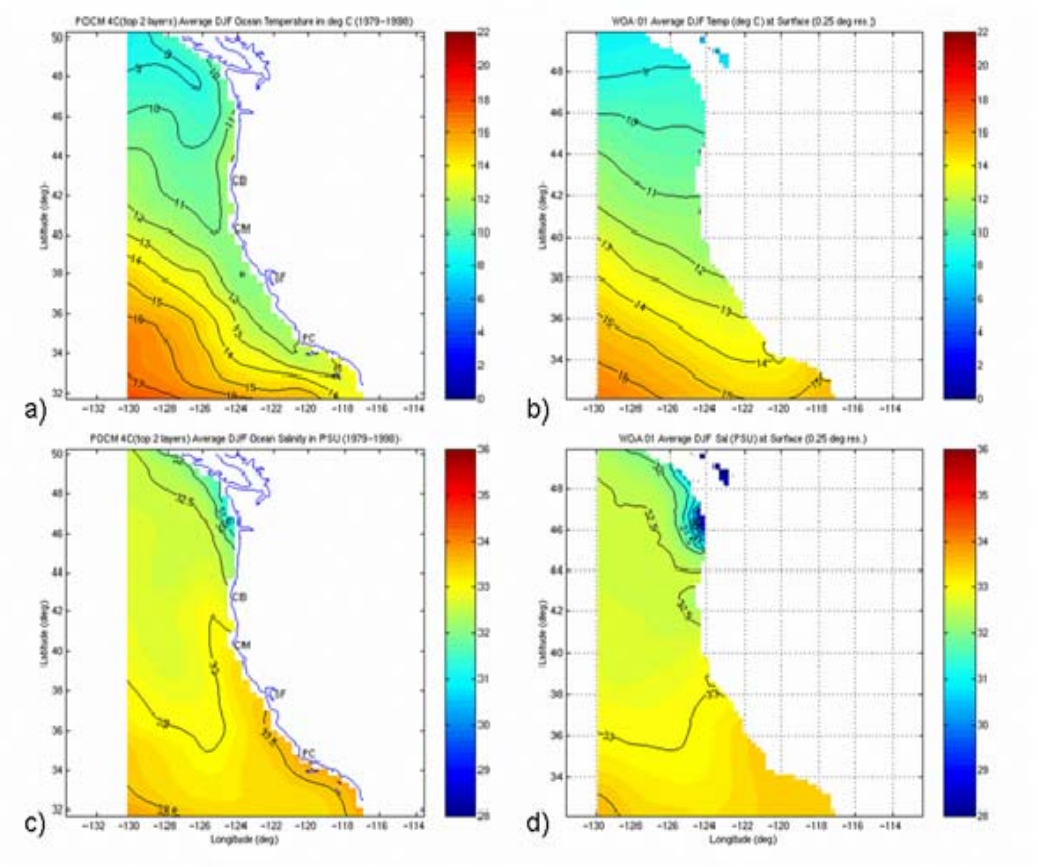

Figure 29. DJF Winter SST and Surface Salinity: (a) POCM 4C SST (°C); (b) Levitus SST (°C); (c) POCM 4C Surface Salinity (PSU); (d) Levitus Surface Salinity (PSU)

Figure 29 illustrates a common feature of the POCM 4C LTMs in all 4 seasons: POCM 4C values are broadly consistent with observations, although SST is generally cooler off the Canadian and California coasts in POCM 4C than in WOA 2001 (Levitus), and is warmer to the southwest of the CCS area of interest. The outflow of fresh water from the Columbia River is seen more strongly in WOA 2001 data than in POCM 4C. Also POCM 4C is distinctly saltier than WOA 2001 along the California coast from south of San Francisco to the vicinity of Cape Blanco.

Figures 30-32 show comparisons cross-sections to about 500 m depth. Again, POCM 4C temperature is in panel a, WOA 2001 temperature is panel b, POCM 4C salinity is panel C, and WOA 2001 salinity is panel d. No interpolation was done in POCM 4C so that the 36.01° N in POCM 4C is compared to 36° N from WOA 2001, 40.11° N with 40° N, and 44.27° N with 44° N. Slight coastline differences can be seen in some figures.

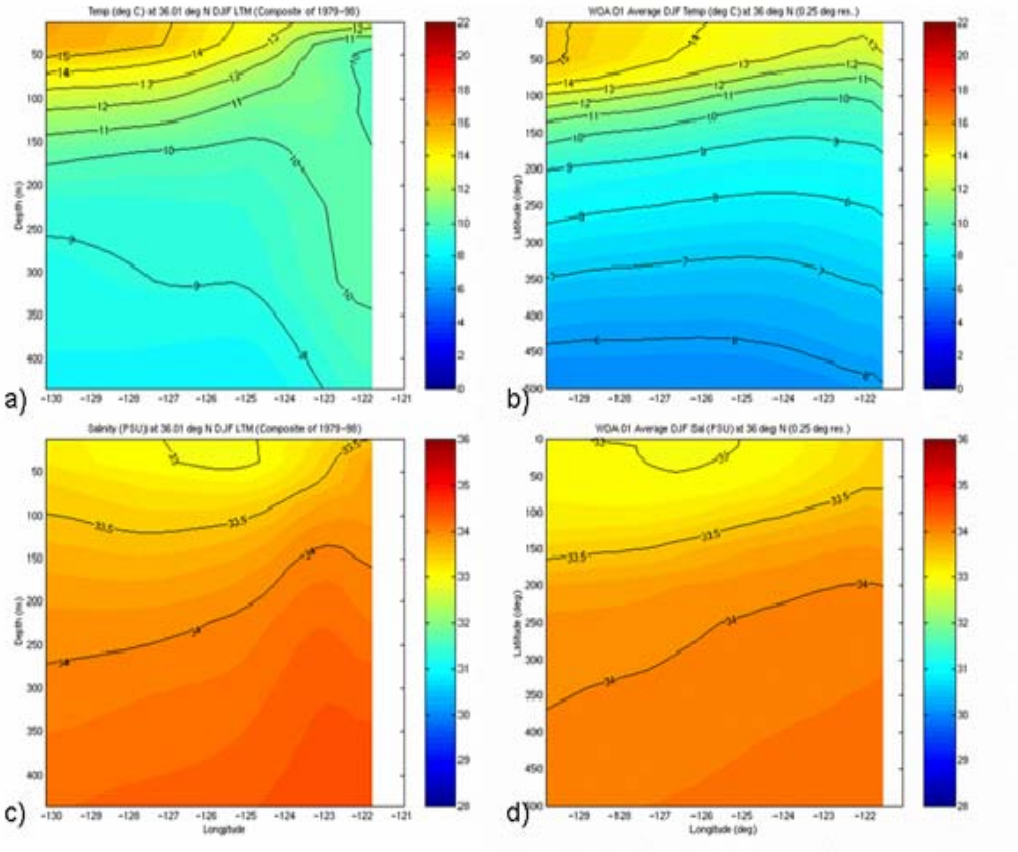

Figure 30. DJF Winter Depth-Longitude Cross-sections at 36° N: (a) POCM 4C Temperature (°C); (b) Levitus Temperature (°C); (c) POCM 4C Salinity (PSU); (d) Levitus Salinity (PSU)

Figure 30 shows some distinct features. Near the coast close to the surface POCM 4C is both colder and saltier than WOA 2001. This implies the model is resolving more upwelling or less downwelling than what is implied in

LTM observations. This is consistent with not having a DC during winter at 36° N. Also POCM 4C is warmer than WOA 2001 between about 200-500 m. This appears to be a systematic bias at 36° N, 40° N, and 44° N for all seasons as can be seen in Figures 30-32, 34-35, and 37-39, and 41-43. POCM 4C also seems to have a systematic salty bias in the upper 500 m compared to WOA 2001 data.

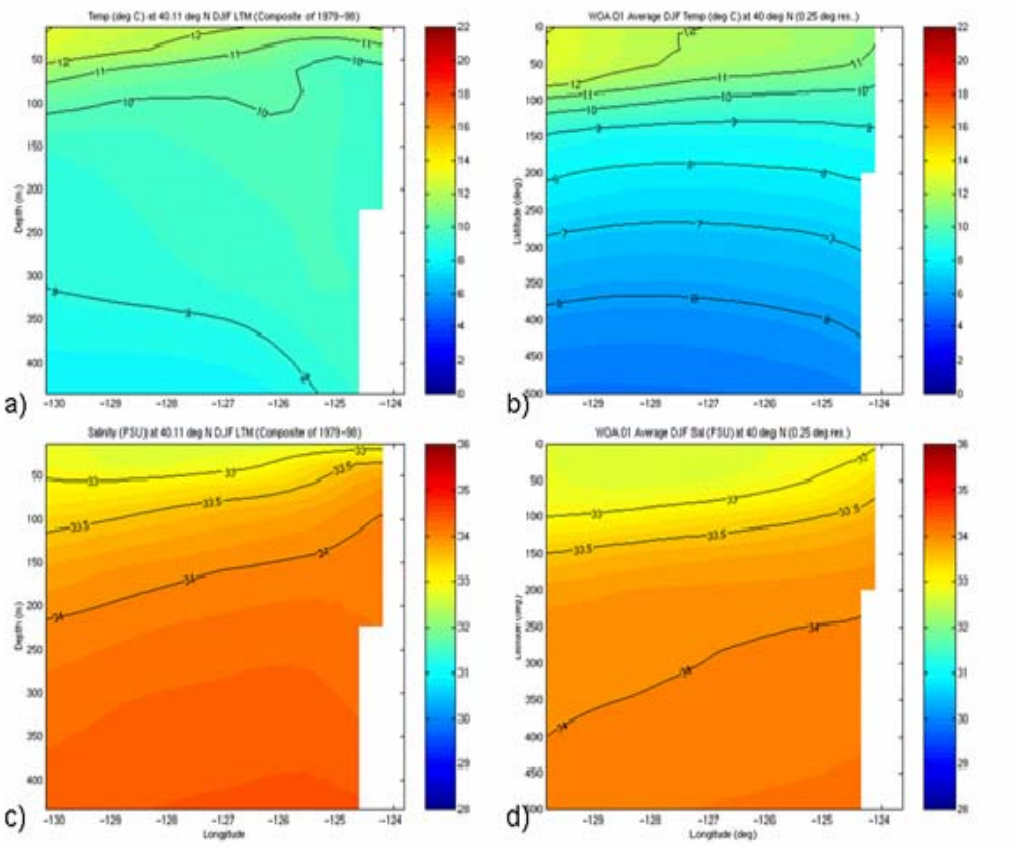

Figure 31. DJF Winter Depth-Longitude Cross-sections at 40° N: (a) POCM 4C Temperature (°C); (b) Levitus Temperature (°C); (c) POCM 4C Salinity (PSU); (d) Levitus Salinity (PSU)

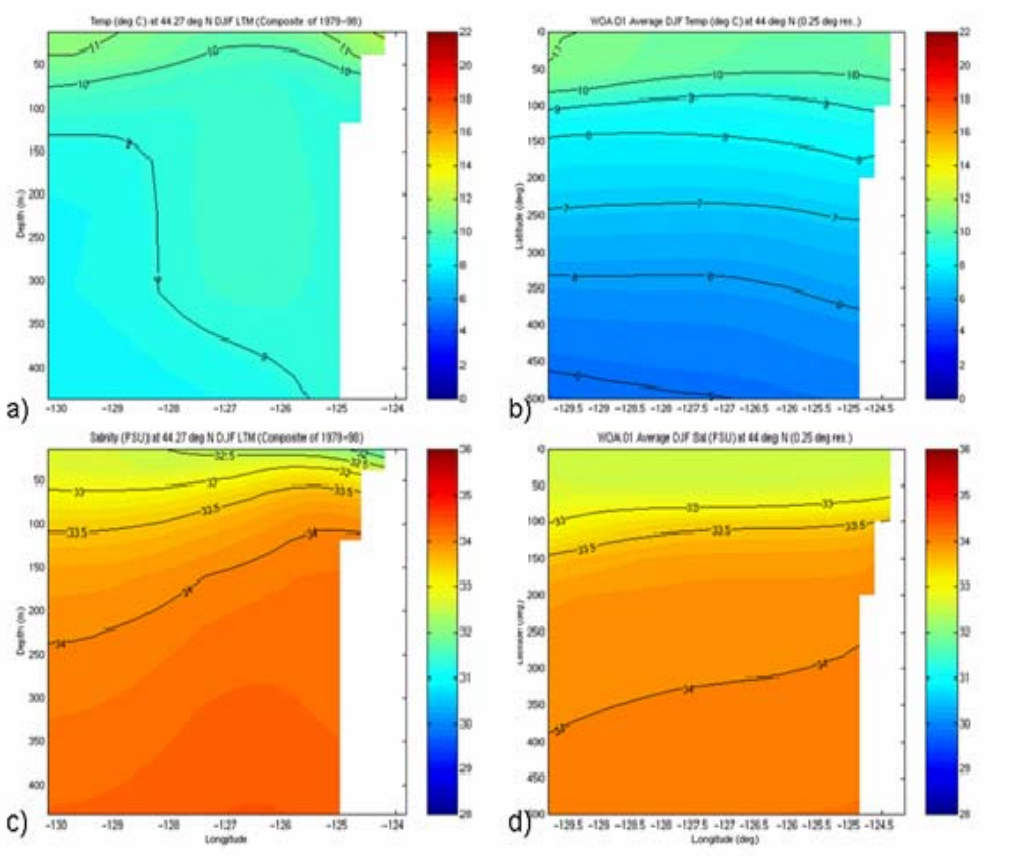

Figure 32. DJF Winter Depth-Longitude Cross-sections at 44° N: (a) POCM 4C Temperature (°C); (b) Levitus Temperature (°C); (c) POCM 4C Salinity (PSU); (d) Levitus Salinity (PSU)

Figure 32a shows POCM 4C with warmer and fresher water than that seen in WOA 2001 data close to the coast. This corresponds with the DC being present in POCM 4C at this latitude.

b. Spring

The same general trends seen for POCM 4C winter apply in spring. The spring transition is indicated in Figure 34 and Figure 35 by isotherms and isohalines that slope upward toward the coast, indicating enhanced upwelling of cold salty water.

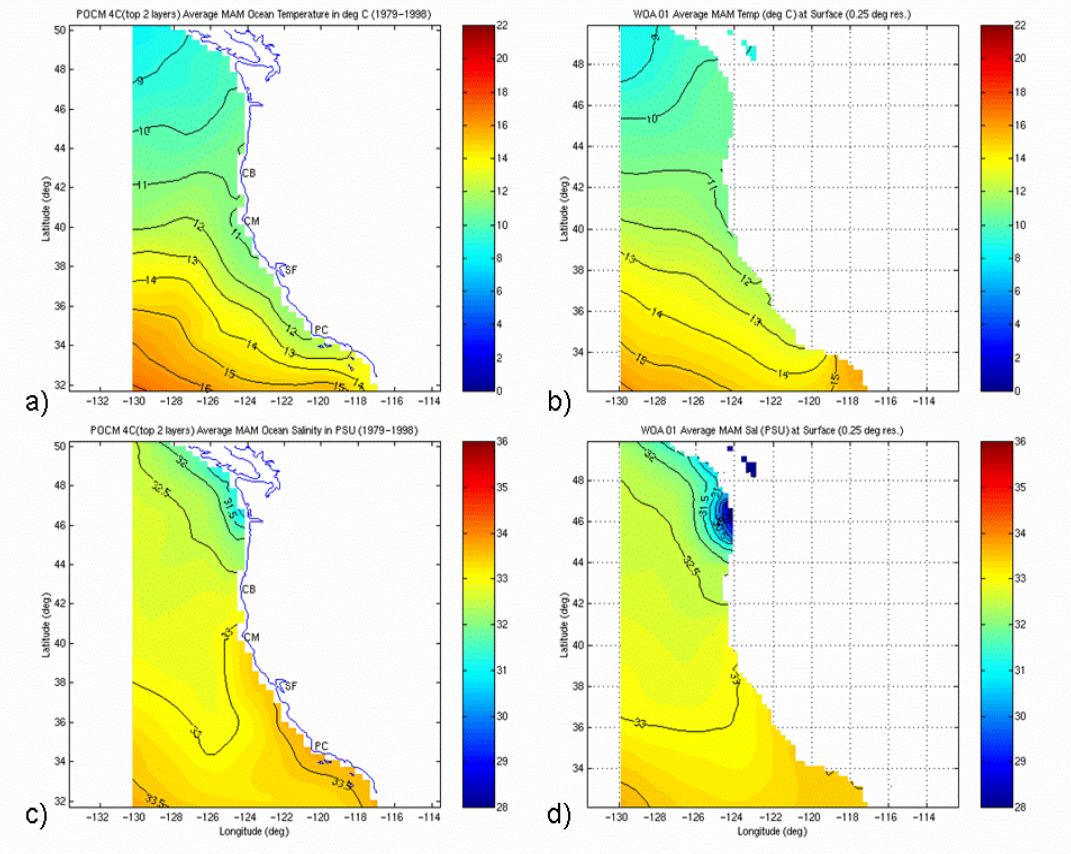

Figure 33. MAM Spring SST and Surface Salinity: (a) POCM 4C SST (°C); (b) Levitus SST (°C); (c) POCM 4C Surface Salinity (PSU); (d) Levitus Surface Salinity (PSU)

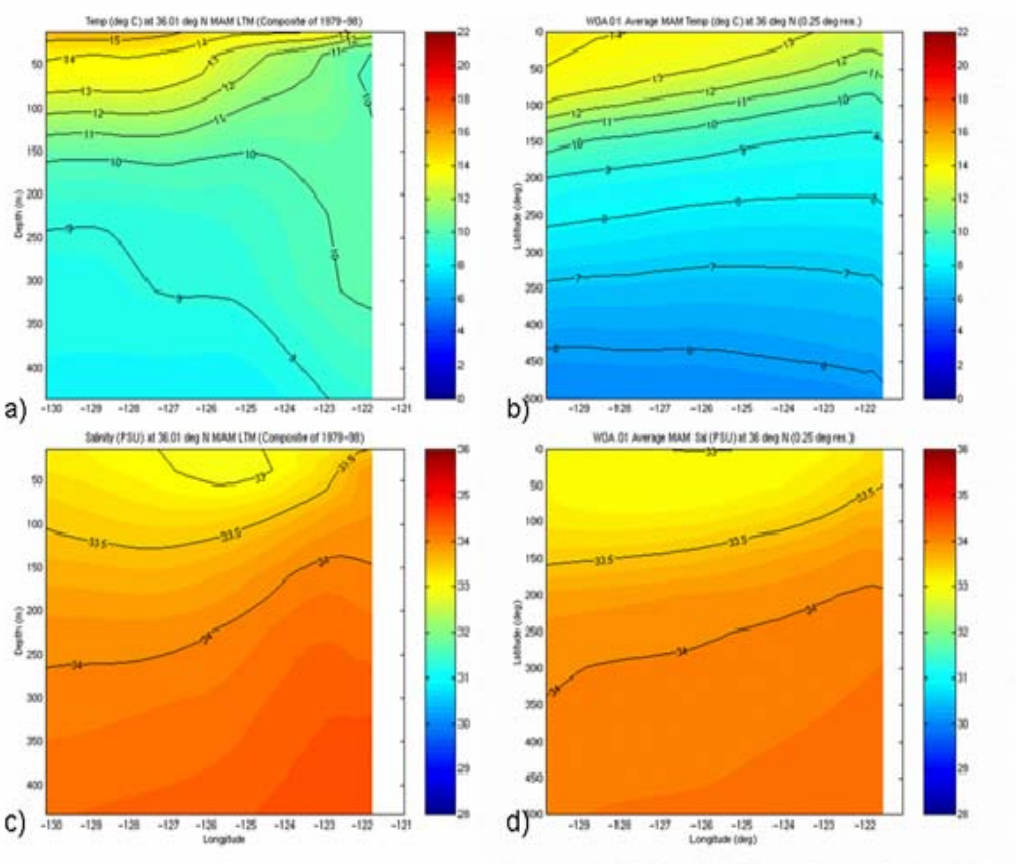

Figure 34. MAM Spring Depth-Longitude Cross-sections at 36° N: (a) POCM 4C Temperature (°C); (b) Levitus Temperature (°C); (c) POCM 4C Salinity (PSU); (d) Levitus Salinity (PSU)

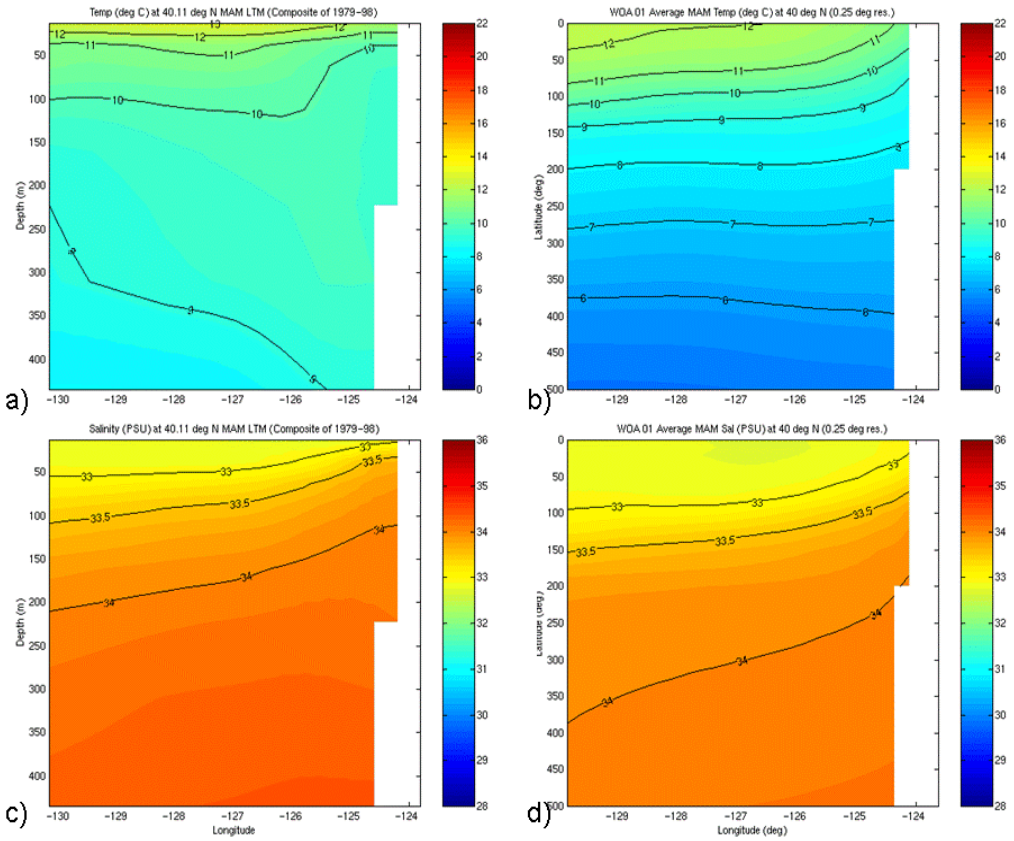

Figure 35. MAM Spring Depth-Longitude Cross-sections at 40° N: (a) POCM 4C Temperature (°C); (b) Levitus Temperature (°C); (c) POCM 4C Salinity (PSU); (d) Levitus Salinity (PSU)

a. Summer

Summer in POCM 4C shows similar patterns to winter and spring (see Figures 29-35). However, the cool bias in POCM 4C along the coast is more pronounced than in other seasons, as is the warm bias in the southwest of the area shown (see Figure 36a).

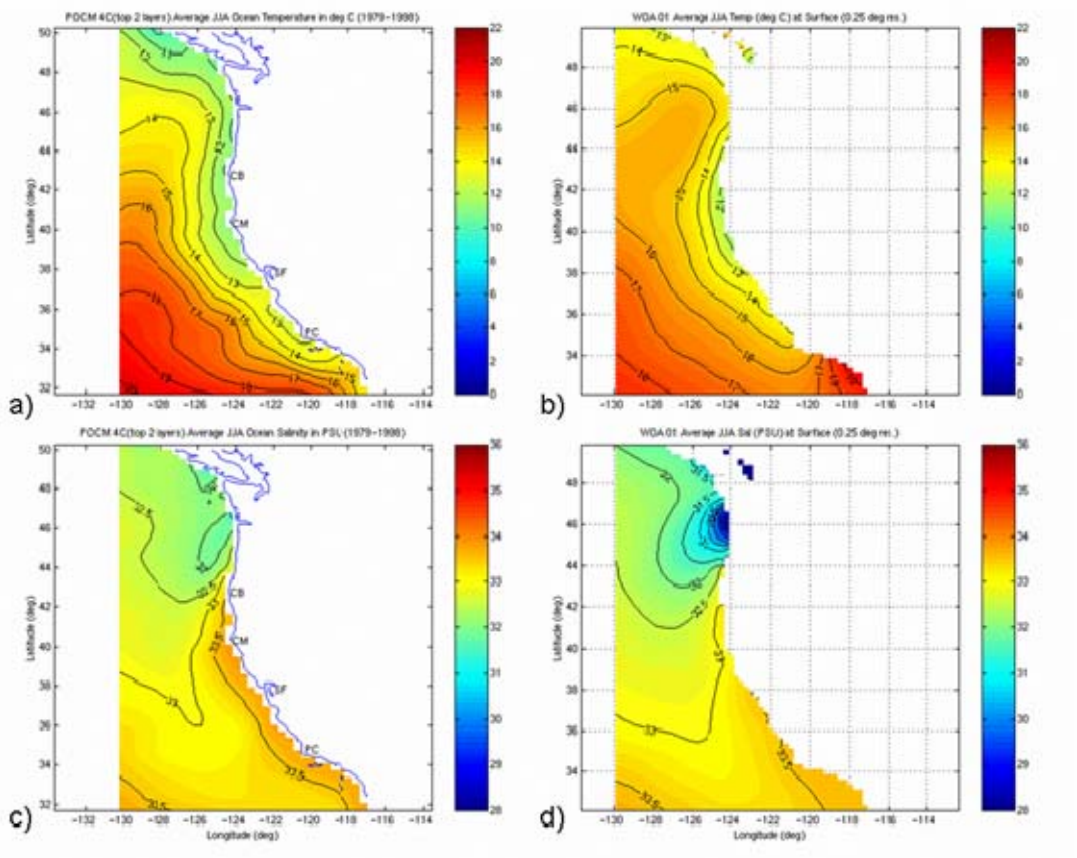

Figure 36. JJA Summer SST and Surface Salinity: (a) POCM 4C SST (°C); (b) Levitus SST (°C); (c) POCM 4C Surface Salinity (PSU); (d) Levitus Surface Salinity (PSU)

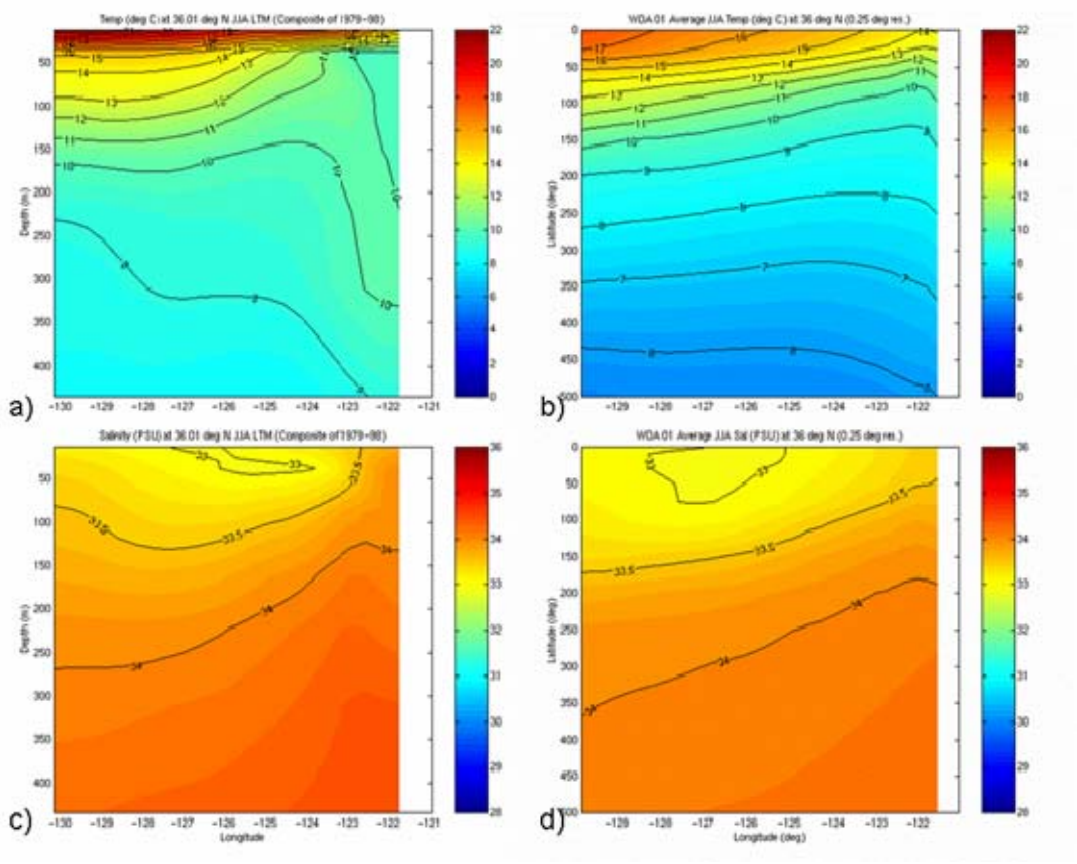

Figure 37. JJA Summer Depth-Longitude Cross-sections at 36° N: (a) POCM 4C Temperature (°C); (b) Levitus Temperature (°C); (c) POCM 4C Salinity (PSU); (d) Levitus Salinity (PSU)

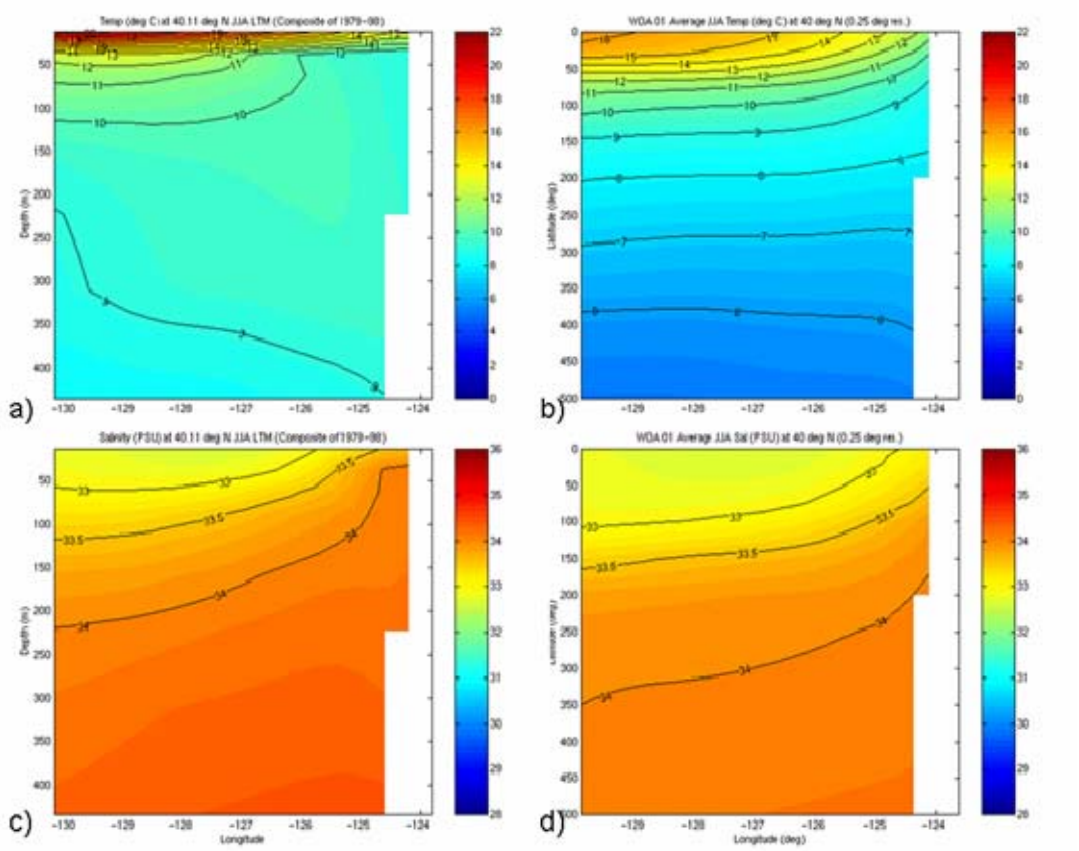

Figure 38. JJA Summer Depth-Longitude Cross-sections at 40° N: (a) POCM 4C Temperature (°C); (b) Levitus Temperature (°C); (c) POCM 4C Salinity (PSU); (d) Levitus Salinity (PSU)

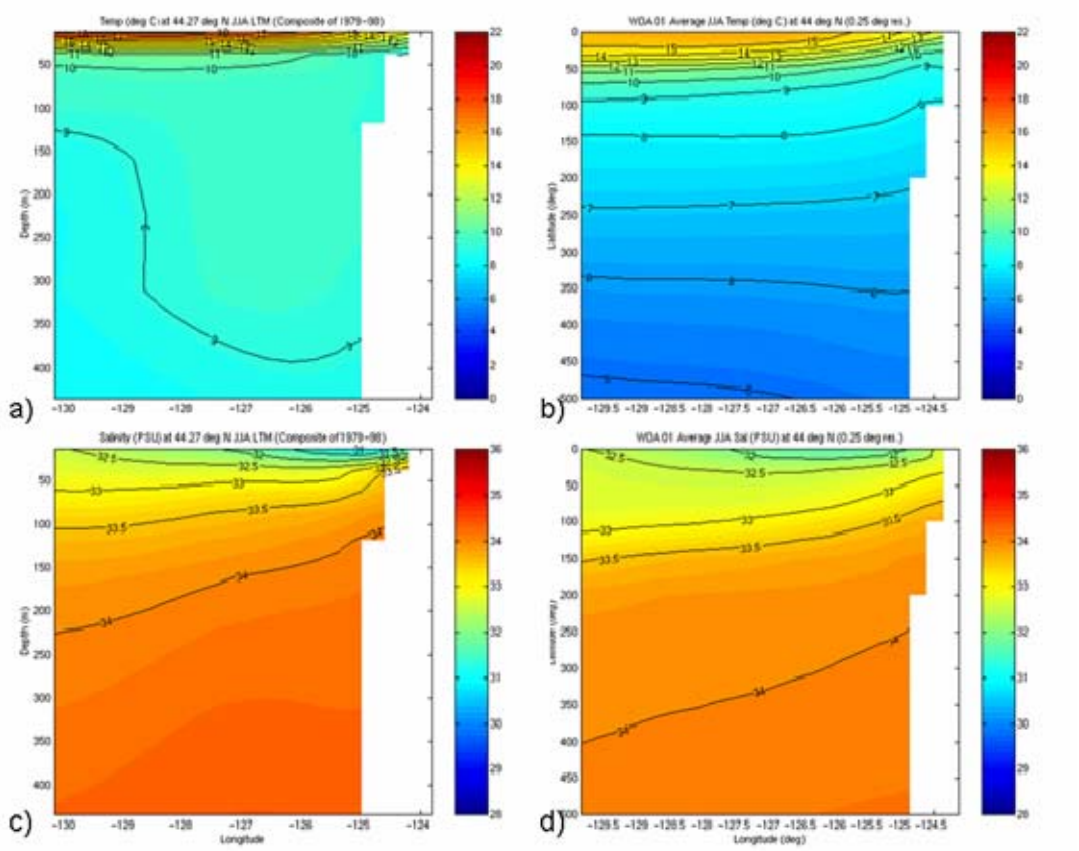

Figure 39. JJA Summer Depth-Longitude Cross-sections at 44° N: (a) POCM 4C Temperature (°C); (b) Levitus Temperature (°C); (c) POCM 4C Salinity (PSU); (d) Levitus Salinity (PSU)

Figures 37-39 show that POCM 4C summer temperatures are not as good a match to WOA 2001 data as is POCM 4C winter and spring temperatures (see Figures 30-32 and 34-35). However, summer salinity values are more consistent between POCM 4C and WOA 2001.

d. Fall

The POCM 4C LTM fall T-S features more closely match those of summer than of winter. The relaxation of upwelling conditions is not very apparent in the cross-sections at 36° N, 40° N, and 44° N (Figure 41-43) as isotherms and isohalines notably still slope upward towards the coast. As with the summer season, temperatures in the upper POCM 4C layers do not match well those seen in WOA 2001.

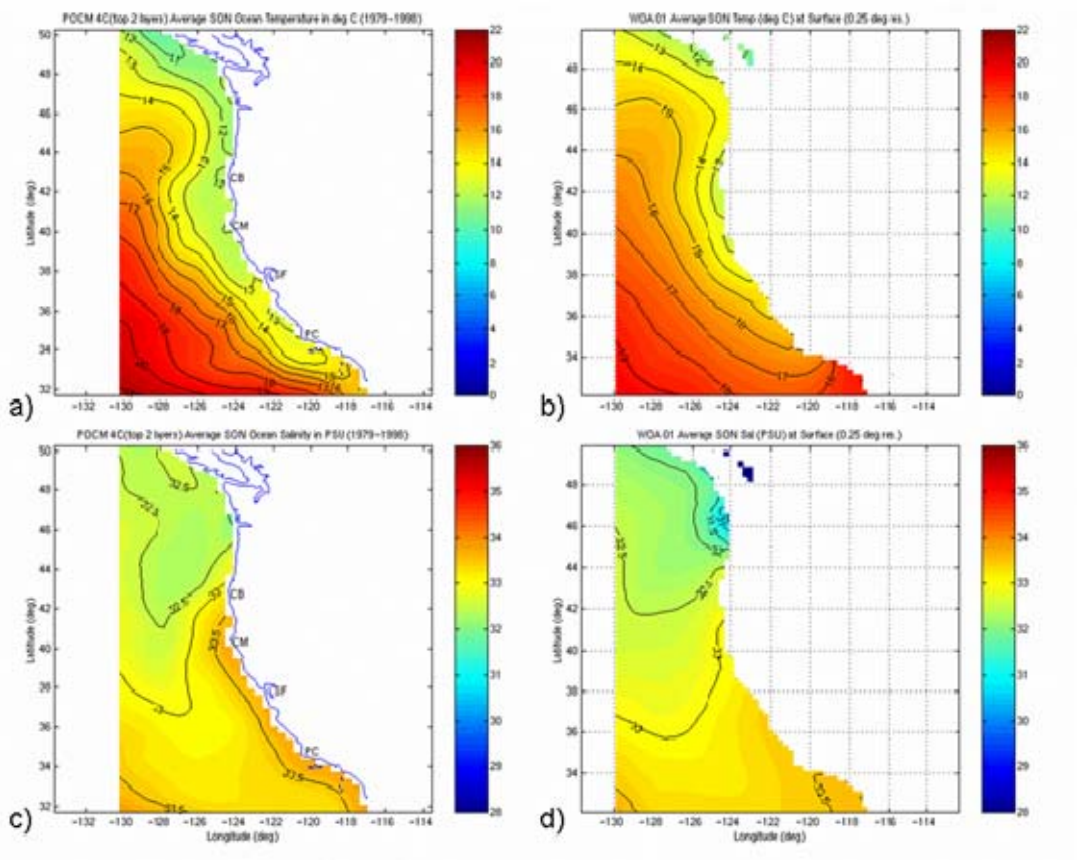

Figure 40. SON Fall SST and Surface Salinity: (a) POCM 4C SST (°C); (b) Levitus SST (°C); (c) POCM 4C Surface Salinity (PSU); (d) Levitus Surface Salinity (PSU)

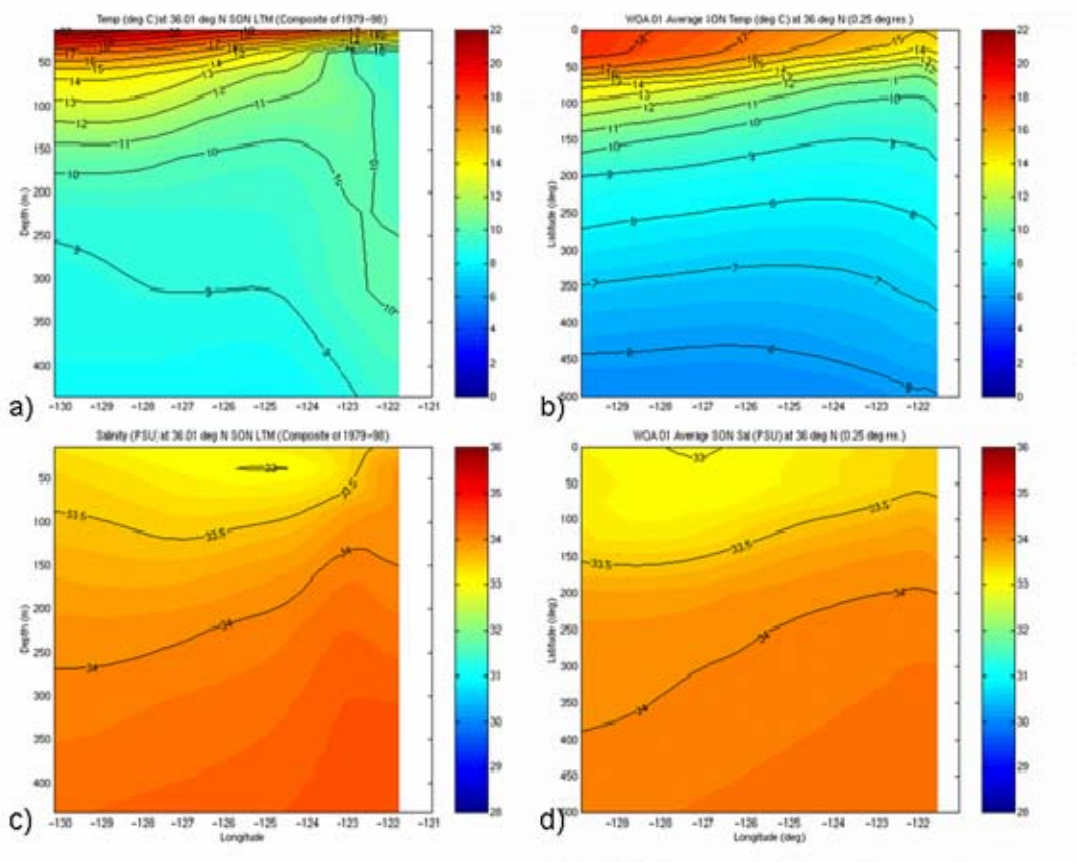

Figure 41. SON Fall Depth-Longitude Cross-sections at 36° N: (a) POCM 4C Temperature (°C); (b) Levitus Temperature (°C); (c) POCM 4C Salinity (PSU); (d) Levitus Salinity (PSU)

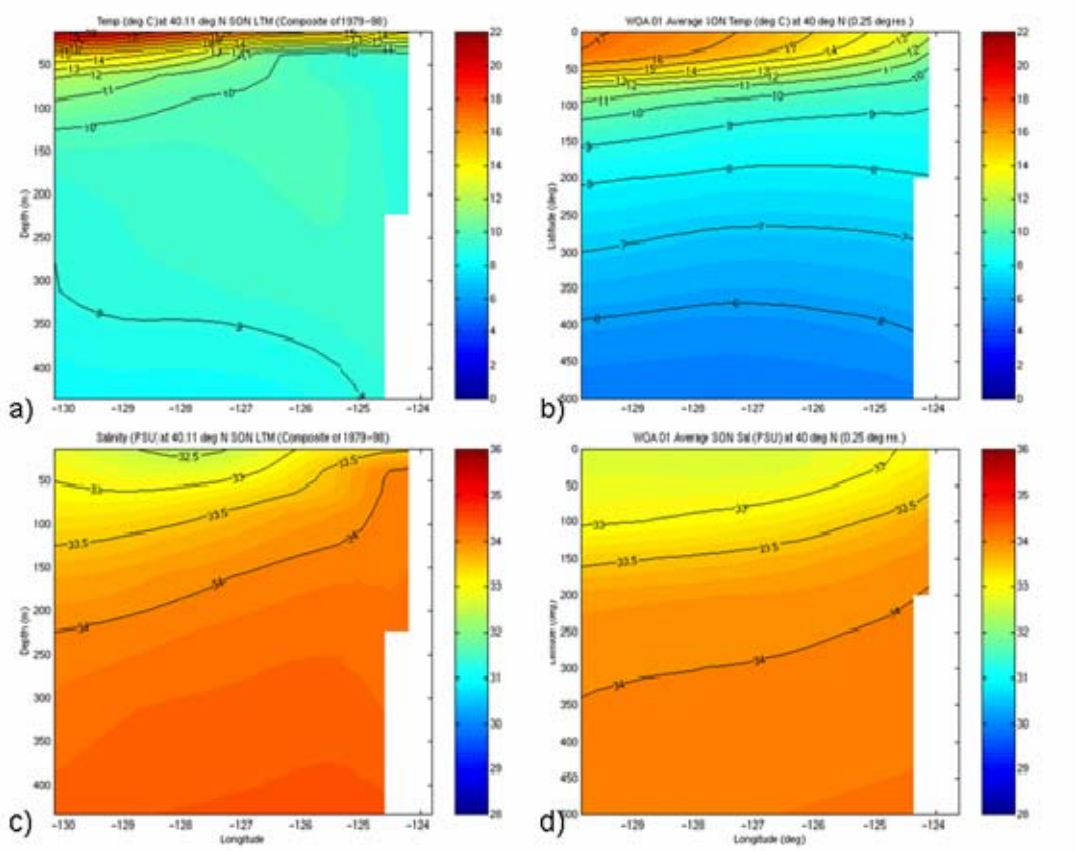

Figure 42. SON Fall Depth-Longitude Cross-sections at 40° N: (a) POCM 4C Temperature (°C); (b) Levitus Temperature (°C); (c) POCM 4C Salinity (PSU); (d) Levitus Salinity (PSU)

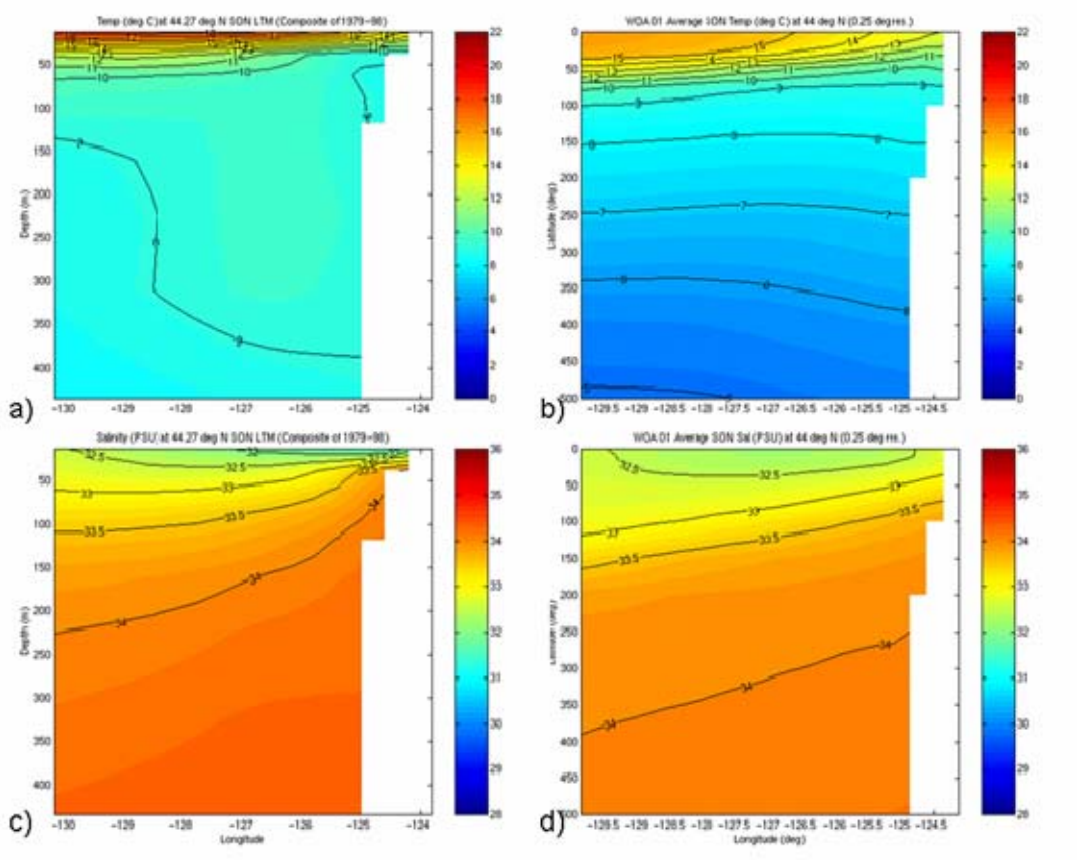

Figure 43. SON Fall Depth-Longitude Cross-sections at 44° N: (a) POCM 4C Temperature (°C); (b) Levitus Temperature (°C); (c) POCM 4C Salinity (PSU); (d) Levitus Salinity (PSU)

3. Summary of LTM Trends in POCM 4C

Consistent with the prior results outlined in Chapter II, currents in POCM 4C are generally weaker than those seen in observational data (see Figures 19-22). POCM 4C simulates the CC in generally the same area as seen in observations, although further offshore during January to June. The maximum equatorward speeds in the CC are also farther offshore than indicated by the observational study of Collins et al. (2003). The DC is not well simulated along the California coast from Point Conception to north of San Francisco during winter. The DC is also farther north in spring than might be expected.

POCM 4C shows some distinct biases in T and S fields (Figures 29-43). Notably, in the upper 500 m of the water column, POCM 4C is generally warmer and saltier than might be expected from observations. The temperature bias is more pronounced than the salinity bias, with ocean temperature remaining in the 9-10 °C range down to 500 m. A cool bias at the surface close to the coastline is also noted in all seasons.

4. Factors Affecting Differences Between POCM 4C LTMs and Observational LTMs

To assess the factors that might create the differences between the POCM 4C LTMs and observational LTMs, we examined several factors. As noted in Chapter II, POCM 4C is forced by wind stress, heat, and freshwater fluxes derived from ECMWF reanalysis and analysis data. Figure 44 shows that the ECMWF wind stress used by POCM 4C follow the seasonal forcing pattern outlined in Chapter I. Note this figure is arranged with winter and spring in the top row, and summer and fall in the bottom. The increase of equatorward wind from winter to spring along the coast associated with seasonal changes in the NPH is apparent. The strongest wind stress is noted in summer, with a slight relaxation during fall, and further relaxation during winter. This suggests that if biases in the POCM 4C wind forcing are involved in creating POCM 4C observational differences, then they are probably relatively subtle biases.

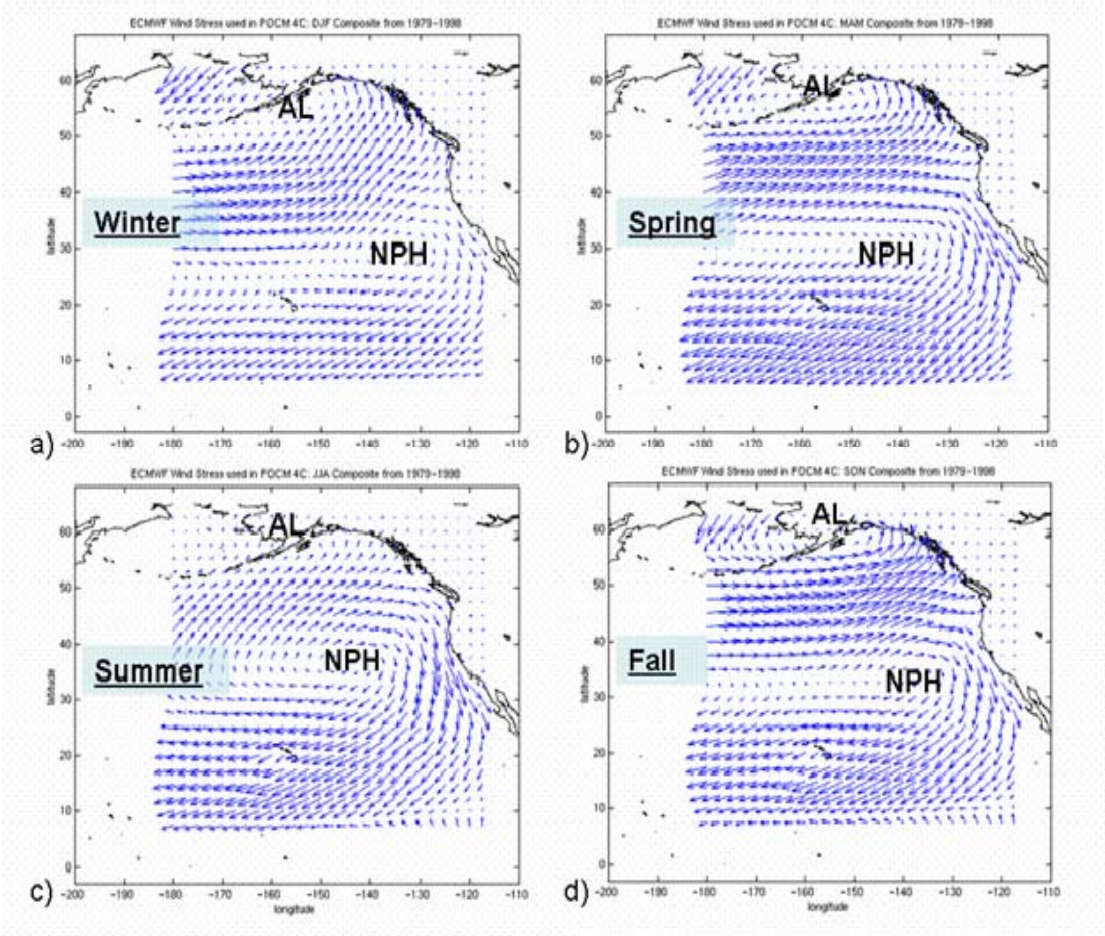

Figure 44. LTM Seasonal ECMWF Wind Stress used in POCM 4C: (a) Winter; (b) Spring; (c) Summer; (d) Fall

Additional external factors may bias POCM 4C LTM fields. The ECMWF forcing fields include climate variability from EN, LN, and other events. Figure 45 below presents several climate indices covering the period of the POCM 4C simulation. A negative NOI generally indicates EN type conditions in the CCS. The Multivariate El Nino/Southern Oscillation (ENSO) index (MEI) is another widely used index to track EN conditions. Large positive (negative) MEI values generally indicate that an EN (LN) is occurring (CDC 2005). Figure 45c displays an index for the PDO. The PDO as mentioned above briefly is a climate

oscillation similar to but on longer time scales than EN/LN. During the so called warm phase of the PDO, EN-type anomalies are seen in the atmosphere and ocean (UW 2005).

During the 1979-98 timeframe covered by the POCM 4C simulation, the PDO was in a warm phase. The twenty year period also included significantly more EN events than LN or neutral conditions. Therefore some bias exists towards EN-type anomalies in the POCM 4C run. That may partially explain the consistent warm and salty biases seen in all seasons, which would correspond to anomalous movement of equatorial waters north. Additionally, reduced upwelling could also account for the warm bias seen in the upper 500 m, but would not correspond to a salty anomaly.

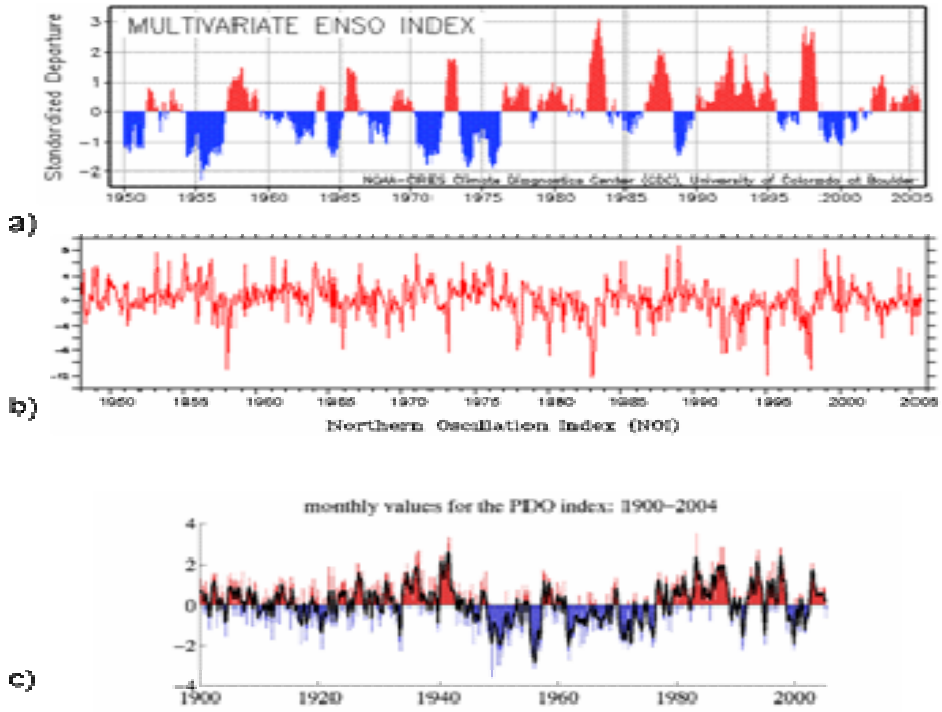

Figure 45. Climate Indices of Note during POCM 4C Run: (a) MEI (From CDC 2005); (b) NOI (From PFEL 2005); (c) PDO Index (From UW 2005);

B. POCM 4C NOVEMBER-MARCH EN/LN/LTM TRENDS

1. Wind Forcing Patterns

As illustrated in Figure 46, the EN composite wind stress anomaly pattern is dominated by a counterclockwise wind anomaly, with northward anomalies along the coast. The opposite holds true in the LN composite. This is consistent with previously reported EN and LN wind anomaly patterns as outlined in Chapter I. These figures confirm that the NOI based November to March composites from POCM 4C are consistent with EN and LN conditions. They also reinforce the idea that EN and LN are opposite phases of the same climate variation.

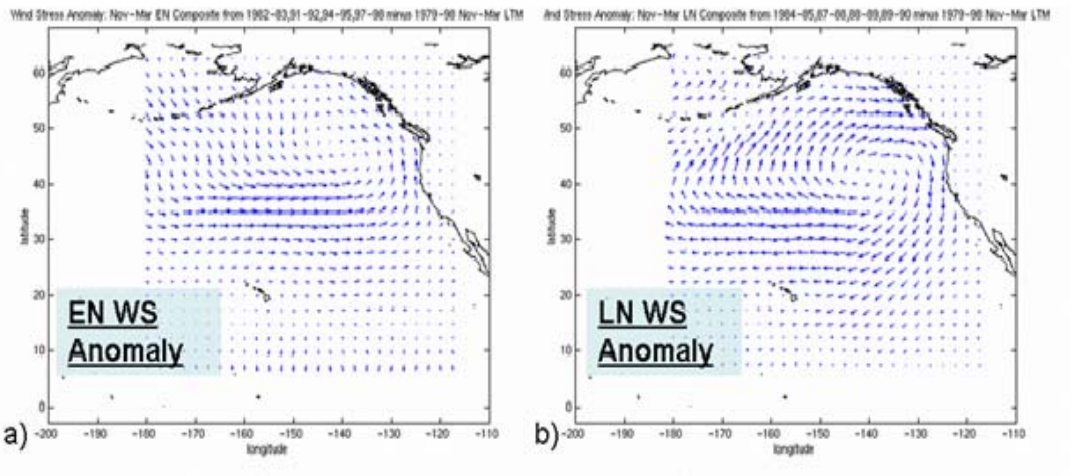

Figure 46. Anomalous Surface Wind Stress Forcing in POCM 4C Smart Climatology Composites: (a) EN; (b) LN)

2. Currents

Figure 47 illustrates the surface currents and current anomalies seen in the POCM 4C EN and LN composites. Both the EN and LN composites show some poleward flow (e.g., the DC, from the Oregon coast northward). However, this flow is

much more pronounced during the EN phase. The anomaly pattern is as discussed in Chapter I: EN has enhanced northward flow/weakened southward flow, while LN has strengthened southward flow all along the coast.

Figure 48 from Huyer and Smith (2002) and Figure 49 from POCM 4C depict current strength off the Oregon coast for EN, LN, and LTM conditions. The area shown is the Newport Hydrographic line, along which several hydrographic surveys per year have been done by Oregon State University for most years over the last four decades. Figure 48 depicts geostrophic rather than actual currents. The EN case in Figure 48 corresponds to November 1997, while LN refers to November 1998. The currents from POCM 4C follow the expected trend: enhanced poleward current along the coast during EN (about double the strength of the LTM), and enhanced equatorward flow during LN (about triple the strength of the LTM). This is also reflected in the in situ data from the Newport line, although the LN case does not appear to be very strong in the observations.

Examining Figure 50 below, the same general pattern is repeated. The CUC strengthens (here by about 15% over the LTM speed), surfaces, and becomes the DC during EN. The CUC is weakened (again by about 15% relative to the LTM) and pushed deeper during LN, while there is increased equatorward flow at the surface. The pattern is again repeated at 36° N as shown in Figure 51, with poleward flow increasing by about 30% relative to the LTM during EN, and equatorward flow increasing by about 60% relative to the LTM during LN.

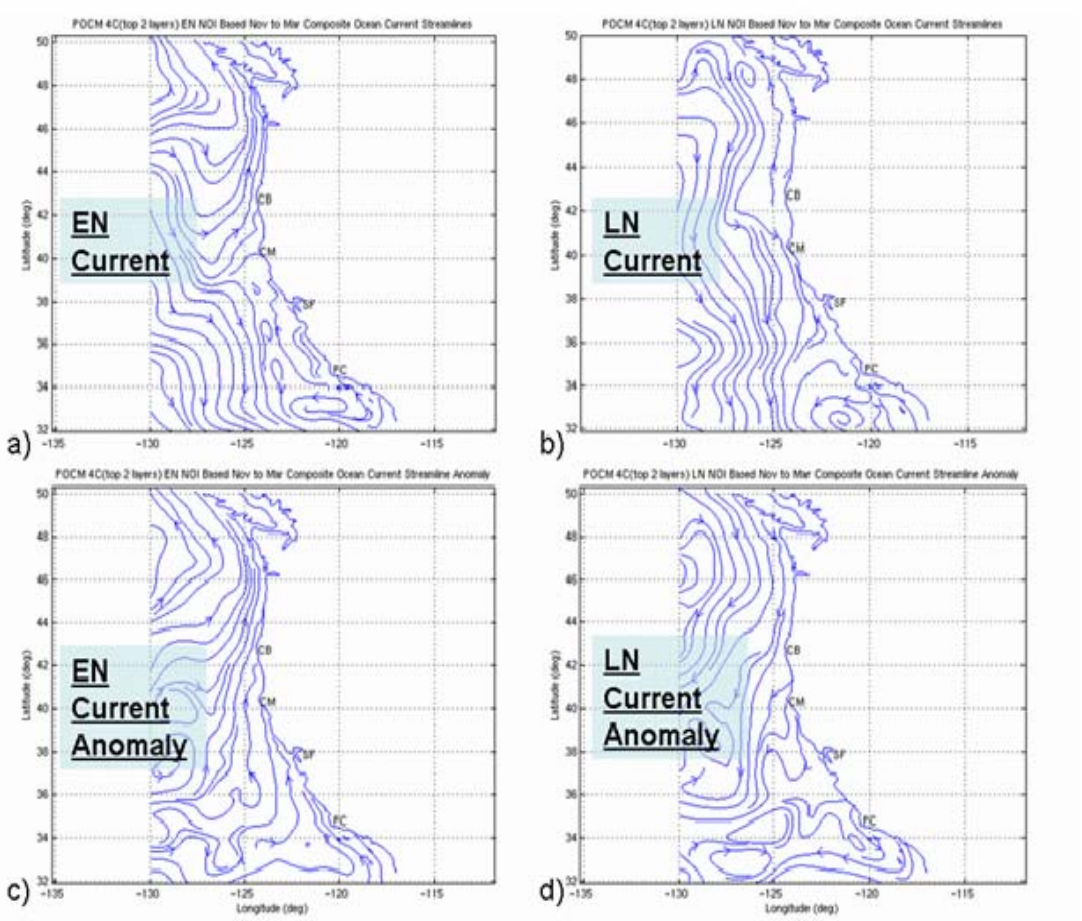

Figure 47. POCM 4C Surface Current Streamlines: (a) EN Current; (b) LN Current; (c) EN Current Anomaly from LTM; (d) LN Current Anomaly from LTM

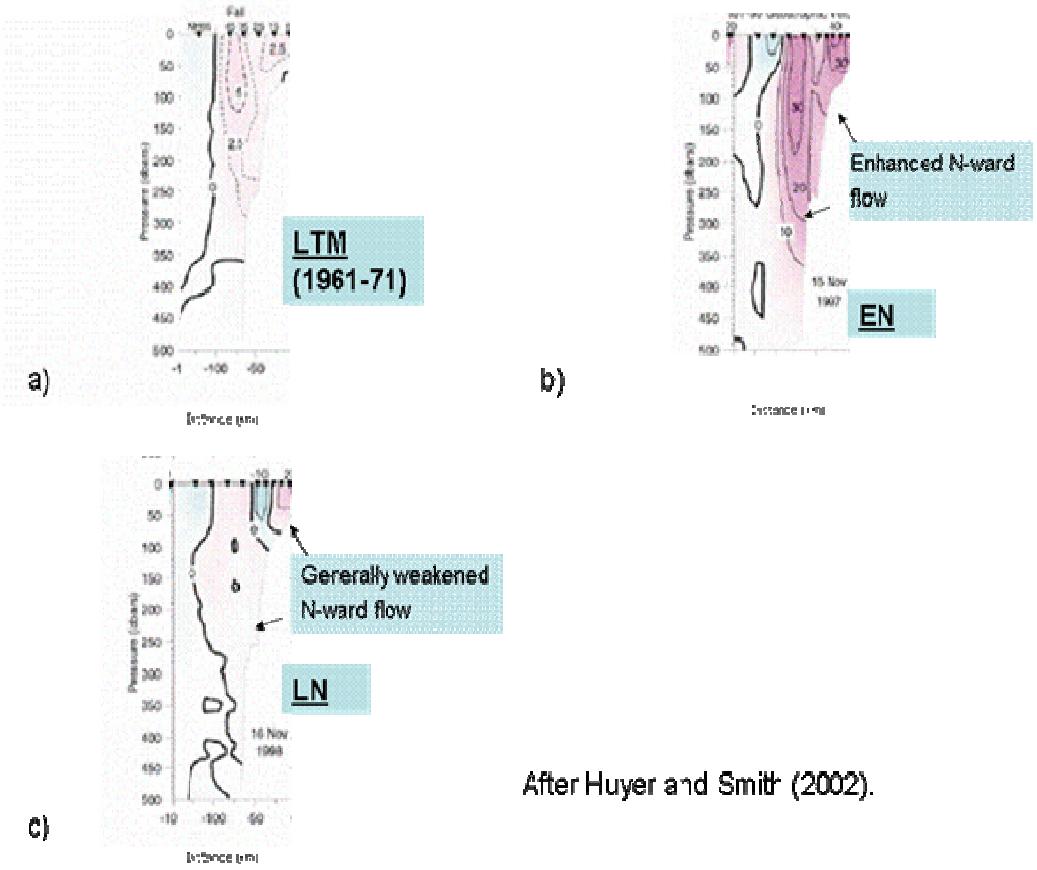

Figure 48. Geostrophic Currents from the Newport Hydrographic Line: (a) Fall LTM; (b) EN 1997; (c) LN (1998)

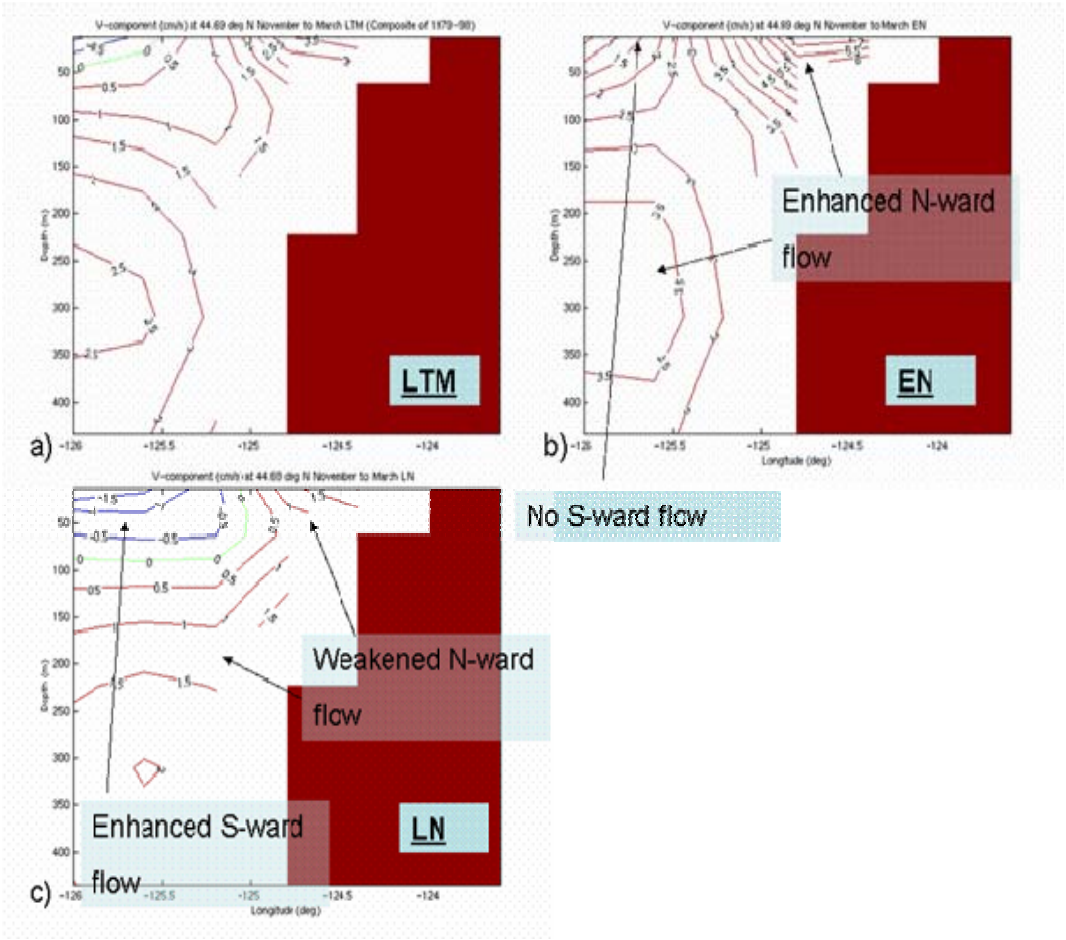

Figure 49. POCM 4C Depiction of V-component of Current Along the Newport Hydrographic Line: (a) November to March LTM; (b) EN; (c) LN

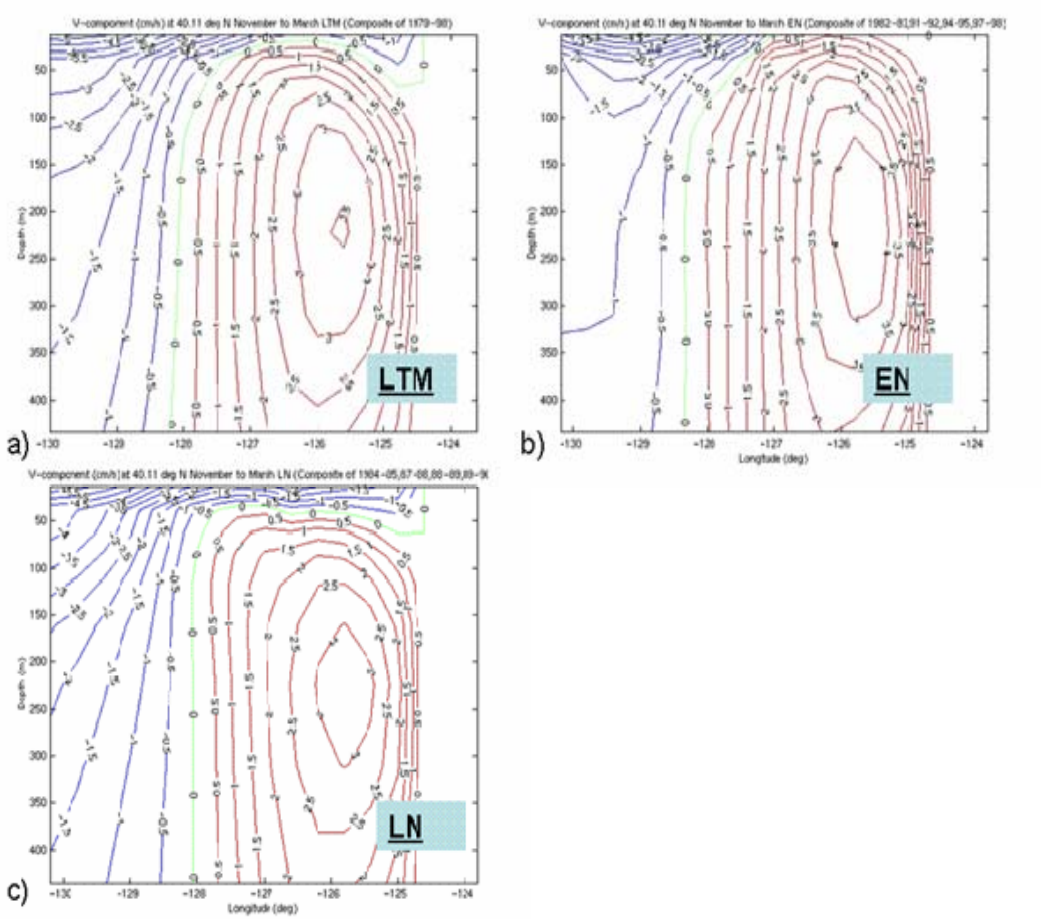

Figure 50. POCM 4C November to March V-Current at 40° N: (a) LTM; (b) EN; (c) LN

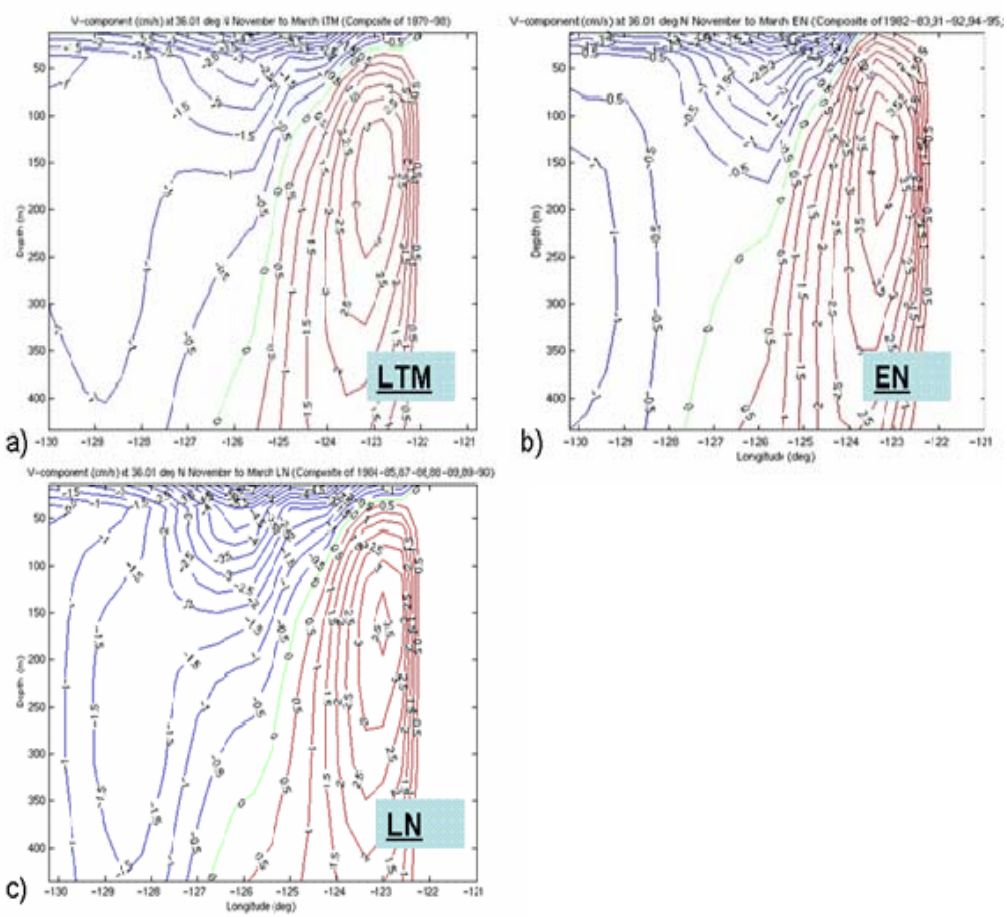

Figure 51. POCM 4C November to March V-Current at 36° N: (a) LTM; (b) EN; (c) LN

3. SSH

Figure 52 compares POCM 4C SSH in the EN and LN composites with satellite SSH using the process described in Chapter II. All figures are plotted with the same color scale and contour interval. Note that both the satellite and POCM 4C data show enhanced SSH along the coast during EN conditions, with low SSH anomalies further offshore between approximately 35°-45° N. The LN view from altimetry data shows low SSH along the coast as has been seen in other cases (e.g., Schwing et al. 2002b). However, the POCM 4C SSH anomaly is weaker than the indicated by altimetry,

and the SSH anomaly is close to zero along much of the California coast.

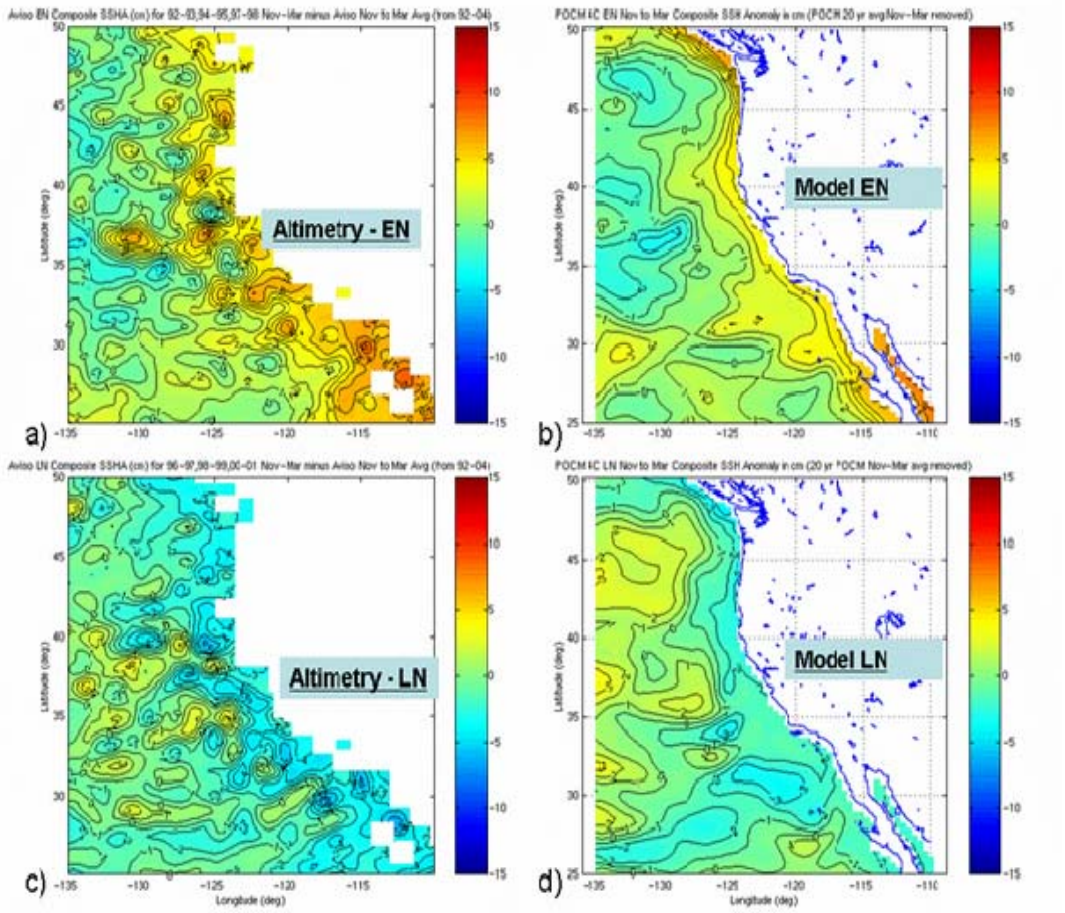

Figure 52. Comparison of Satellite and POCM 4C November to March SSHA: (a) Aviso EN; (b) POCM 4C EN; (c) Aviso LN; (d) POCM 4C LN

4. Temperature

A large area view of sea surface temperature anomaly (SSTA) is shown in Figure 53 POCM 4C was compared to the NOAA Optimally Interpolated SST Version 2 (i.e., Reynolds SST; Reynolds et al. (2002)). Reynolds SST fields are available for several decades, and are a blended product of satellite and in situ observations. Although not a perfect representation, the Reynolds SST does provide a historical standard to compare against. Reynolds SST data from the

exact same months as used in the EN and LN composites were downloaded, averaged into composites, and the Reynolds 1961-1990 LTM was subtracted to provide anomalies.

Panels a and b of Figure 53 show POCM 4C simulations of EN and LN respectively, while panels c and d show the Reynolds SSTA fields for EN and LN. Both POCM 4C and Reynolds EN and LN composites show the expected EN/LN patterns (cf. Schwing et al. 2002b): anomalously warm (cool) temperatures are seen along the coast during EN (LN). This figure reveals an interesting feature of the POCM 4C SSTAs. In both the EN and LN case, along the central California coast, the POCM 4C SSTAs are opposite to the Reynolds SSTAs and to other the EN and LN SSTAs found in many prior studies (e.g., Schwing et al. 2002b). For example, in the POCM 4C EN composite a cool anomaly is shown along the coast from Cape Mendocino to Cape Blanco. In both the EN and LN cases, the POCM 4C and Reynolds SSTAs have the same sign north of Cape Blanco and south of Point Conception, although the POCM 4C SSTAs are weaker.

Figure 54 and Figure 55 are similar to Figure 48 and Figure 49 above, showing data for the same dates and locations. Again, panel a represents LTM conditions, panel b EN, and panel c LN. However temperature is shown instead of currents. The x-axis of the observed data (Figure 54) is labeled in kilometers, while the POCM 4C data (Figure 55) is labeled in degrees longitude, but the figures cover approximately the same geographic area. The POCM 4C and observed temperature anomalies are similar. During EN conditions, isotherms can be seen to dip towards the coast more strongly than in the LTM, while during LN the isotherms tend to level out with respect to the LTM. This

is consistent with warmer than normal water along the coast during EN due to decreased upwelling. During LN cooler temperatures than normal close to the coast, caused by enhanced upwelling, would be expected.

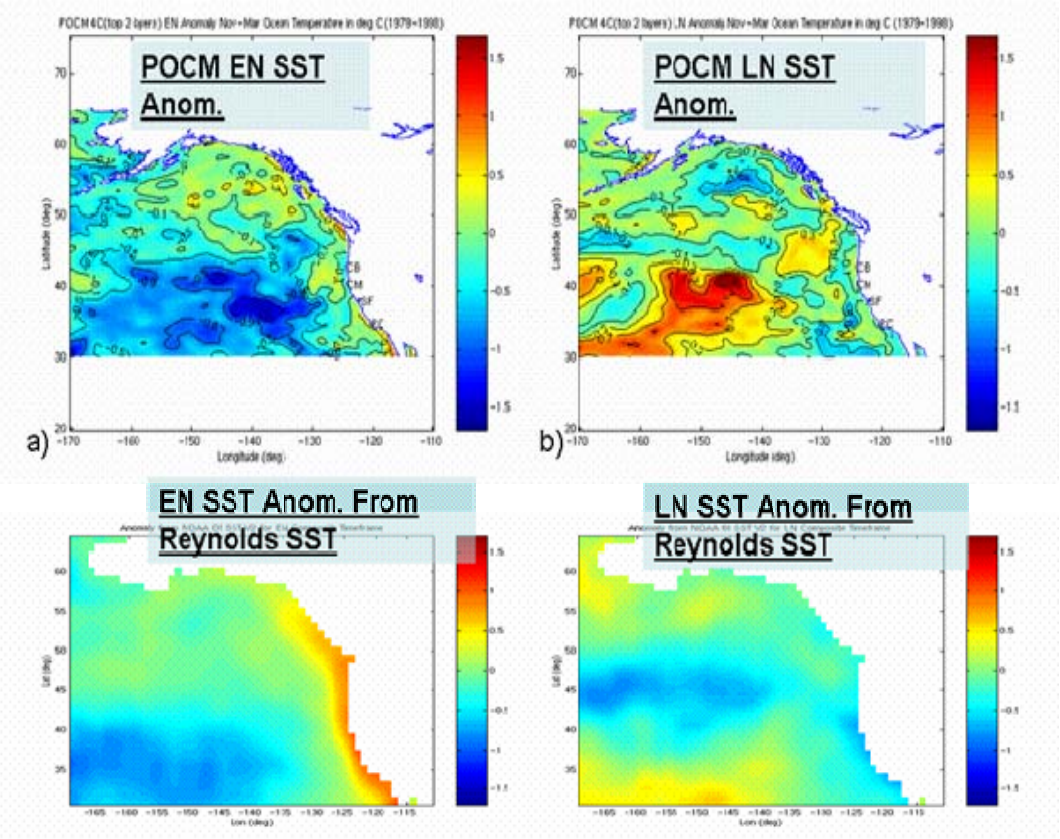

Figure 53. Comparison of Anomalies in POCM 4C and NOAA Optimally Interpolated V2 SST: (a) POCM 4C EN SSTA; (b) POCM 4C LN SSTA; (c) Reynolds EN SSTA; (d) Reynolds LN SSTA

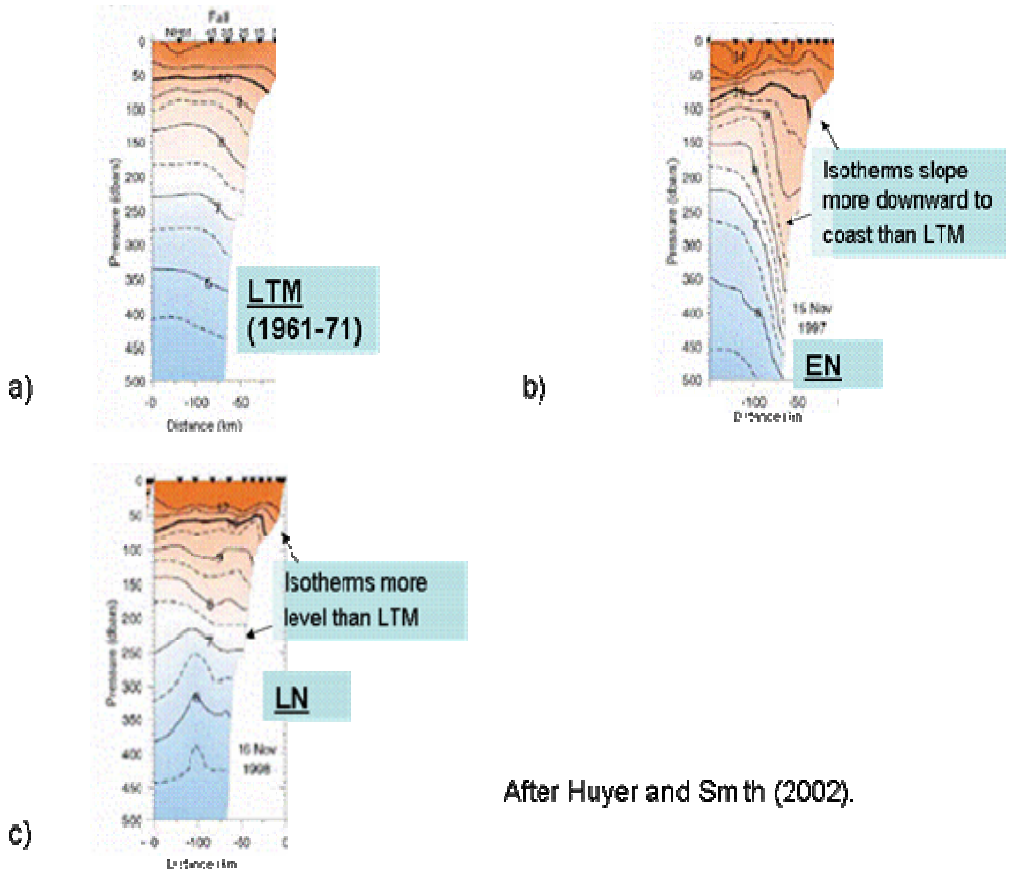

Figure 54. Temperature along the Newport Hydrographic Line: (a) Fall LTM; (b) EN 1997; (c) LN (1998)

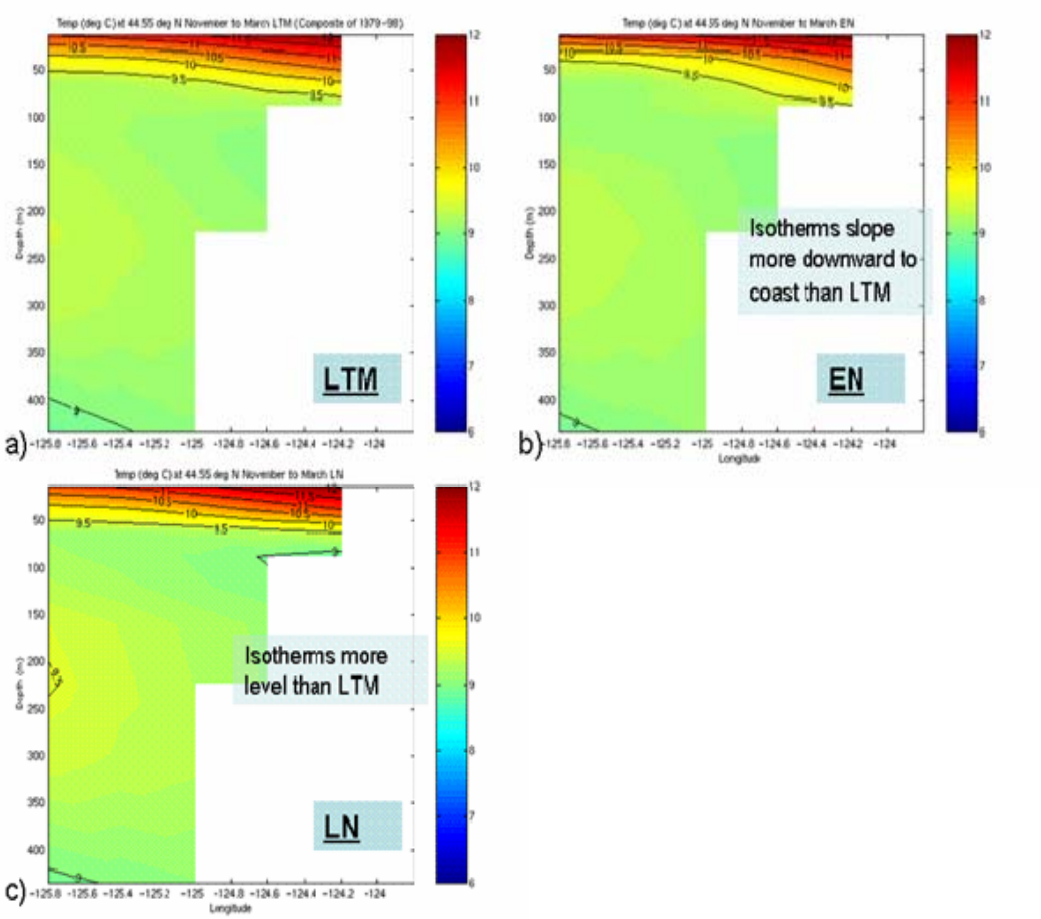

Figure 55. POCM 4C Depiction of Temperature along Newport Hydrographic Line: (a) November to March LTM; (b) EN; (c) LN

5. Salinity

Figure 56 and Figure 57 of salinity below cover the same time periods and geographic range as the above depictions of the Newport hydrographic line. Again panel a represents LTM, panel b EN, and panel c LN. The geographic area shown in observations is matched as closely as possible in the POCM 4C figure. The in situ data shows that during an EN condition, isohalines close to the close sloped sharply downward relative to the LTM. Such an effect is not obvious in the POCM 4C plots, although the EN composite shows fresher water than the LTM close to the coast. During LN, the in situ data shows close to the coast

the isohalines sloping in the opposite direction to that of EN. Again this is not as clearly simulated in the POCM 4C LN composite, and the LN composite shows fresher water at the surface than the POCM 4C LTM. However, the waters along the coastal margin are saltier overall than in the LTM case, from about 50 m depth and deeper. Taken together the observational figures (Figure 54 and 56) indicate anomalously warm and salty water along the coast during EN, while the POCM 4C figures (Figure 55 and 57) indicate anomalously warm and fresh water. Warm and fresh anomalies are the expectation in this area during EN (see Chapter I). Thus it would be interesting to look at other observations from the Newport Line during different EN events.

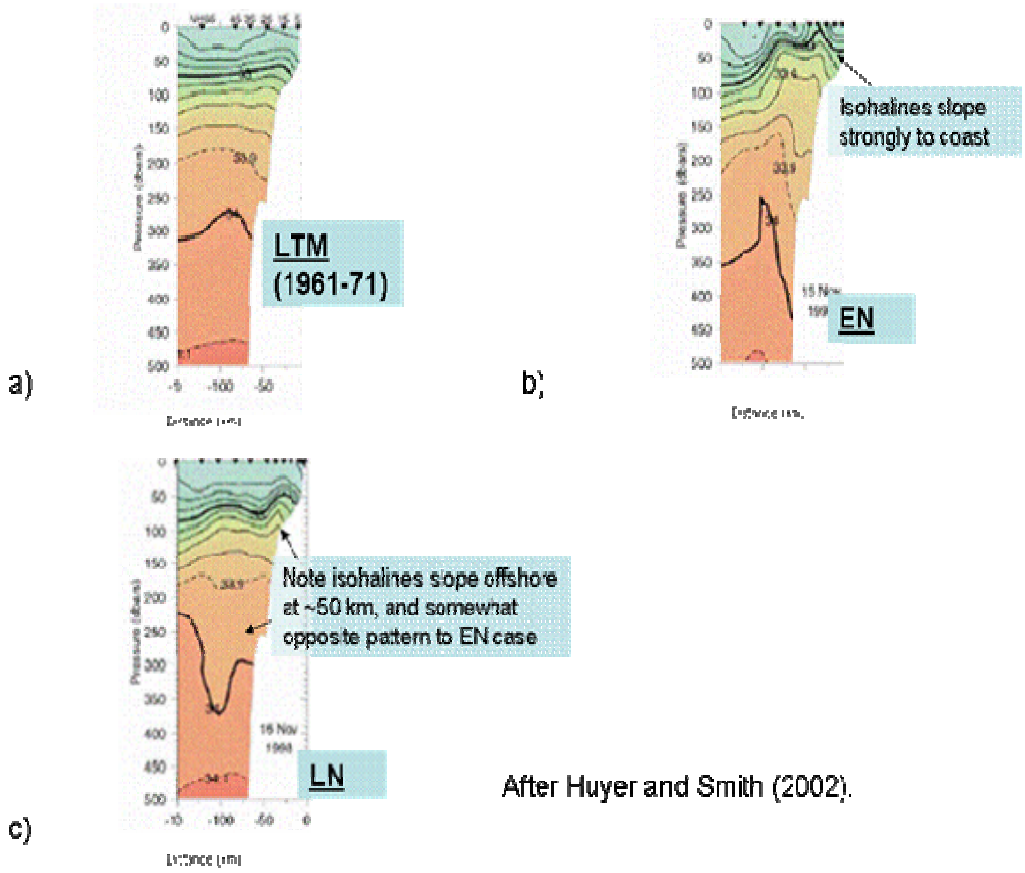

Figure 56. Salinity along the Newport Hydrographic Line: (a) all LTM; (b) EN 1997; (c) LN (1998)

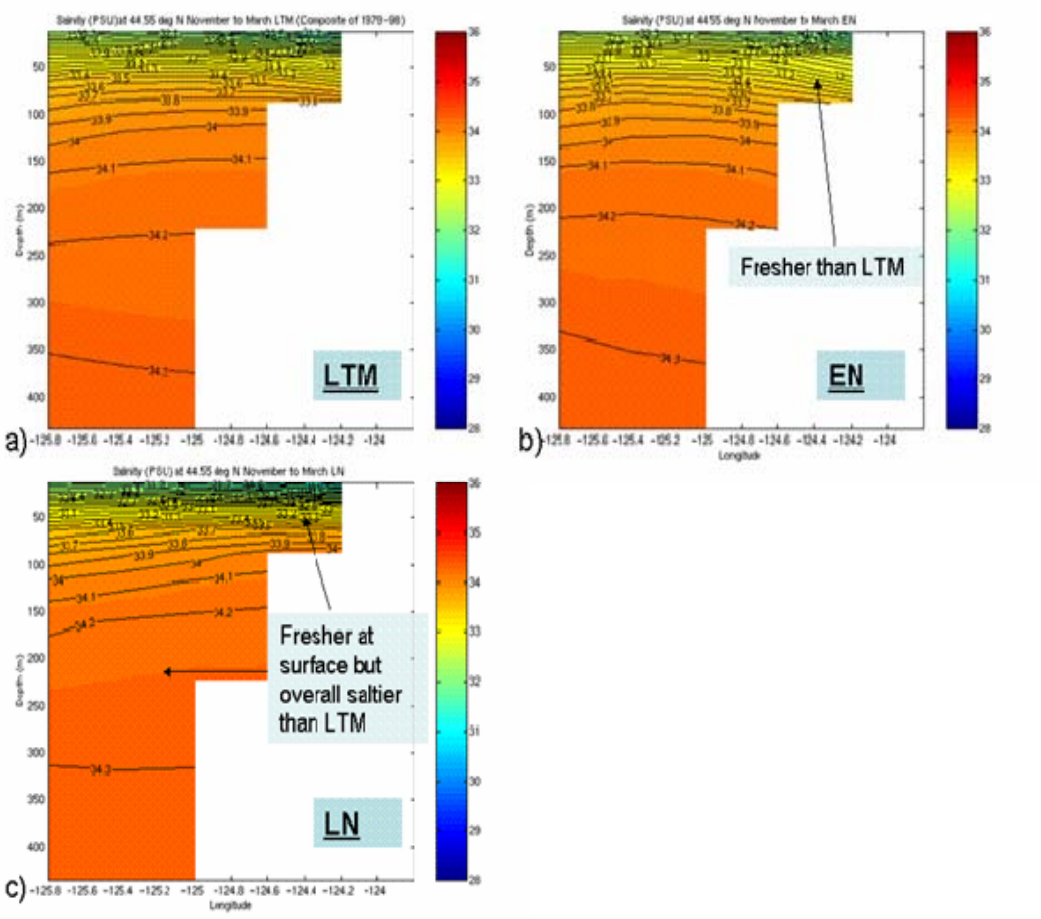

Figure 57. POCM 4C Depiction of Salinity along the Newport Hydrographic Line: (a) November to March LTM; (b) EN; (c) LN

6. Wind Stress Variability

Wind stress (WS) and wind stress curl (WSC) are of great importance in Ekman processes. They effect upwelling and downwelling and hence temperature and salinity anomalies. Figure 58 and Figure 59 below present the wind stress and wind stress curl anomalies calculated from the 2.5° resolution ECMWF forcing fields used in POCM 4C. Note that the color bar for WSC has been reversed, so that blue temperatures correspond to positive WSC (this was done because positive WSC typically leads to Ekman pumping and cool anomalies). Panel a in each figure shows the SST

anomaly from POCM 4C, panel b shows the WSC anomaly calculated from ECMWF, and panel c shows the ECMWF WS anomaly over the POCM 4C SSTA. Note that the WSC pattern for EN of negative curl along the coast in the CCS and positive curl over much of the NPH/AL is opposite to the LN pattern. Note in the EN composites the general association along the coast of negative SSTA with positive WSCA, indicating that Ekman pumping anomalies contributed to the SSTAs.)

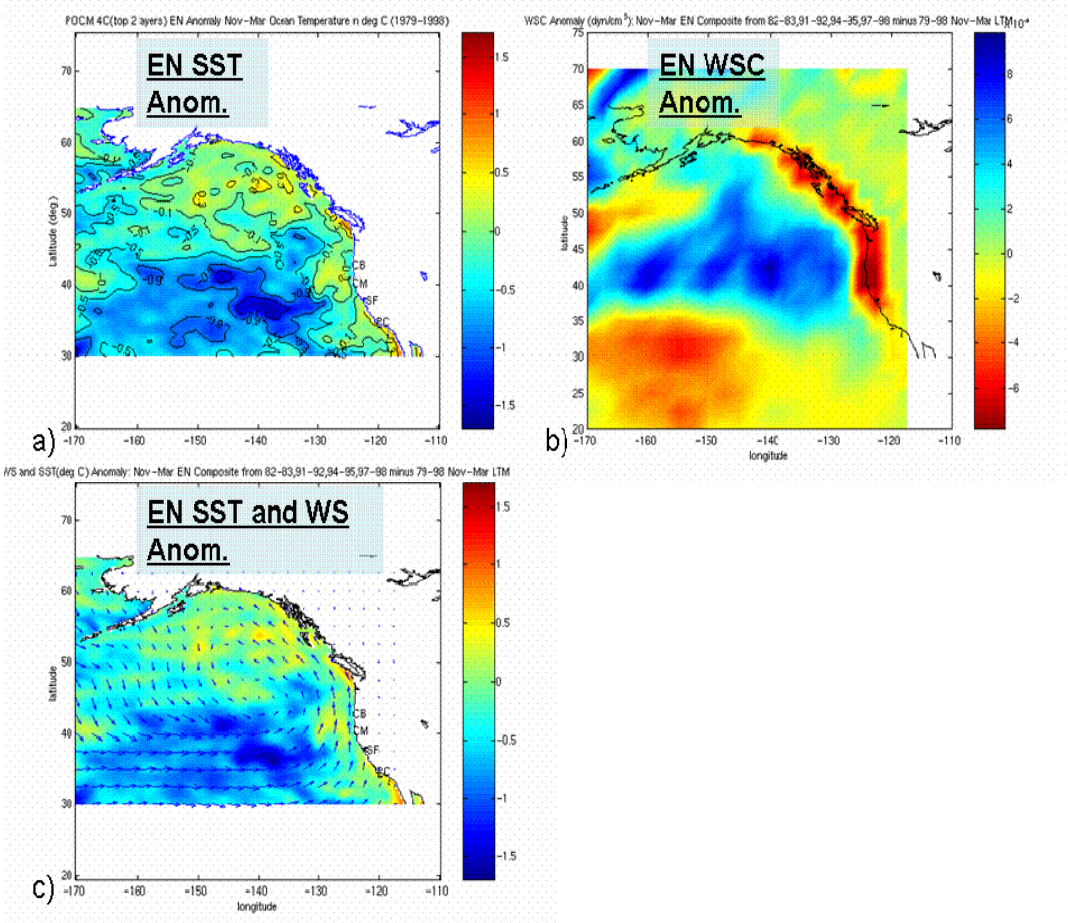

Figure 58. Wind Stress, Wind Stress Curl, and SST Anomalies for EN Composite: (a) POCM 4C EN SSTA; (b) ECMWF EN WSCA; (c) POCM 4C EN SSTA and ECMWF WS Anomaly

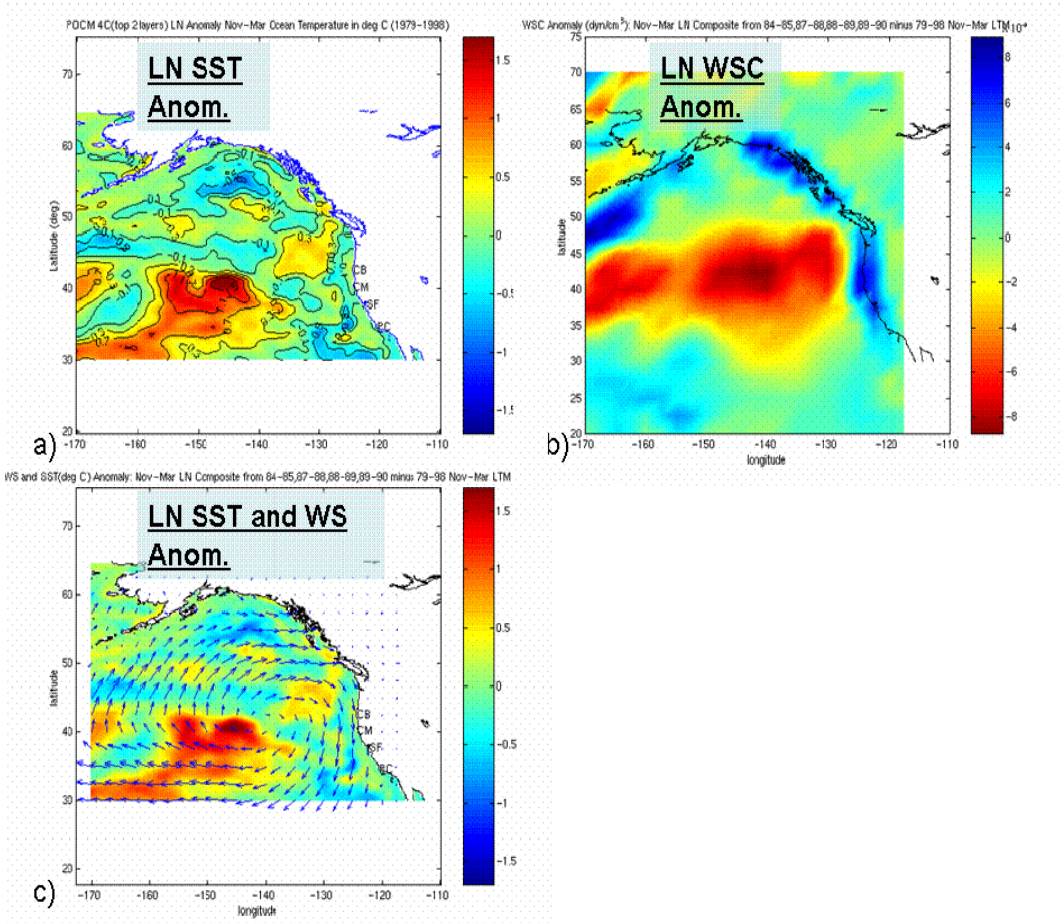

Figure 59. Wind Stress, Wind Stress Curl, and SST Anomalies for LN Composite

THIS PAGE INTENTIONALLY LEFT BLANK

IV. DISCUSSION AND CONCLUSIONS

A. SUMMARY OF RESULTS

An atmospheric climate index, representing the connection between the tropical western Pacific and the northeast Pacific in the vicinity of the CCS, was used to selectively average output from a 20-year run of an ocean climate model. Composites, or smart climatologies, representing EN and LN conditions were made from such selective averages. The oceanic conditions from the model composites were found to be broadly consistent with previously published studies on EN and LN. Overall, the patterns of anomalies from LTM conditions in variables such as salinity, temperature, and currents were opposite in sign in the EN composite to the LN composite, as expected for opposite phases of the same climate variation. This indicates that the model derived smart climatologies provide realistic indications of ocean climate variations and are an improvement on exclusively using traditional climatologies.

B. SMALLER SCALE COMPARISONS, USE OF SMART CLIMATOLOGY IN A TEST CASE

For Naval operations, such as ASW or amphibious landings, areas on the order of a hundred kilometers or less are of particular interest. Additionally, geographic areas of this scale are often sampled on oceanographic cruises and could provide valuable in situ data to compare with climatologies. Therefore, it is interesting to compare POCM 4C climatologies to in situ data as a test case on a smaller scale. Initially, our intent was to compare POCM 4C currents with in situ current observations. However, finding sufficient numbers of current measurements, at

consistent depths and with long and overlapping time series, was quite difficult. So instead, temperature and salinity cross-sections were examined.

Hydrographic line P is located off the Canadian Pacific coast and has been regularly sampled for decades (IOS 2005). Its location is shown in Figure 60. Plots of analyzed cruise sample data are available online at http://www-sci.pac.dfo-mpo.gc.ca/osap/projects/linepdata/default_e.htm, accessed 2005. These are included below for comparison with POCM 4C depictions of the LTM, EN, and LN composites, and the EN and LN composite anomalies along line P as simulated in POCM 4C.

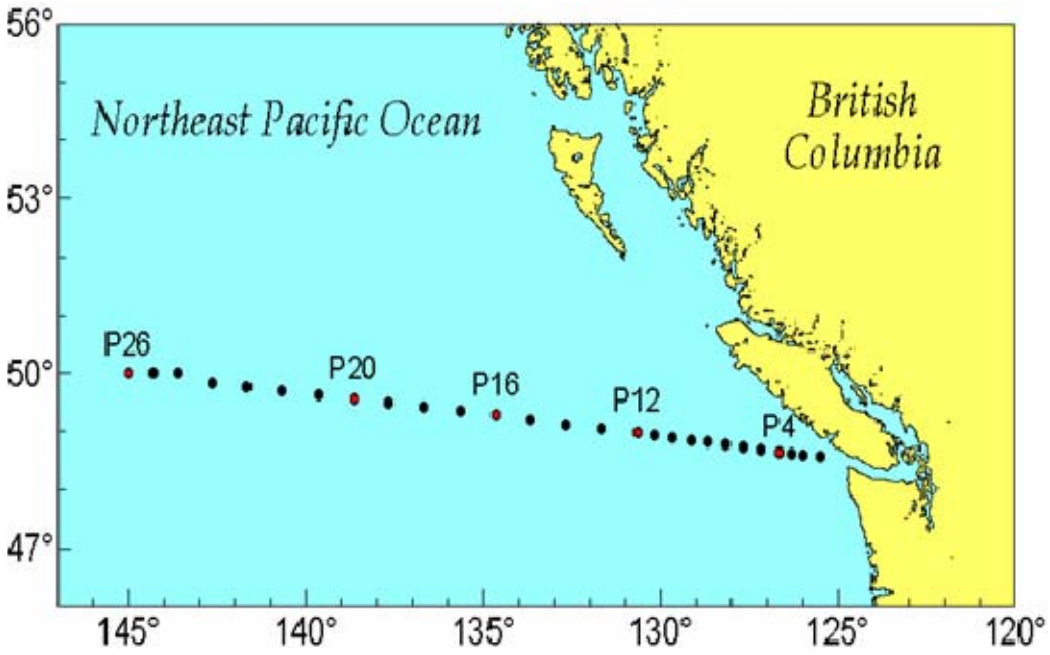

Figure 60. Line P Location (From IOS (2005)): Standard sampling stations (e.g., P4, P20 – all red and black dots) are Noted

First we examine temperature fields directly. Figure 61 below shows a distance versus depth cross-section of observational temperature data from November 1982, an EN

like month as indicated by its NOI, along with the POCM 4C November to March LTM and EN and LN smart climatologies. Panel a is the observed data, panel b is the POCM 4C EN November-March composite, panel c is the POCM 4C 20 year LTM November-March (traditional climatology), and panel d is the POCM 4C LN November-March composite. The lines in the upper right corner of each panel indicate the upper 500 m of the water column and the area shoreward of 130° W longitude, which has been the focus area of previous cross-sections. Figure 62 panel a shows February 1999, a LN like month as indicated by its NOI. Panels b-d of Figure 62 are as in Figure 61. The upper right hand corner of each panel corresponds to point P1, and the upper left corner of each panel is point P26.

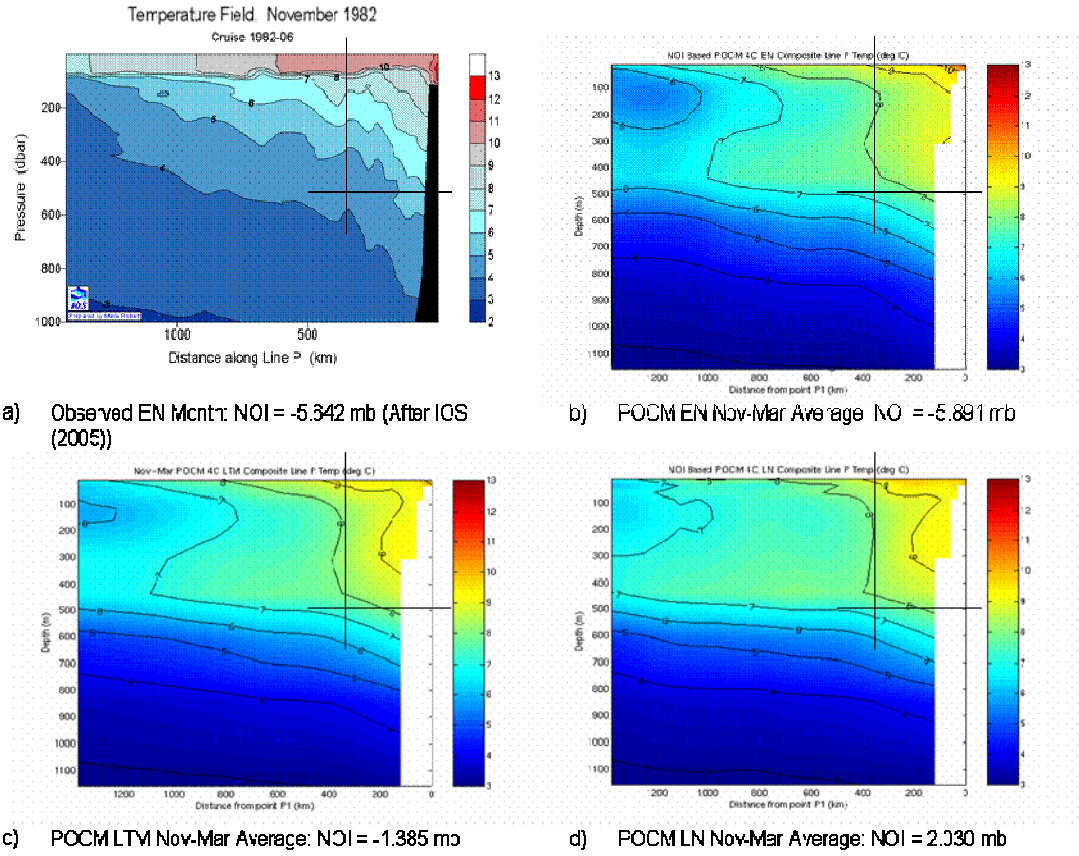

Figure 61. In situ Temperature (˚C) Along Line P During EN vs. POCM 4C Climatologies

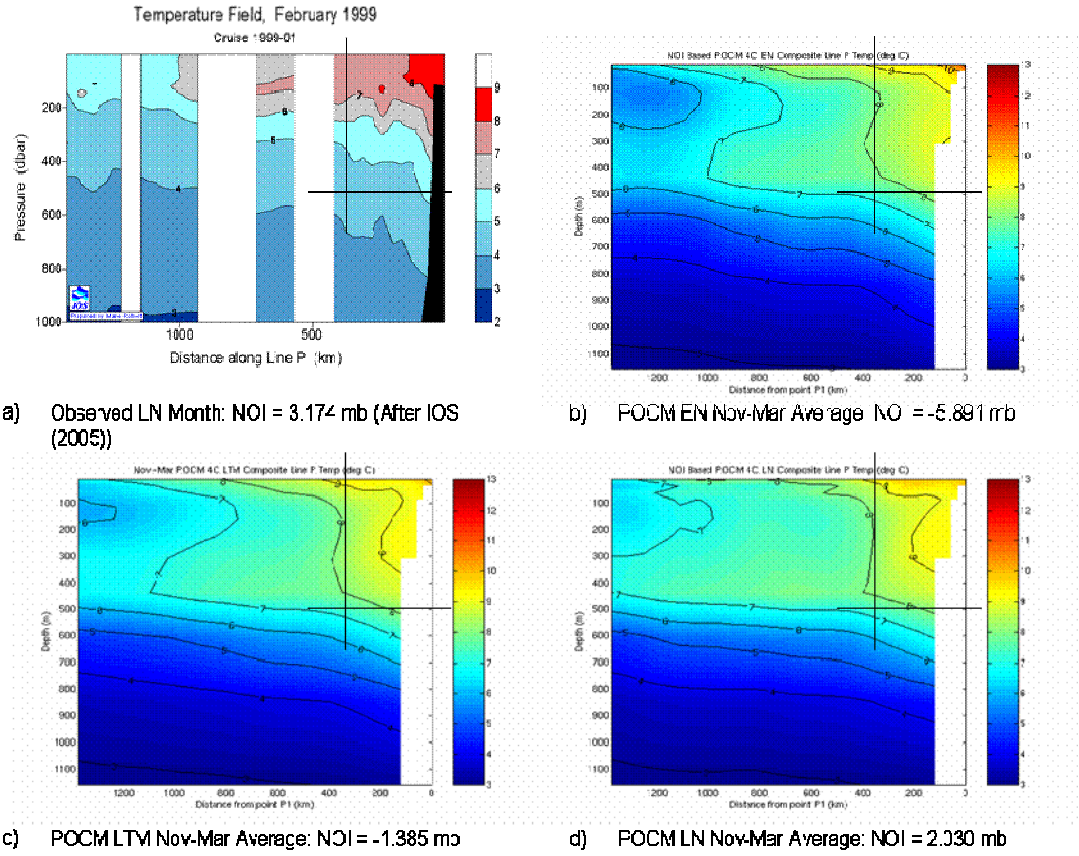

Figure 62. In situ Temperature (˚C) Along Line P During LN vs. POCM 4C Climatologies

For November 1982, a significant feature in the observations is the warm mixed layer concentrated in the upper 100 m of the water column, for about 700 km from point P1. Further west, the temperature at the surface is cooler. The POCM 4C EN composite roughly follows this pattern. By contrast, both the POCM 4C LTM and LN November-March composites show much deeper mixed layers close to point P1. Additionally, the LN composite is much warmer at the surface from about 400-1000 km from P1. This implies that the EN composite is the best match to the observations.

For February 1999, observations show a deeper and broader warm mixed layer, extending several hundred

kilometers seaward of what was observed in 1982. Both the POCM 4C LTM and LN composite show a similar deep mixed layer. However, the LN composite shows warmer surface waters further to the west than either observations or the LTM composite. Thus in this case the LTM traditional climatology from POCM 4C may be the best match. This may indicate other climate variability besides LN was affecting line P at this time.

Detecting the subtle variability among the above temperature plots can be difficult, especially since the variability within POCM 4C is generally less than that seen in observations. Therefore, comparisons of observed anomalies from the observed LTM with POCM 4C EN and LN anomalies from the POCM 4C LTM are made below. Figure 63 and Figure 64 both represent EN anomalies, since February 1998 was part of the 1997-98 EN. Both figures show warm temperature anomalies at the surface at the eastern edge of line P (close to coast). Comparison of the two figures shows several other matches, although the overall pattern is not identical. Figure 65 and Figure 66 represent EN salinity anomalies. Except for a fresh surface anomaly 600 - 800 km from P1 in the POCM 4C data, the in situ data and POCM 4C composite show a good match in the pattern of positive and negative anomalies (note that the anomaly signs match, not the anomaly magnitudes).

Figures 67-69 represent temperature anomalies during LN. Note that the POCM 4C LN anomaly matches the observational data from the 1988 LN quite well out to over 1000 km from the beginning of line P. Note also that POCM 4C better matched the November 1984 field than the December 1988 field. Thus the smart climatology LN composite may be

capturing some of the variability that was present in 1984 and 1988, but additional factors may be affecting the observations.

Figures 70-72 compare salinity during LN conditions. In this case the LN composite matches the data from the 1984 quite well, but actually shows the opposite pattern at almost all locations to the 1988 LN data.

This comparison of model composites with observed data along line P is somewhat inconclusive. In several cases, the model reproduces the observed patterns in temperature, salinity, and their anomalies fairly closely. In other cases there are notable differences. Since more than EN or LN variability will affect conditions along line P this may indicate that the NOI is tracking the variability caused by EN or LN, but cannot track other variability present in specific years. Thus using smart climatology along line P may best reflect the ocean state in limited circumstances, such as when EN or LN is the dominant forcing in the ocean. Also, a more sophisticated smart climatology using more than one climate index might capture more variability, and better represent line P conditions than a LTM.

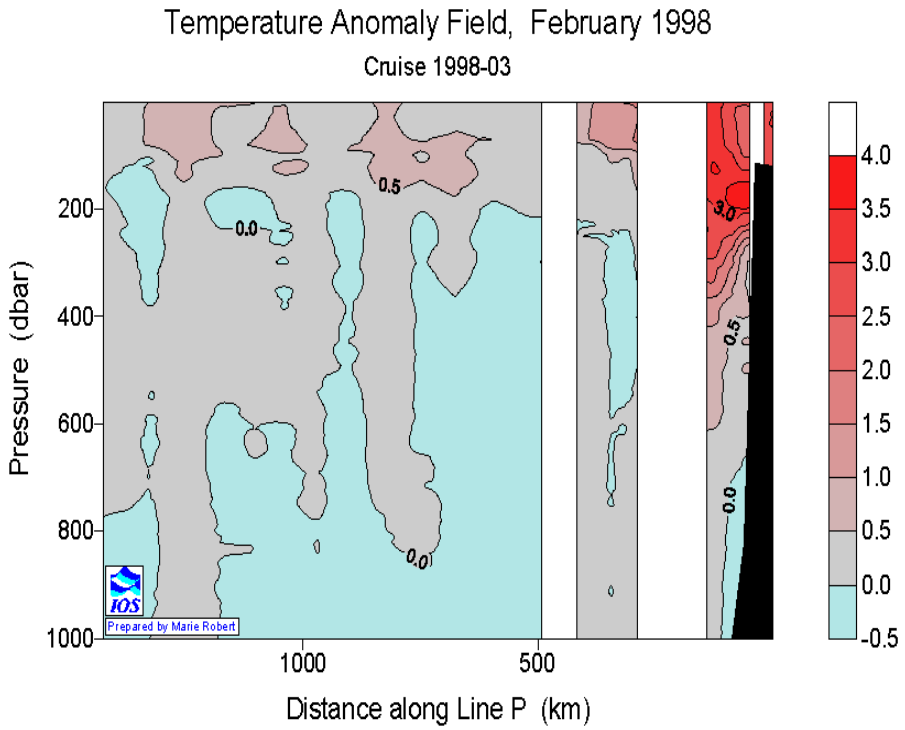

Figure 63. Line P In Situ Temperature Anomaly for February 1998 (From IOS (2005))

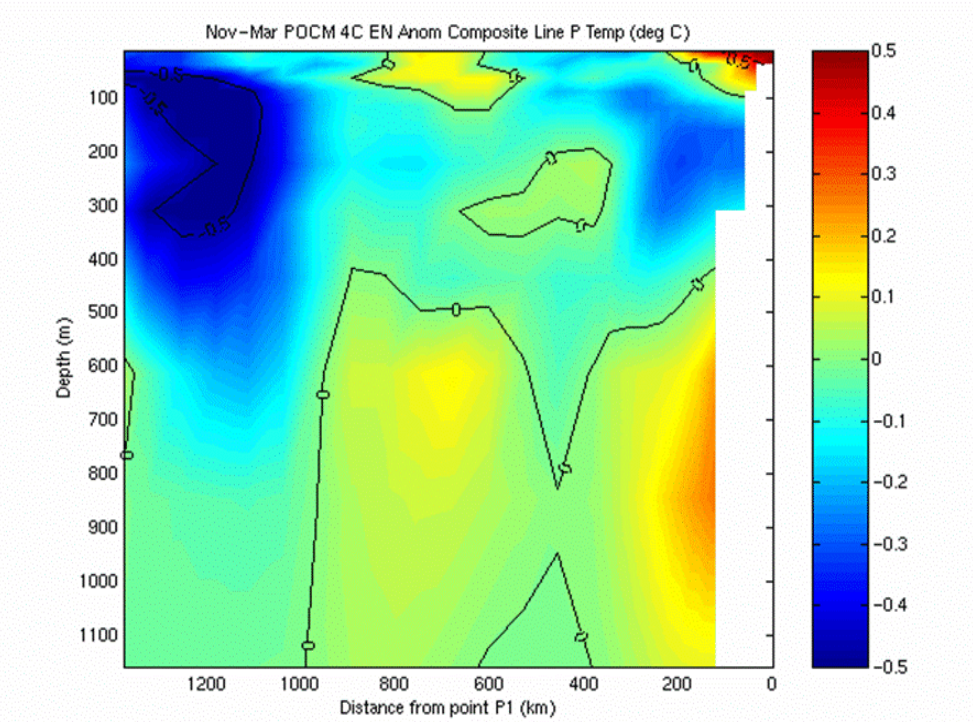

Figure 64. POCM 4C EN Composite Temperature Anomaly Along Line P

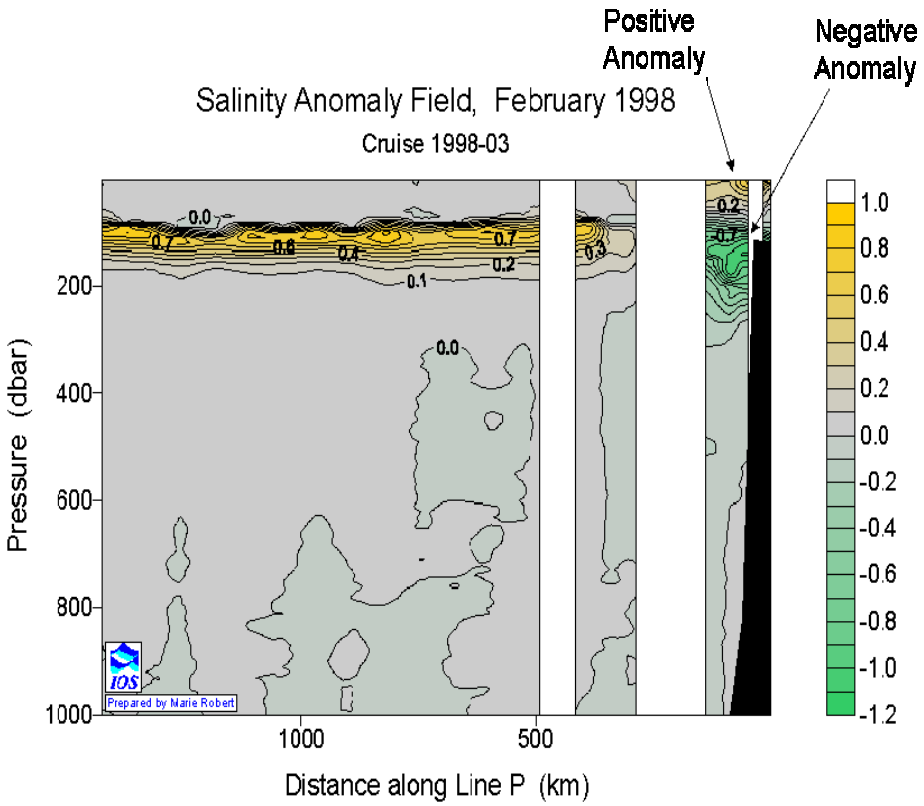

Figure 65. Line P In Situ Salinity Anomaly for February 1998 (From IOS(2005))

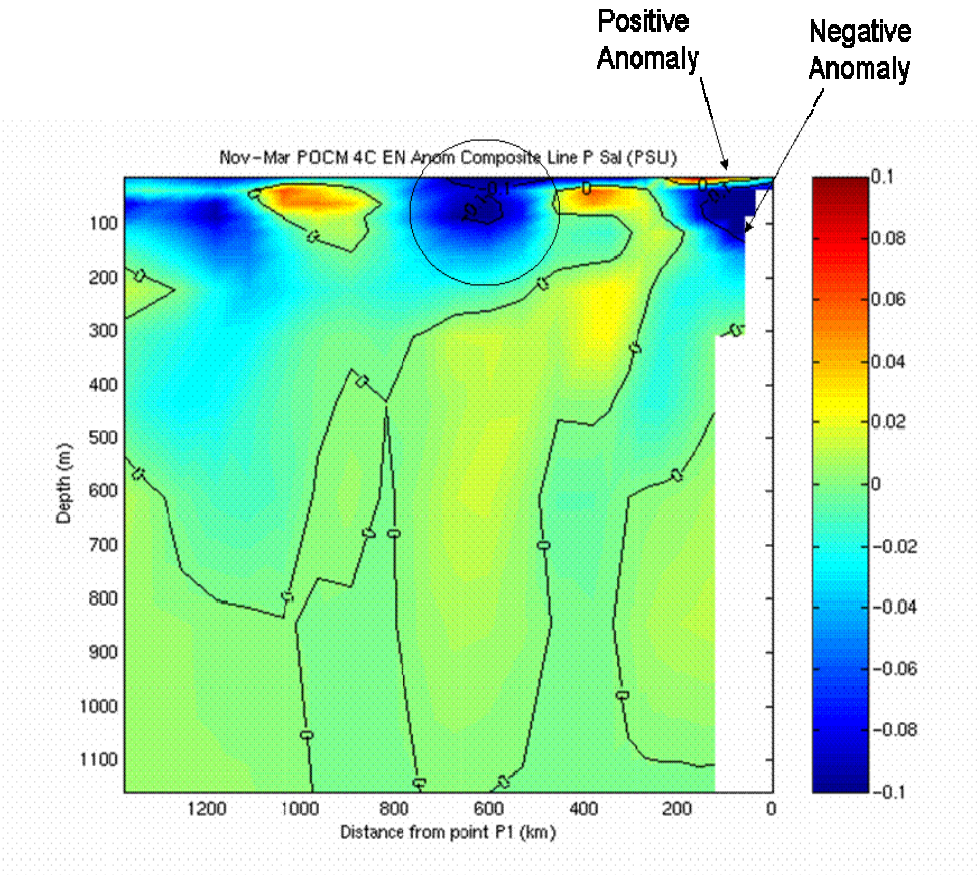

Figure 66. POCM 4C EN Composite Salinity Anomaly Along Line P

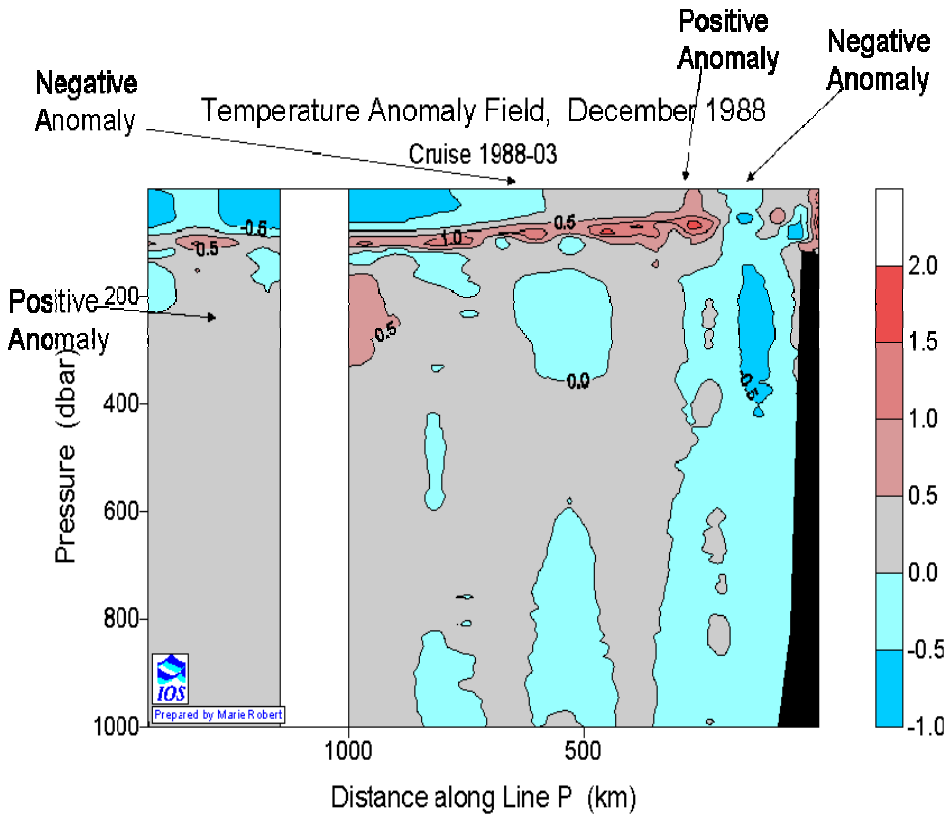

Figure 67. Line P In Situ Temperature Anomaly for December 1988 (From IOS (2005))

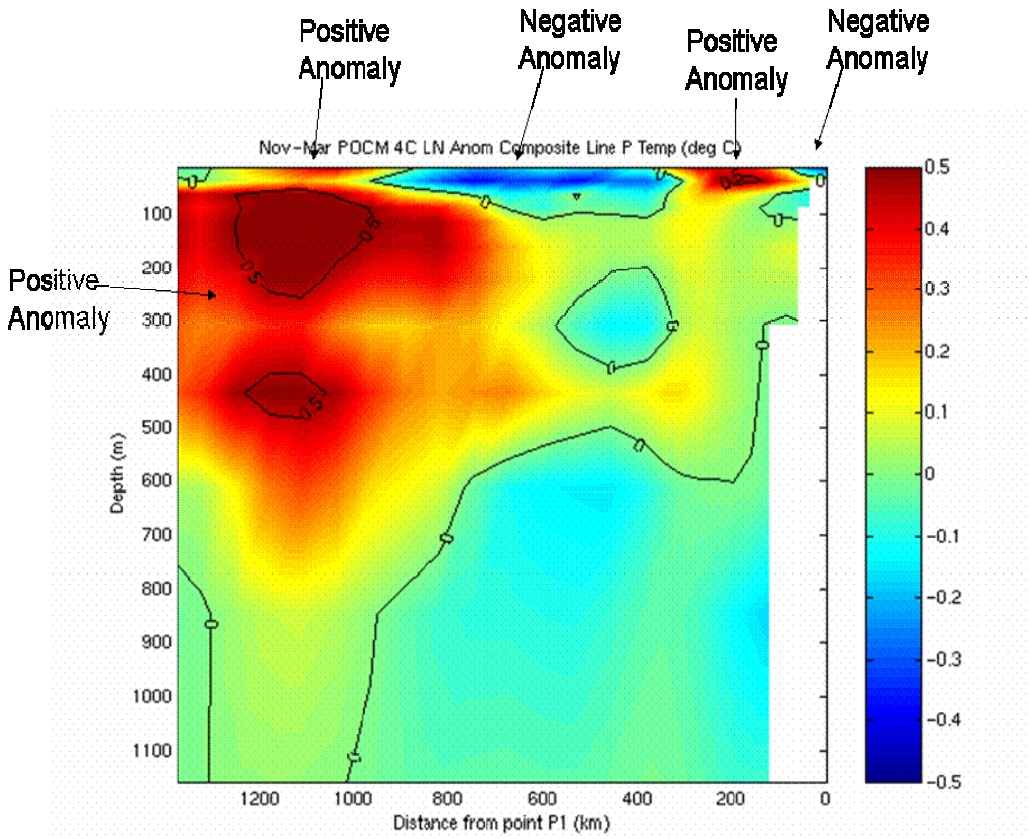

Figure 68. POCM 4C LN Composite Temperature Anomaly Along Line P

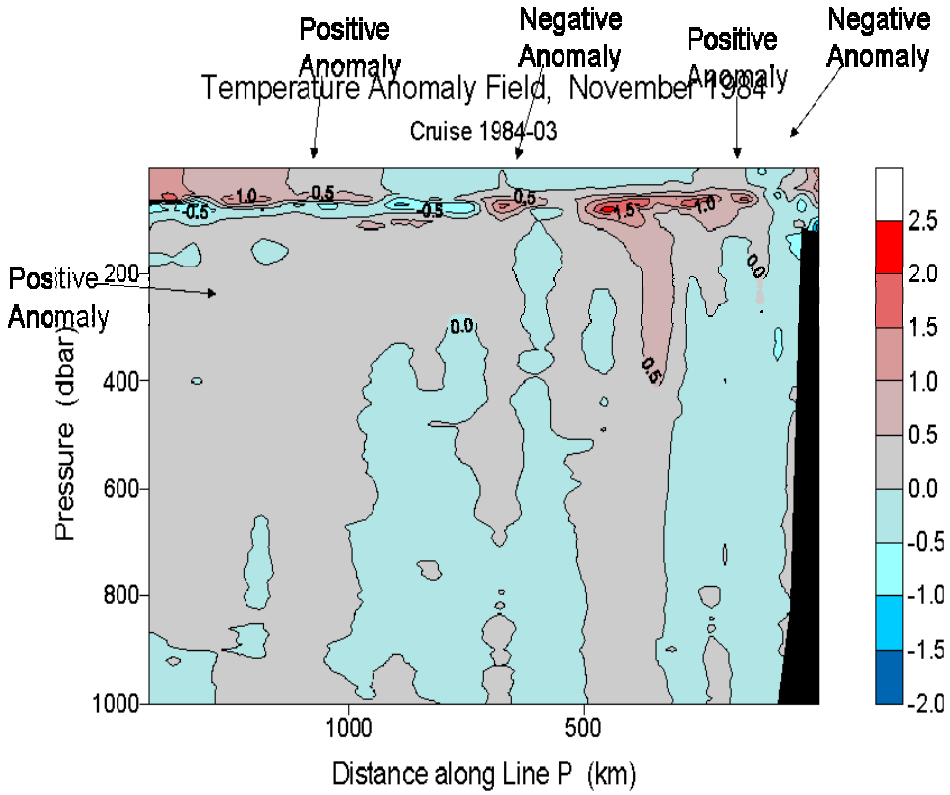

Figure 69. Line P In Situ Temperature Anomaly for November 1984 (From IOS(2005))

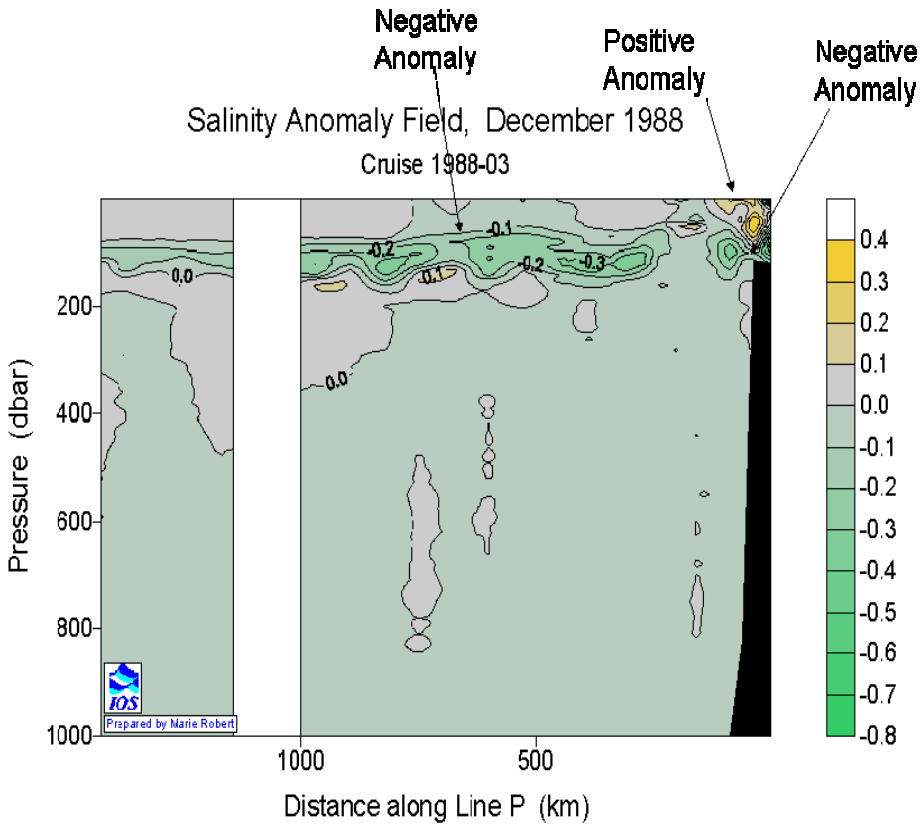

Figure 70. Line P In Situ Salinity Anomaly for December 1988 (From IOS(2005))

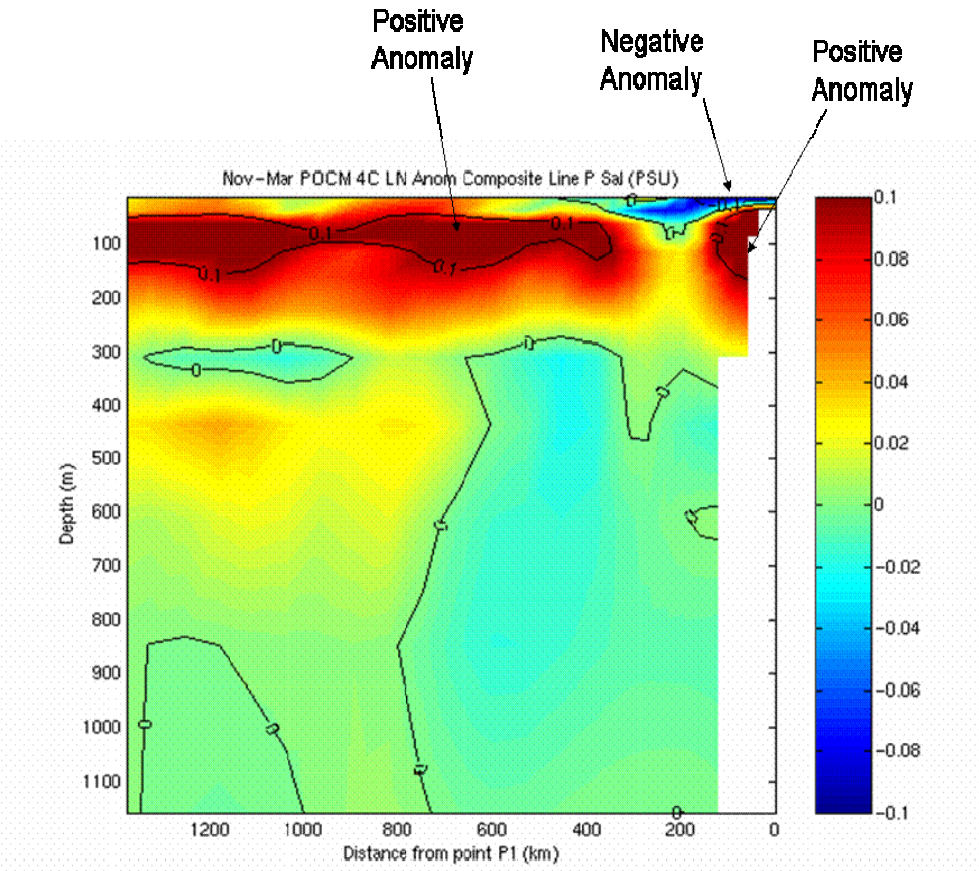

Figure 71. POCM 4C LN Composite Salinity Anomaly Along Line P

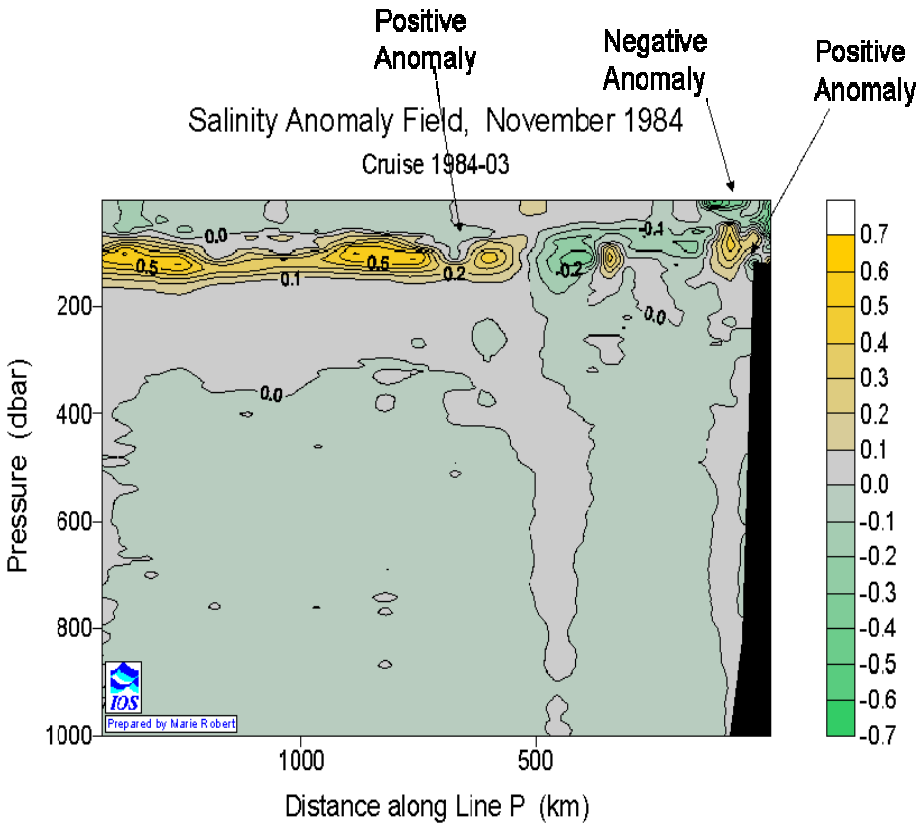

Figure 72. Line P In Situ Salinity Anomaly for November 1994 (From IOS(2005))

C. DISCUSSION

1. Comparison of Model vs. Observed Data

The EN and LN composites from POCM 4C were broadly consistent with observed data. Namely, the CC was weakened and the DC was strengthened during EN, with the opposite occurring during LN. SSH during EN was anomalously high along the coastline in both POCM 4C and satellite altimetry data. During LN, conditions were reversed and anomalously low coastal SSH was simulated by the model and observed in satellite altimetry fields.

The broad scale patterns of EN and LN salinity anomalies simulated by POCM 4C was a weak match to observations. For example the patterns seen in salinity

data reported by Huyer and Smith along the Newport hydrographic line are not clearly repeated by POCM 4C. However, the large patterns seen in POCM 4C, such as fresher water close to the coast during EN, are consistent with observed salinity anomalies during EN or LN. This is not too unexpected since as was mentioned in both Chapter 2 and 3, POCM 4C does not simulate salinity as accurately as other variables.

The POCM 4C simulation of temperature along the coast was not as realistic as was SSH. Reynolds SST shows anomalously warm temperatures all along the coast during EN, and anomalously cool temperatures along the coast during LN. POCM 4C reflected this pattern except for a portion of the central California coast where anomalously cool temperatures were seen in the EN composite, and anomalously warm temperatures were seen in the LN composite. In an effort to determine the source of these inconsistent anomalies, plots of anomalous currents were overlaid on plots of salinity and temperature anomalies along several latitudinal and longitudinal lines. No consistent pattern matching anomalous east-west or north-south flow with temperature or salinity anomalies was noted. Therefore, anomalous advection of external waters into the central California coast region was ruled out as a source of the unexpected anomalies.

As seen in figures in Chapter 3, the patterns of WS and WSC during EN and LN are consistent with warm anomalies all along the coast during EN, and cool anomalies during LN. Therefore, wind forcing cannot be used to explain the cool anomaly along the central California coast during EN, and the warm anomaly along the central California coast

during LN. These unexpected anomalies could be a function of the individual EN and LN events simulated in POCM 4C. For instance, the strong 1982-83 EN event in POCM 4C shows strong warm temperature anomalies everywhere along the coast. Further analysis is warranted of the individual years in the composite, as well as other sources of temperature anomalies such as anomalous mixing or heat flux. In addition, differences in resolution and sampling could be a factor.

Comparisons of POCM 4C EN and LN composites to Line P hydrographic data were inconclusive. At times the POCM 4C EN composite anomaly pattern seemed a better match to observations from an EN month than the LN composite, and vice versa. However, the POCM 4C composite anomalies certainly did not match the patterns of observed anomalies exactly. Since the large-scale surface temperature and salinity anomaly patterns are broadly consistent with observations this may simply indicate that a higher resolution model should be used for such a comparison or that the NOI cannot characterize the ocean down to the scale of 100s of meters of depth over horizontal scales on the order of 100 km.

2. Comparison of EN and LN in the Model

As has been mentioned several times, the patterns of anomalies seen in the POCM 4C EN and LN composites were almost always opposite. For example, if a warm anomaly was seen at a particular location during EN, a cold anomaly was seen in the LN composite. This reinforces the idea that EN and LN are opposite phases of the same climate variation

This research utilized a model simulation relatively short for climate studies. For example, four November to

March periods out of a possible twenty were averaged together to create the EN composite. Thus for each variable at each grid point in the POCM 4C EN and LN composites, the value was the average of only four events. The challenge statistically is to show that the set of four EN events is distinct from the set of four LN events. To do this, a Kolmogorov-Smirnov (K-S) test for two samples was carried out. This test is sensitive to differences in both the mean and variance of two data sets. Like the Student t-test it is appropriate for use with small samples, but unlike the t-test the K-S test does not make any assumptions about the distribution of the datasets (Conover 1999).

The null hypothesis for the K-S test is that the two datasets being compared are in fact from the same distribution. The null hypothesis not being rejected is indicated by a zero value for the test. If the null hypothesis is rejected, the two datasets are different and a value of one is returned. So for each POCM 4C grid-point the set of four EN values was taken as one dataset and the four LN values as the other dataset. The K-S test is built into the MATLAB statistics package, and was done at each grid point for temperature, salinity, and the u and v components. Note that values of 1 for the test are denoted by red, while values of 0 are denoted by blue. No other values are returned by the MATLAB function (kstest2). Results are shown for the upper model layer in the four figures below for a 90% confidence level. In other words, where the figures show a value of 1 for the K-S tests there is a 9 in 10 chance that the 2 phases are distinct.

As can readily be seen in figures 73-76, the null hypothesis is rejected over the largest area along the

coast for the u and v current components. Thus the K-S test suggests that the EN and LN currents simulated by POCM 4C are distinctly different from one another in the CCS. This is consistent with the large differences in current anomalies seen between the EN and LN composites. For temperature and salinity data, the null hypothesis is rejected over much smaller geographic areas. The smallest area is for salinity, but since POCM 4C has been shown to not handle salinity as well as temperature this is not unexpected. It is also interesting to note that at the 90% confidence level, the null hypothesis is rejected for temperature and velocity along the Washington State to Vancouver Island coastline, including shoreward portions of hydrographic Line P. Thus the NOI based composites from POCM 4C may be most applicable to this portion of coastline, rather than over the whole CCS. For temperature and salinity, the EN-LN phase differences follow trends previously reported (see Chapter I) except in the region around 35° N 150° W. The variability seen in POCM 4C may be related to the longer period signal of the North Pacific Index (Tokmakian 1998).

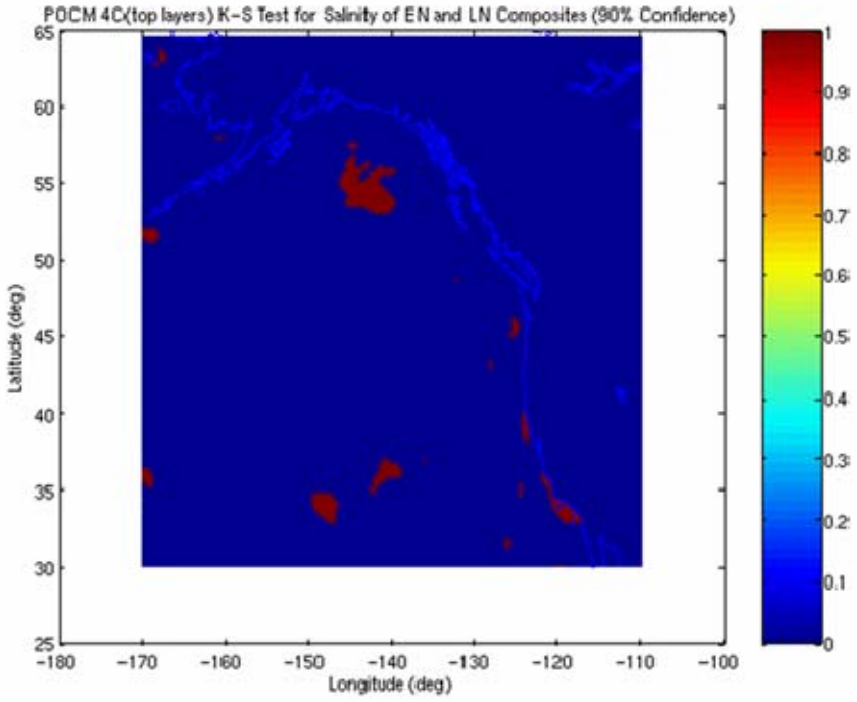

Figure 73. K-S Test for Salinity Between POCM 4C EN and LN Composites

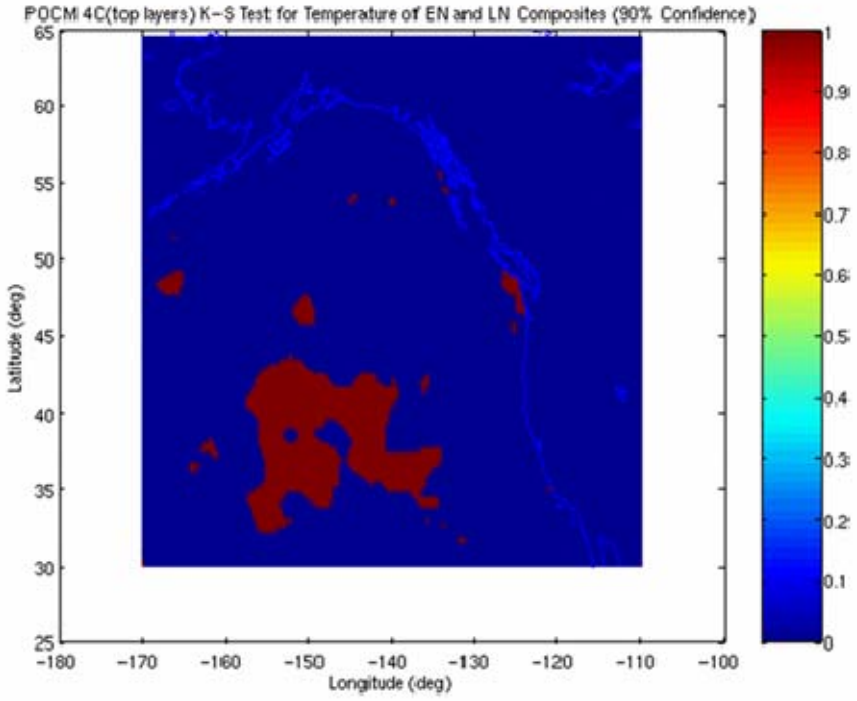

Figure 74. K-S Test for Temperature Between POCM 4C EN and LN Composites

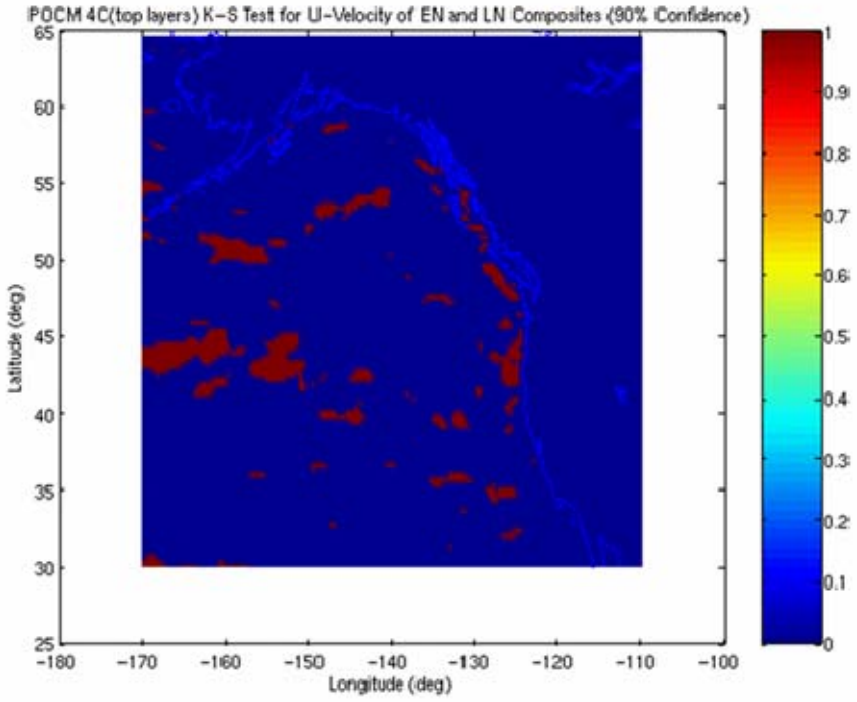

Figure 75. K-S Test for U-component of Current Between POCM 4C EN and LN Composites

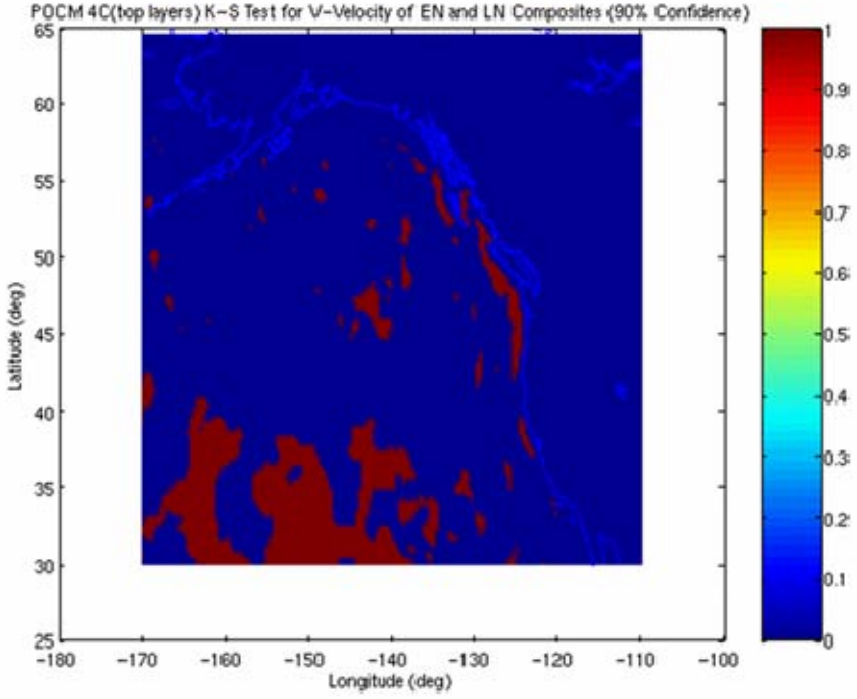

Figure 76. K-S Test for V-component of Current Between POCM 4C EN and LN Composites

C. CONCLUSIONS

The NOI, an atmospheric climate index, does characterize the state of the ocean to some extent. NOI based EN/LN composites from POCM 4C capture well the character of large EN/LN variations over the CCS, although those variations are weaker in POCM 4C than in observational data. The POCM 4C EN and LN smart climatologies might be used to estimate initial conditions in certain areas, as shown by the comparisons with Line P observations, better than is possible with traditional LTM climatologies. Mixed results were seen when attempting to look at specific hydrographic lines on smaller scales. Statistical tests suggest that the POCM 4C EN and LN composites are most different in the Washington State and Vancouver Island coastal areas. So, the NOI based composites of EN and LN conditions created in this study may be most useful in a limited region along the United States-Canada border.

D. RECOMMENDATIONS FOR FUTURE WORK

1. Temporal Coverage

One of the major constraints on this research was the time period covered by POCM 4C. Twenty years of data is less than the often used traditional climatology standard of thirty years. As was mentioned above, the period from 1979-1998 was dominated by EN events and was part of a warm phase of the PDO. Therefore, in future studies it would be useful to have model output covering a longer time span that is more equally representative of EN and LN events. In this case, the model LTM would be more representative of a real world thirty year or longer LTM, and the pattern of anomalies from the LTM would also be more similar to those obtained from observations. So, a warm EN bias in the 1979-

1998 data could be balanced with data from cool LN biased periods. Additionally, comparisons could be made of EN/LN events during warm phases of the PDO with EN/LN events during cool phases of the PDO.

Another advantage of a longer model run would be having more EN and LN events to sample and create composites from. Common variability among EN or LN events would be reinforced in the averaging, while non-EN or non-LN related variability would be smoothed out. Thus, for example, a composite of more EN events would be more representative of the variability caused just by EN and less representative of other variability.

At the same time, it would be interesting to look at NOI based composites covering smaller portions of time. Instead of looking at a 5 month average over an EN or LN event, it would be interesting to look at just one month in particular. This would facilitate comparisons with hydrographic data, as continuous samples for one hydrographic line for periods longer than a month are rare. Such a study in combination with studies of longer time periods might also help quantify over what time scales an index like the NOI is providing useful information about the ocean

2. Different Model Choices

POCM 4C is an excellent choice for studying ocean climate variability on the large scale. However, a logical next step is to focus on smaller areas. In particular, it would be interesting to look at oceanographic features close to the coast in more detail, and over the span of 100 km or less. A natural choice would be a higher resolution ocean model, either a higher resolution global model such

as the Parallel Ocean Program (POP) which is related to POCM 4C or a regional high resolution or mesoscale ocean model.

Another issue is the coupling of the atmosphere and ocean. As POCM evolved, forcing did become more realistic from version 4A to version 4C. However, it would be interesting to do a similar project to the research presented here with a fully coupled atmosphere-ocean model. Several options are available (see for instance Saha et al. (2005)). Using a coupled atmosphere-ocean model would allow a closer look at feedbacks between the ocean and atmosphere, whereas this study has focused on atmospheric forcing of the ocean.

3. Geographic Area

Finally, it would be interesting to do a similar study in a western boundary current (WBC) region. WBC areas such as the Gulf Stream or Kuroshio have generally stronger currents than the CCS, and have large mesoscale features such as warm core and cold core rings (Pickard and Emery 1990). If a suitable atmospheric climate index characterizing large fluctuations in a WBC region can be selected, it may be easier to see large variations in temperature, salinity, and current patterns. In such a case EN and LN may not be the climate variations studied, but as long as the climate variability is large compared to normal seasonal variability, the research could be beneficial.

E. NAVAL RELEVANCE

This thesis serves as a demonstration of the concept that the climate state of the ocean may be characterized by a carefully chosen atmospheric climate index. Using such a climate index, selected composites of ocean conditions

corresponding to different climate regimes can be made. Since historical ocean observations are not uniformly dense enough in time or space to make meaningful composites, ocean models present the best source of proxy data. The conditions seen in the composites are consistent with real world observations, better match ocean variability than traditional climatology, and the differences between the composites are statistically significant. Therefore further research into using the techniques described in this study is warranted.

The Navy has a particular interest in ocean conditions for anti-submarine warfare, search and rescue, and navigation. The speed of sound in water, and hence the tactical and strategic placement of sensors, is highly dependent on temperature and salinity variability. There is currently an increased focus on the use of AUVs and UUVs, particularly for environmental sampling. These craft have limited range and endurance, hence their launch and search areas need to be optimized. Search and rescue operations could be enhanced by a better depiction of where ocean currents may carry missing personnel or equipment. Ships, submarines, amphibious landing craft, and special warfare units all require accurate ocean current information to plan optimum navigation tracks. Additionally, the ocean models used by the Navy would benefit from more accurate boundary and initial conditions. Using smart climatology for the ocean and atmosphere shows promise for improving the products provided to the warfighter by the Naval Meteorology and Oceanography Community.

As a final thought, Figure 77 is included below. On the left of the figure we see traditional climatology from

static MODAS. The next panel shows the difference between static and dynamic MODAS. The third panel is from an intensive ocean survey. It is easily seen that the dynamic MODAS figure improves on traditional climatology. Some of the possibilities raised by this thesis are annotated on the figure and in the far-right panel. Smart climatology may someday be blended with dynamic MODAS, or some similar product, to gain an even more useful depiction of the ocean. Or perhaps smart climatology will eventually provide another useful option when MODAS is unavailable.

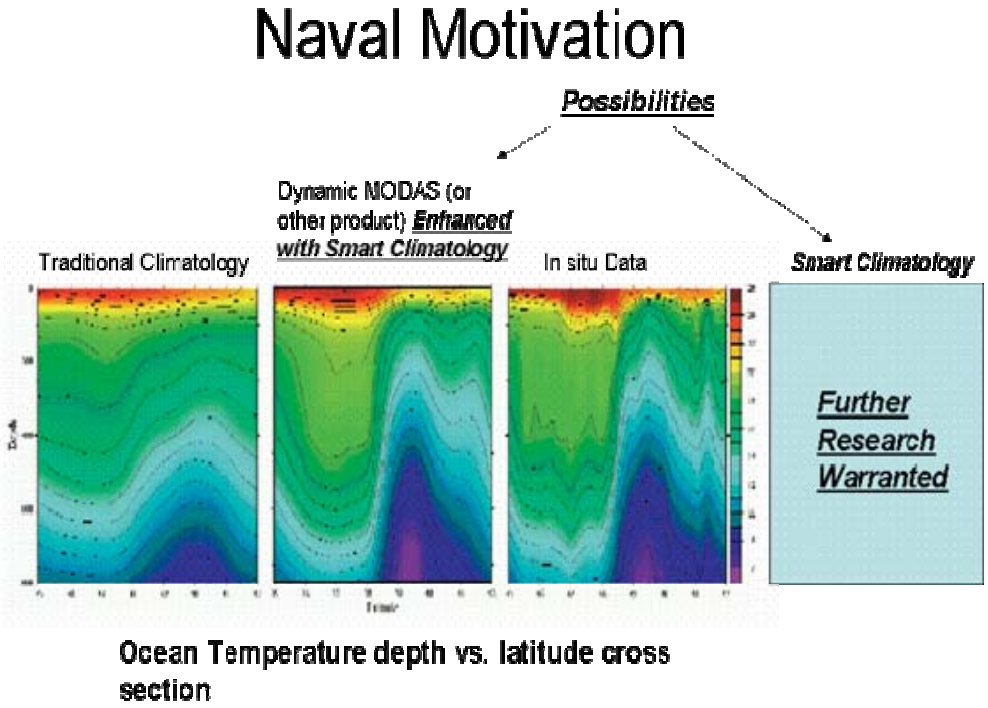

Figure 77. Naval Motivation: Depth-Latitude Cross-sections of Temperature Showing Current and Possible Climate Tools

LIST OF REFERENCES

Barth, J.A., S.D. Pierce, and R.L. Smith, 2000: A separating coastal upwelling jet at Cape Blanco, Oregon and its connection to the California Current System. ***Deep-Sea Res. II,*** **47**, 783-810.

Boyer, T., S. Levitus, H. Garcia, R.A. Locarnini, C. Stephens, and J. Antonov, 2005: Objective Analyses of Annual, Seasonal, and Monthly Temperature and Salinity for the World Ocean on a 0.25° Grid. ***Int. J. Climatol.,*** **25**, 931-945.

Bryan, K., 1969: A Numerical Method for the Study of the Circulation of the World Ocean. ***J. Comput. Phys,*** **4**, 347-376.

Cane, M.A., 1983: Oceanographic Events during El Nino. ***Science,*** **222**, 1189-1195.

Carton, J.A., G. Chepurin, X. Cao, and B. Giese, 2000: A Simple Ocean Data Assimilation Analysis of the Global Upper Ocean 1950-95. Part I: Methodology. ***J. Phys. Oceanogr.,*** **30**(2), 294-309.

CDC, cited August 2005: Multivariate ENSO Index [Available online from http://www.cdc.noaa.gov/ENSO/enso.mei_index.html].

Chelton, D.B. and R.E. Davis, 1982: Monthly Mean Sea-Level Variability Along the West Coast of North America. ***J. Phys. Oceanogr.,*** **12**, 757-784.

CNES, cited August 2005: Aviso Website [Available online from http://www.jason.oceanobs.com/].

Collins, C.A., C.G. Castro, H. Asanuma, T.A. Rago, S.K. Han, R. Durazo, and F.P. Chavez, 2002: Changes in the hydrography of Central California waters associated with the 1997-98 El Nino. ***Prog. Oceanogr.,*** **54**, 129-147.

Collins, C.A., J.T. Pennington, C.G. Castro, T.A. Rago, and F.P. Chavez, 2003: The California Current System off Monterey, California: physical and biological coupling. ***Deep-Sea Res. II,*** **50**, 2389-2404.

Conkright, M.E., J.I. Antonov, O. Baranova, T.P. Boyer, H.E. Garcia, R. Gelfeld, D. Johnson, R.A. Locarnini, P.P. Murphy, T.D. O'Brien, I. Smolyar, and C. Stephens, 2002: ***World Ocean Database 2001, Volume 1: Introduction.*** S. Levitus, Ed., NOAA Atlas NESDIS 42, U.S. Government Printing Office, Wash., D.C., 167 pp., CD-ROMs.

Conover, W.J., 1999: ***Practical Nonparametric Statistics.*** Wiley, 584 pp.

Danielson, E.W., J. Levin, E. Abrams, 2003: ***Meteorology.*** McGraw Hill, 558 pp.

Estis, F., and B. Tsugawa, Eds., 2004: The Federal Plan for Meteorological Services and Supporting Research Fiscal Year 2005. OFCM Document FCM P1-2004, 248 pp.

Fox, D.N., W.J. Teague, C.N. Barron, M.R, Carnes, and C.M. Lee, 2002a: The Modular Ocean Data Assimilation System (MODAS). ***J. Atmos. and Oceanic Tech.,*** **19**, 240–252.

Fox, D.N., C.N. Barron, M.R. Carnes, M. Booda, G. Peggion, and J.V. Gurley, 2002b: The Modular Ocean Data Assimilation System (MODAS), ***Oceanography,*** **15(1)**, pp 22-28.

Gangopadhyay, A., W.G. Leslie, P.J. Haley Jr., P.F.J. Lermusiaux, and A.R. Robinson, cited July 2005: A working Paper on the California Current System: Its features, scales of variability and modeling domain initialization [Available online from http://www.smast.umassd.edu/modeling/ccs.pdf]

Gille, S.T., D.P. Stevens, R.T. Tokmakian, and K.J. Heywood, 2001: Antarctic Circumpolar Current response to zonally averaged winds. ***J. Geophys. Res.,*** **106(C2)**, 2743-2759.

Gould, J.W., 2003: WOCE and TOGA – The Foundations of the Global Ocean Observing System. ***Oceanography,*** **16(4),** pp. 24-30.

Grembowicz, K. P., and B.S. Howell, 2002: Quality Control of Ocean Temperature and Salinity Profile Data. ***Oceans 2002 IEEE/MTS Conference Proceedings,*** Biloxi, MS, Oceans 2002 IEEE/MTS Conference Committee, 1253-1257.

Hearn, C. G., 2002: ***Tracks in the Sea - Matthew Fontaine Maury and the Mapping of the Oceans.*** International Marine, 278 pp.

Hickey, B. M., 1998: Coastal Oceanography of Western North America from the Tip of Baja California to Vancouver Island. ***The Sea***, **11**, 345-393.

Huyer, A., R.L. Smith, and J. Fleischbein, 2002: The coastal ocean off Oregon and northern California during the 1997-8 El Nino. ***Prog. Oceanogr.***, **54,** 311-341.

IOS (Institute of Ocean Sciences, Department of Fisheries and Oceans, Canada, cited September 2005: Line P Time-Series Program [Available online from: www-sci.pac.dfo-mpo.gc.ca/osap/projects/linepdata/default_e.htm]

Jayne, S. R. and R. Tokmakian, 1997. Forcing and sampling of ocean general circulation models: impact of high-frequency motions. ***J. Phys. Oceanogr.***, **27**, 1173-1179.

Johnson, M.A., and J.J. O'Brien, 1990: The Northeast Pacific Ocean Response to the 1982-1983 El Nino. ***J.Geophys. Res.***, **95 (C5)**, 7,155-7,166.

Killworth, P.D., D. Stainforth, D.J. Webb, and S.M. Paterson, 1991: The Development of a Free-Surface Bryan-Cox-Semtner Ocean Model. ***J. Phys. Oceanogr.***, **21**, 1333-1348.

Martin, S., 2004: ***An Introduction to Ocean Remote Sensing.*** Cambridge University Press, 454 pp.

Matano, R.P., E.J. Beier, P.T. Strub, and R. Tokmakian, 2002: Large-Scale Forcing of the Agulhas Variability: The Seasonal Cycle. ***J. Phys. Oceanogr.,*** **32**, 1228-1240.

Matthews, P.E., M.A. Johnson, and J.J. O'Brien, 1992: Observation of Mesoscale Ocean Features in the Northeast Pacific Using Geosat Radar Altimetry Data. ***J.Geophys. Res.,*** **97 (C11)**, 17,829-17,840.

Miller, A.J., and N. Schneider, 2000: Interdecadal climate regime dynamics in the North Pacific Ocean: theories, observations and ecosystem impacts. ***Prog. Oceanogr.,*** **47**, 355-379.

Miller, A.J., J.C. McWilliams, N. Schneider, J.S. Allen, J.A. Barth, R.C. Beardsley, F.P. Chavez, T.K. Chereskin, C.A. Edwards, R.L. Haney, K.A. Kelly, J.C. Kindle, L.N. Ly, J.R. Moisan, M.A. Noble, P.P. Niiler, L.Y. Oey, F.B. Schwing, R.K. Shearman, and M.S. Swenson, 1999: Observing and Modeling the California Current System, ***Eos, Transactions, American Geophysical Union,*** **80**, 533-539.

Murphree, T., S.J. Bogard, F.B. Schwing, and B. Ford, 2003a: Large scale atmosphere-ocean anomalies in the northeast Pacific during 2002. ***Geophys. Res. Lett.,*** **30(1)**, 8026, doi:10.1029/2003GL017303..

Murphree, T., P. Green-Jessen, F.B. Schwing, and S.J. Bogard, 2003b: The seasonal cycle of wind stress curl and its relationship to subsurface ocean temperature in the Northeast Pacific. ***Geophys. Res. Lett.,*** **30(9),** 1469,doi:10.1029/2002GL016366.

Mysak, L.A., 1986: El Nino, Interannual Variability and Fisheries in the Northeast Pacific Ocean. ***Can. J. Fish. Aquat. Sci.,*** **43**, 464-497.

NAVO, cited July 2005: GDEMV 3.0 [Available online from https://128.160.23.42/gdemv/gdem_desc_v30.html].

NRL, cited July 2005: Near Real-Time Depiction of the California Current System [Available online from http://www7320.nrlssc.navynavy.mil/ccsnrt/].

Oceanographer of the Navy, 2000: Strategy for Research and Development: A Roadmap to a Vision of Operational Oceanography, 18 pp. [Available from Technical Director Oceanographer of the Navy (CNO 096T), U.S. Naval Observatory, 3450 Massachusetts Avenue NW, Washington, DC 20392.]

Pennington, J.T., and F.P. Chavez, 2000: Seasonal fluctuations of temperature, salinity, nitrate, chlorophyll and primary production at station H3/M1 over 1989-1996 in Monterey Bay, California. ***Deep-Sea Res. II,*** **47**, 947-973.

PFEL, cited 2005: The Northern Oscillation Index (NOI) [Available online from http://www.pfel.noaa.gov/products/PFEL/modeled/indices/NOIx/noix.html].

Pickard, G.L., and W.J. Emery, 1990: ***Descriptive Physical Oceanography - An Introduction (5^{th} edition).*** Butterworth-Heinemann, 320 pp.

Pierce, S.D., R.L. Smith, P.M. Korso, J.A. Barth, and C.D. Wilson, 2000: Continuity of the poleward undercurrent along the eastern boundary of the mid-latitude north Pacific. ***Deep-Sea Res. II,*** **47**, 811-829.

Ramp, S.R., J.L. McClean, C.A. Collins, A.J. Semtner, and A.S. Hays, 1997a: Observations and modeling of the 1991-1992 El Nino signal off central California. ***J.Geophys. Res.,*** **102 (C3)**, 5553-5582.

Ramp, S.R., L.K. Rosenfeld, T.D. Tisch, and M.R. Hicks, 1997b: Moored observations of the current and temperature structure over the continental slope off central California. ***J. Geophys. Res.,*** **102 (C10)**, 22,877-22,902.

Reeves, R. W., and D.J. Gemmill, Eds., 2004: ***Climate Prediction Center - Reflections on 25 Years of Analysis, Diagnosis, and Prediction.*** U. S. Government Printing Office, 107 pp.

Reynolds, R.W., N.A. Rayner, T.M. Smith, D.C. Stokes, W. Wang, 2002: An Improved In Situ and Satellite SST Analysis for Climate. *J. Clim.*, **15(13)**, 1609-1625.

Saha, S., S. Nadiga, C. Thiaw, J. Wang, W. Wang, Q. Zhang, H. M. van den Dool, H.L. Pan, S. Moorthi, D. Behringer, D. Stokes, G. White, S. Lord, W. Ebisuzaki, P. Peng, P. Xie, 2005: The NCEP Climate Forecast System. Submitted to *The Journal of Climate.*

Schwing, F.B., T. Murphree, and P.M. Green, 2002a: The Northern Oscillation Index (NOI): a new climate index for the northeast Pacific. *Prog. Oceanogr.*, **53**, 115-139.

Schwing, F.B., T. Murphree, L. deWitt, L., and P.M. Green, 2002b: The evolution of oceanic and atmospheric anomalies in the northeast Pacific during the El Niño and La Niña events of 1995-2001. *Prog. Oceanogr.*, **54**, 459-491.

Semtner, A.J. and R.M. Chervin, 1988: A Simulation of the Global Ocean Circulation With Resolved Eddies. *J.Geophys. Res.*, **93 (C11)**, 15,502-15,522.

Semtner, A.J. and R.M. Chervin, 1992: Ocean General Circulation From a Global Eddy-Resolving Model. *J.Geophys. Res.*, **97 (C4)**, 5493-5550.

Semtner, A.J., 1995: Modeling Ocean Circulation. *Science,* **269**, 1379-1385.

Stammer, D., R. Tokmakian, A. Semtner, and C. Wunsch, 1996: How well does a ¼° global ocean model simulate large-scale oceanic observations. *J. Geophys. Res.*, **101 (C11)**, 25,779-25,811.

Stephens, C., J.I. Antonov, T.P. Boyer, M.E. Conkright, R.A. Locarnini, T.D. O'Brien, and H.E. Garcia, 2002: *World Ocean Atlas 2001, Volume 1: Temperature.* S. Levitus, Ed., NOAA Atlas NESDIS 49, U.S. Government Printing Office, Wash., D.C., 176 pp.

Strub, P. T., and C. James, 2000: Altimeter-derived variability of surface velocities in the California Current System: 2 Seasonal Circulation and eddy statistics. *Deep-Sea Res. II*, **47**, 831-870.

Strub, P. T., and C. James, 2002a: Altimeter-derived surface circulation in the large-scale NE Pacific Gyres. Part 1. seasonal variability. ***Deep-Sea Res. II***, **53**, 163-183.

Strub, P.T., and C. James, 2002b: Altimeter-derived surface circulation in the large-scale NE Pacific Gyres. Part 2: 1997-1998 El Nino anomalies. ***Prog. Oceanogr.***, **53**, 185-214,

Strub, P.T., and C. James, 2002c: The 1997-1998 oceanic El Nino signal along the southeast and northeast Pacific boundaries – an altimetric view. ***Prog. Oceanogr.***, **54**, 439-458.

Tokmakian R. T., cited 1996: A Note on a Global Comparison of Tide Gauge Sea Levels with a Model's Sea Surface Heights. [Available online at www.oc.nps.navynavy.mil/~rtt/paper/sea level.html]

Tokmakian, R., 1998: A High Resolution Ocean Model with Variable Forcing of Wind, Heat, and Freshwater: Initial Evaluation. ***International WOCE Newsletter, 32.***

Tokmakian, cited August 2005: Model Grid Horizontal and Vertical Definition [Available online from http://www.oc.nps.navynavy.mil/~rtt/Histinfo 0.25].

Tokmakian, R., Challenor, P. G., 2000: On the joint estimation of model and satellite sea surface height anomaly errors, ***Ocean Modelling***, **1 (1)**, 1, 39-52.

UW, cited 2005: The Pacific Decadal Oscillation. [Available online from http://tao.atmos.washington.edu/pdo/].

Wooster, W.S., and D.L. Fluharty, Eds.,1985: ***El Nino North – Nino Effects in the Eastern Subarctic Pacific Ocean.*** Washington Sea Grant Program, 312 pp.

THIS PAGE INTENTIONALLY LEFT BLANK

INITIAL DISTRIBUTION LIST

1. Defense Technical Information Center
   Ft. Belvoir, Virginia

2. Dudley Knox Library
   Naval Postgraduate School
   Monterey, California

3. Philip A. Durkee, Department of Meteorology
   Naval Postgraduate School
   Monterey, California

4. Mary L. Batteen, Department of Oceanography
   Naval Postgraduate School
   Monterey, California

5. Tom Murphree, Department of Meteorology
   Naval Postgraduate School
   Monterey, California

6. Robin T. Tokmakian, Department of Oceanography
   Naval Postgraduate School
   Monterey, California

7. Leslie K. Rosenfeld, Department of Oceanography
   Naval Postgraduate School
   Monterey, California

8. Steven Ramp, Department of Oceanography
   Naval Postgraduate School
   Monterey, California

9. Curtis A. Collins, Department of Oceanography
   Naval Postgraduate School
   Monterey, California

10. Richard Siquig
    Naval Research Lab
    Monterey, California

11. Joel Feldmeier
    Monterey, California

12. John and Judith Feldmeier
    Monroe, Michigan

13. John Feldmeier
National Optical Astronomy Observatory
Tucson, Arizona